Near-End Crosstalk Cancellation in xDSL Systems

by

Rajeev Conrad Nongpiur
BTech.(Hons) Indian Institute of Technology - Kharagpur, 1998

A Dissertation Submitted in Partial Fulfillment of the Requirements
for the Degree of

DOCTOR OF PHILOSOPHY

in the Department of Electrical and Computer Engineering

Supervisors: Dr. A. Antoniou and Dr. D.J. Shpak

ABSTRACT

In xDSL technology, high-speed data are transferred between the central office and the customers, or between two or more central offices using unshielded telephone lines. A major impairment that hinders the increase in data-rate through the twisted-pair line is near-end crosstalk (NEXT) between the adjacent twisted pairs. DSL systems with overlapping transmit and receive spectra are susceptible to NEXT which significantly increases the interference noise in the received signal and also reduces the reliability and availablity of the system. One way to cancel the NEXT in the received signal is to deploy adaptive filters. However, if adaptive filters are deployed to cancel every possible NEXT signal from the other twisted pairs, the computational complexity increases in proportion to N^2 where N is the number of twisted pairs in the bundle and, therefore, it becomes prohibitive even for small values of N. In this dissertation, four new methods for NEXT reduction are proposed. The methods aim at reducing computational complexity while maintaining speed and performance.

In Chapter 3 an efficient NEXT cancellation system is proposed. The new system first detects the NEXT signals present in the received signal and then assigns adaptive filters to cancel the most significant NEXT signals detected. The detection process uses a fast and efficient algorithm that estimates the crosscorrelation between the transmitted and received signal. By subtracting the adaptive filter estimates of the NEXT signals that have been detected and assigned adaptive filters for cancellation, the magnitude of smaller NEXT signals can be estimated more accurately during the NEXT detection stage. The new system offers an overall computational complexity of order N. This represents a large reduction in the computational effort relative to that in previous NEXT cancellation system which offer computational complexities of order N^2.

In Chapter 4, the NEXT cancellation system proposed in Chapter 3 is implemented using frequency-domain least-mean-square (FDLMS) adaptive filters to cancel the NEXT

signals. Several schemes for assigning the adaptive filter step sizes are explored. It has been found that by making the step sizes proportional to the magnitude of the NEXT signals during the initial phases of adaptation and then making them all equal during the later phases, the convergence rate can be significantly improved. And by returning after convergence to step sizes that are proportional to the magnitudes of the NEXT signals, a much better tracking performance is achieved.

In Chapter 5, a new technique that reduces the computational complexity in adaptive filters for NEXT cancellation is proposed. In this technique, the filter length of each adaptive filter is adjusted according to the strength of the NEXT signal. Since the NEXT signals from the other twisted pairs are typically of different magnitudes, using such a technique leads to a significant reduction in the total number of filter taps when compared with fixed-length adaptive filters. The NEXT cancellation is started by using adaptive filters with minimum filter lengths. As the adaptation progresses, the filter length of each adaptive filter is adjusted according to the magnitude of the NEXT signal. Upon convergence, another algorithm is deployed which readjusts the filter lengths of those adaptive filters that are too long or too short.

Chapter 6 deals with another new method to mitigate NEXT based on a wavelet denoising technique. In xDSL systems, the received signal typically has greater power in the lower end of the frequency spectrum whereas the NEXT signal has greater power in the higher end. The wavelet technique takes advantage of the difference between the power spectrum of the received signal and that of the NEXT to mitigate the crosstalk noise. In addition, the method has a low computational complexity which makes it fast, efficient, and well suited for high data-rate applications.

Table of Contents

List of Tables

List of Figures

List of Abbreviations

2B1Q	2 binary 1 quaternary
ADSL	Asymmetric digital subscriber line
AWG	American wire gauge
BRI	Basic rate ISDN
CAP	Carrierless AM/PM
CO	Central office
CSA	Carrier service area
DFE	Decision feedback equalizer
DMT	Discrete multitone
DSL	Digital subscriber line
FDD	Frequency division duplexing
FDI	Feeder distribution interface
FDLMS	Frequency domain LMS
FEXT	Far-end crosstalk
HDSL	High bit-rate DSL
HDSL2	Second generation HDSL
ISDN	Integrated service digital network
ITU	International Telecommunications Union
LMS	Least mean square
MAD	Median absolute deviation
NEXT	Near-end crosstalk
NLMS	Normalized LMS
OPTIS	Overlapped PAM with interlocking spectra
PAM	Pulse amplitude modulation
PIC	Primary inter-exchange carrier

PSD	Power spectral density
QAM	Quadrature amplitude modulation
SDSL	Single-pair symmetric DSL
SIR	Signal to interference ratio
UTP	Unshielded twisted pair
VDSL	Very-high-data-rate DSL

Acknowledgement

I would like to express my deepest gratitude to Dr. Andreas Antoniou for his guidance, advise, and support throughout my graduate studies; I am especially thankful for the special attention and the extra time he has spent in teaching me invaluable lessons on how to develop and present new ideas. I am also deeply grateful to Dr. Dale Shpak for his encouragement and support and for his many insightful comments that opened new doors during the course of my research. It was Dr. Antoniou and Dr. Shpak who encouraged me to go for my PhD rather than settle just for a master's degree, and their continuous support and guidance gave me the confidence and vigor to achieve much more than what I had initially aimed for. I feel privileged to have had them as my supervisors.

I am especially thankful to Drs. Wu-Sheng Lu and Pan Agathoklis for always being available to answer my questions, listen to my ideas, give advice, and for serving as members of my Supervisory Committee. I thank Dr. Michela Serra, outside member of my Supervisory Committee, for her pertinent comments and Dr. Martin Bouchard, my External Examiner, for his perceptive comments and suggestions in improving my thesis.

I wish to thank Ms. Vicky Smith, Ms. Catherine Chang, Ms. Monica Bracken, Ms. Lynne Barrett, and Ms. Mary-Anne Teo for all their help during my graduate program. Thanks are also due to Steve Campbell, John Dorocicz, and Erik Laxdal for making sure that the computer systems are free from hackers and that the latest and greatest software applications are installed on the computers of the DSP Lab.

My life in Uvic would have been pretty dull and miserable without my friends: Many thanks to Debasish Sasmal for all his help over the years; it was Debasish who encouraged me to come to Uvic for my graduate studies – a decision that I am pleased to have made. I would like to thank Apurva and Paramesh, my apartment mates, including Pratibha and Manjinder for being such helpful and understanding friends. When it comes to living 'life to the lees', as in Tennyson's Ulysses, I owe it to Brad and Stuart: the 'wings and prawns nights' on Wednesdays at Maudes, the parties ... flaming sambuka ..., the camping and

ski trips, the midnight frisbee golfs, and the coffee breaks at Finnertys are some of the pleasurable moments, with them, that immediately come to mind. I would also like to thank Watheq, Nanyan, Yajun, Xianmin, Deepali, Sabbir, Newaz, Mohammed Yasein, and Rafik for all their help and for the enjoyable discussions that we had in the DSP Lab. My special thanks to Doug and Bev Biffard for making my stay in Victoria all the more pleasant and enjoyable; the 100 and more scuba-dives – around Victoria, at Race Rocks, and in the wrecks of the G.B. Church, HMCS Mackenzie, and HMCS Cape Brenton – that I did with them are some of my most enjoyable experiences. I am also thankful to Seigo Sakamoto for teaching me how to fly the Cessna 150 and the 172, and for helping me obtain my PPL. Thanks are also due to Kate for all her help and to her family.

Finally, I would like to thank Monisha, my sister, and Vijay, my brother, for their love and support. Most of all, my parents receive my deepest gratitude and love for their dedication and unremitting support. This thesis is also to commemorate my father who unfortunately passed away more than two years ago – as he glances from above, I do not think he will be disappointed with the way things evolved so far.

Dedication

TO MY MOTHER AND FATHER

Chapter 1

Introduction

A subscriber line is the means whereby a telephone user is connected to the telephone network. Through it, the user transmits information to a local switch to be distributed to other subscribers on the same network or interconnected networks. Due to their ubiquity, subscriber lines are the most economical means of connecting to customers. During the 1970s and early 1980s the telephone subscriber lines were also used as voice frequency analog data links. With the advent of powerful and inexpensive computers however the demand for higher data transmission rates grew. This compelled communication system designers to look beyond the voice channel bandwidth of 3 kHz in order to exploit a greater portion of the frequency spectrum. For telephone lines, the bandwidth beyond 3 kHz is severely limited by loop attenuation and crosstalk noise. However, with advances in signal processing, echo and crosstalk cancellation, and modulation techniques developed during the 1980s, a significant portion of these limitations can be overcome. Hence, the loop plant has rapidly evolved from a simple voice-frequency system to a sophisticated access system for high-speed digital services. This brought about the development of the digital loop carrier and the digital subscriber line.

1.1 Digital Subscriber Lines

In this section, the makeup of a typical loop structure that connects the customer premises to a central (or switching) office (CO) is described. This is followed by a description of

the different types of digital subscriber line (DSL) services that are currently in use. Since in most of our simulation experiments HDSL and HDSL2 were used, these systems are described in more detail.

1.1.1 Cabling in a Typical Subscriber Loop

A typical subscriber loop consists of a pair of insulated copper wires having a gauge that ranges from 26 to 19 AWG (approximately 0.4 to 0.91mm). The insulating dielectric is usually polyethylene, but some paper-insulated pairs are also still in service. Fig. 1.1 shows a typical loop plant. At one end is a multipair feeder cable that starts from the CO and ends at a feeder distribution interface (FDI). The feeder cable has up to 50 binder groups, each of which may contain 12, 13, 25, 50 or 100 pairs. At the feeder distribution interface (FDI), the feeder cable is divided into several smaller distribution cables each consisting of up to 50 pairs. Each distribution cable is then separated into many individual drop-wire pairs for distribution to customer premises.

Within each cable, the two wires of each pair are twisted around each other to form an unshielded twisted pair (UTP). And to reduce the coupling that causes crosstalk, the adjacent pairs are made to have different rates of twist.

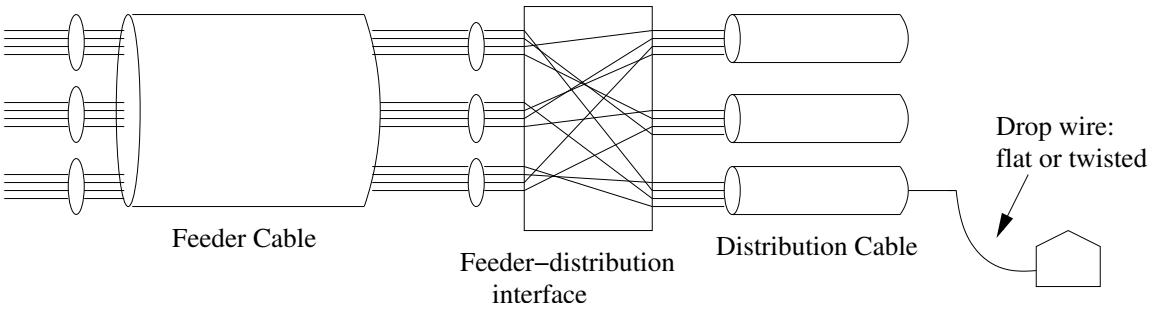

Figure 1.1. *Typical loop plant.*

1.1.2 Types of DSL Systems

The DSL family includes the integrated services digital network (ISDN), high bit-rate DSL (HDSL), HDSL2, single-pair symmetric DSL (SDSL), single-pair high-speed DSL (SHDSL), asymmetric DSL (ADSL), and very-high-data-rate DSL (VDSL). The International Telecommunications Union has already standarized ISDN, ADSL, and HDSL. The ITU-T Recommendations G.995.1 [1] provides a comprehensive overview of ADSL and HDSL recommendations. HDSL2, SHDSL, and VDSL are currently in the process of being standardized. SDSL is not standardized but has been deployed at various bit rates up to 2.32 Mbit/s. Some basic characteristics of the different DSL services are listed below:

• ISDN. Basic rate ISDN (BRI) was initially aimed at providing a uniform global network for telephony and data communication. Using an 80 kHz bandwidth, it offers a 160 kbit/s bidirectional data transmission consisting of two 64 kbit data channels and a 16 kbit/s control channel. It uses the simple 2B1Q, 4-level pulse amplitude modulation (PAM), and baseband transmission with echo cancellation. Three variants of ISDN, with different line codes, exist in different parts of the world as specified in the appendices of ITU Recommendation G.961 [2].

• HDSL. An HDSL transceiver operates at five times the data rate of BRI or standard DSL. The required signal processing power, however, could be 25 times greater because the discrete channel and echo path impulse responses contain five times as many samples due to a sampling rate that is five times higher. The stated transmission throughput improvement of HDSL over ISDN-DSL is also facilitated by a restricted physical reach in its carrier service area (CSA) operation range. Three HDSL systems are specified in the ITU-T recommendation G.961 [3]. The first system uses two or three pairs in parallel: each pair transports bidirectionally at a bit rate of 784 kbit/s. The second system uses only two pairs in parallel: each pair transports bidirectionally at a bit rate of 1168 kbit/s. The third system uses only one pair with an increased bit rate of 2320 kbit/s, bidirectionally. The line codes for all the systems are either 2B1Q or carrierless amplitude/phase (CAP) modulation [6]. The CAP modulation has a single carrier and is similar to quadrature amplitude

modulation (QAM). In North America, 2B1Q HDSL with a data rate of 784 kbit/s on each pair is universal.

• HDSL2. Although HDSL2 is classified as 'second generation' system, it is not a second-generation HDSL. Instead, it is more of a complement to the existing HDSL. HDSL2 offers the same 1.544 Mbps capacity that HDSL offers, but it does it on one pair of copper wires rather than two pairs. HDSL2 offers three signifiant improvements: (1) full T1 transmission rate of 1.544 Mbps over a single copper pair with a reach of 12,000 feet, (2) equal or better spectral compatibility than traditional HDSL, and (3) interoperability with other DSL systems. HDSL2 uses overlapped pulse amplitude modulation with interlocking spectra (OPTIS). OPTIS uses overlapped but nonidentical spectrum for upstream and downstream transmission. Essentially, it is a hybrid between a symmetrically echo-cancelled transmission and an FDM system that uses echo cancellation and asymmetric spectrums for upstream and downstream transmissions. In characterizing the worst-case noise conditions for North America, it has been noted that the noise environments at the central office and the customer remote terminals are significantly different. OPTIS takes advantage of this fact by carefully shaping the upstream and downstream transmit spectra for maximum performance in the worst-case noise condition that occurs at either end of the loop. Spectral shaping also minimizes OPTIS spectral crosstalk into other services. In the upstream direction, the transmit spectrum is severely limited beyond 250 KHz in order to minimize interference into the downstream ADSL spectrum. At the same time, the upstream power spectral density (PSD) is boosted in the range of 200 to 250 KHz, a region where the receiver at the customer remote terminal experiences a relatively good signal-to-noise ratio (SNR) in the presence of the mixed crosstalk noise that may exist on the loop. To counteract the effect of boost in the upstream spectrum, the OPTIS downstream PSD is notched in the region of 200 to 250 KHz. This notch corresponds to the boost in the upstream channel and is referred to as the interlock. By interlocking the upstream and downstream signals, OPTIS crosstalk into other services is minimized.

HDSL2 uses a combination of decision feedback equilization (DFE) and Tomlinson

precoding [4] to overcome the attenuation on the line. However, in high-noise conditions, a wrong decision by the DFE slicer can cause propagation of errors that will be fed to the Veterbi decoder [5]. While the Veterbi decoder works well with independent errors it does not function well with burst errors. To get around this error propagation problem, HDSL2 uses Tomlinson precoding. The DFE is used during the startup training of the transceiver to determine the line equalization characteristics. Before the loop is fully activated, each modem on either end of the line will share DFE equalization coefficients, which will be used to set the characteristics of the transmit precoder. Before the loop activates, the DFE block switches off and the precoder switches on for the duration of the connection. By using transmit precoding rather than DFE in the receiver, error propagation in the Veterbi decoder is minimized thereby improving the performance of the decoder block.

• SDSL is not standardized but has been deployed. It uses 2B1Q line code on one twisted pair and offers various symmetric data rates up to 2.32 Mbit/s. Its advantages over HDSL and HDSL2 are variable data rates, lower cost, and greater range.

• SHDSL uses 16-level PAM with trellis codes [7]. As in SDSL, the bit rate can be adjusted from 300 kbit/s to 2.32 Mbit/s depending upon the length of the loop. SHDSL has been developed primarily to address interoperability issues: the shape of its transmitted signal PSD has been designed taking into consideration the spectral characteristics of line coding and transmission techniques of other systems in the network. SHDSL is a modified version of HDSL2 that uses trellis coded PAM with 16 levels of encoding (rather than the 4 levels provided by 2B1Q) to provide better spectral efficiency than SDSL. By using trellis coding, Viterbi decoding and Tomlinson precoding techniques, the error rate and SNR are as good as those in SDSL, if not better. SHDSL also has a much sharper roll-off than SDSL. Thus, the potential for interference with an ADSL customer is greatly reduced while requiring less power. Overall, SHDSL causes less disturbance to ADSL equipped loops, and ensures better spectral compatibility with existing deployment.

• ADSL uses one twisted pair to offer asymmetric data transmission between the customer and CO. The upstream and downstream data rates are 640 kbit/s and 6 Mbit/s, re-

spectively, for a service radius of approximately 12000 ft, and 176 kbit/s and 1.544 Mbit/s for a radius of approximately 18000 ft. The modulation technique is discrete multitone transmission (DMT) [8, 10] with most systems also adopting frequency-division duplexing (FDD) between the upstream and downstream transmissions. Since ADSL uses the frequency spectrum that is above the voice band, it can therefore allow simultaneous usage of the voice band for telephone services.

- VDSL is an extension of ADSL technology with a shorter loop length than ADSL. Due to this shorter loop length, it can use a wider bandwidth and therefore offers a higher data rate than ADSL. The downstream bit rate ranges from 13 Mbit/s to 53 Mbit/s and the upstream bit rate from 1.6 Mbit/s to 26 Mbit/s. One standard of VDSL uses DMT modulation while another standard uses CAP modulation. FDD is also used between the upstream and downstream transmissions.

1.2 Noise Environment for xDSL Sytems

The twisted pair subscriber loops were originally designed for the transport of analog voice signals. As such, their termination impedances were designed so that the balance is best in the voice band. At the higher frequencies where the DSL systems operate there is a large imbalance between the termination impedance and loop. This imbalance causes the twisted pairs to pick up detrimental differential signals from other sources. Such undesirable signals include crosstalk, radio signal interference (RFI), and impulse noise.

1.2.1 Crosstalk

Crosstalk between twisted pairs in a multipair cable is the dominant impairment in most DSL systems. The causes of crosstalk are capacitve and inductive couplings between the twisted pairs (or, more precisely, imbalance between the twisted pair couplings). If one pair is considered the interferer, then the voltages and currents induced by the interferer onto the other pairs travel in both directions: those that continue in the same direction as the

interfering signal add up to form far-end crosstalk (FEXT); those that come back towards the source of the interferer add up to form near-end crosstalk (NEXT). This is conceptually illustrated in Fig. 1.2 where the thickness of the lines showing the crosstalk is a crude indication of the strength of the signal. If both NEXT and FEXT occur in an xDSL system, NEXT will in general be much more severe. NEXT increases with frequency and at VDSL frequencies (up to 15 MHz) it would be intolerable. Therefore, VDSL systems are designed to avoid NEXT altogether using FDD techniques.

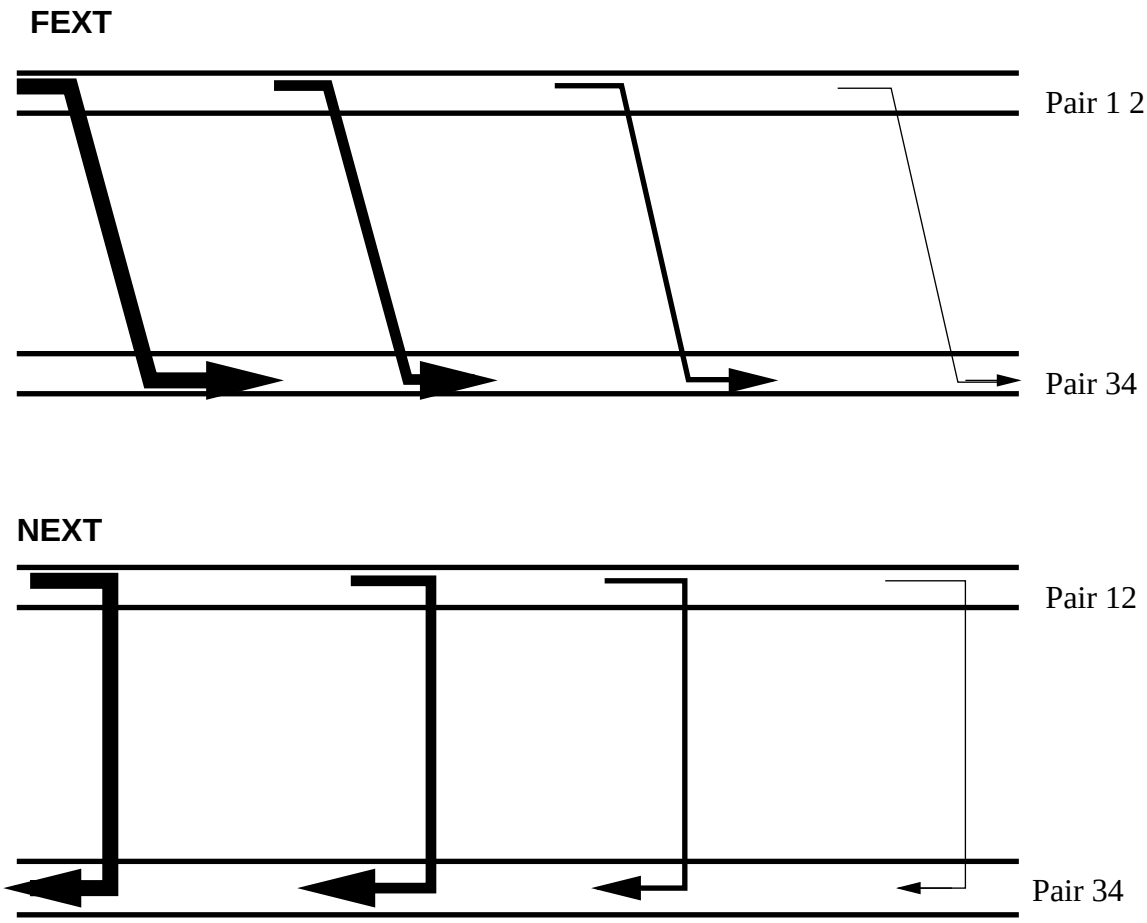

Figure 1.2. *Interpair coupling causing FEXT and NEXT.*

1.2.2 Radio Frequency Interference

In twisted pair telephone lines, the aerial segments such as the drop wires can act like antennae. Because of line imbalance, these lines pick up external radio frequency noise causing interference or ingress noise at the DSL receiver. The ingress noise level can sometimes be larger than the crosstalk level and therefore it cannot be ignored by designers. Conversely, this line imbalance can also cause the lines to emit DSL signals thereby causing interference to other RF receivers, like for example, AM and amateur radio where the operating frequency spectrum overlaps with that of the DSL system.

1.2.3 Impulse Noise

Impulse noise is short-term nonstationary interference from high-power electrical sources such as lightning strikes, power lines, switching transients of machinery, arc welders, and the like. To partially avert problems caused by impulse noise, DSL systems have a 6 dB design margin.

1.3 NEXT in xDSL Systems

In larger telecom cables, the twisted pairs are grouped in 25 pair units and each unit is wrapped with coloured tape to form a binder group. Many binder groups are combined together with a common physical and electrical shield to form a cable. Within the cable however, there is crosstalk between the twisted pairs due to capacitive and inductive couplings. In the voice band crosstalk is minimal — one can hardly hear the voice energy from an adjacent pair because the crosstalk loss is usually more than 80 dB while the voice channel loss is less than 20 dB. However, at the higher frequencies that DSL systems operate, it becomes intolerable [17] [18].

In general, the effect of cable crosstalk is minimized not only by the use of good insulation materials between the twisted pairs but also by adopting different rates of twist

among adjacent twisted pairs in a binder group. Even the binder groups are twisted so that no two groups are adjacent for long runs. However, since differential twisting of twisted pairs is intended for reducing crosstalk in the voice band, it is inadequate at DSL operating frequencies where the interpair couplings are still significant. Consequently, in DSL technology where the signal bandwidth reaches into the MHz range, crosstalk noise is still the major limiting factor to the achievable throughput.

1.3.1 Characteristics of NEXT

NEXT is strongest at the point where the transmitter transfers the signal to the cable. Therefore, any receiver adjacent to the transmitter will receive the NEXT signal in addition to the intended signal. The NEXT signal can significantly lower the signal-to-interference ratio (SIR) of the received signal. And if the intended signal does not dominate the interferers, then NEXT becomes a problem. NEXT interference is common in symmetric systems like ISDN DSL, HDSL, and HDSL2 where similar transmitters are installed on both ends of the twisted pair.

The NEXT that is produced within a binder group full of collocated transceivers is called worst-case NEXT. And if the NEXT is between similar systems, like for example, DSL to DSL, HDSL to HDSL, or T1 to T1, then it is called ‘self NEXT’.

Due to cable design and manufacturing variations, the amount of NEXT between twisted pairs can differ with cable type. However, at the same time, the amount of NEXT also depends upon the NEXT couplings between the twisted pairs which, in turn, depends upon the frequency and the relative location of the pairs within the binder group. At a given frequency, the NEXT loss is defined as the power sum of the crosstalk from all the other twisted pairs in a cable binder group. In most crosstalk simulation models, the 1% worst-case NEXT loss is used. This means that on the average, at a given frequency, 1% of the twisted pairs will have a NEXT loss which is worse (less) than the NEXT model.

When simulating DSL systems, the commonly adopted PSD model for NEXT is one

due to Werner et al. [11], and it is given by

$$|H_{NEXT}(f,n)|^2 = S(f)X_N f^{\frac{3}{2}} n^{0.6} \tag{1.1}$$

where $|H_{NEXT}(f,n)|^2$ is the 1% worst-case crosstalk power, f is the frequency, n is the number of disturbing systems, X_N is a scalar constant, and $S(f)$ is the PSD of the interfering system. In this model, it is assumed that all of the pairs involved are of the same binder group, all have the same length, and all have interferers that are of the same type. In a mixed environment where the bundle has i different types of interferers, the crosstalk power is given by

$$|H_{NEXT}(f,n)|^2 = \left[\sum_{i=1}^{N} (S_i(f)X_N f^{\frac{3}{2}} n_i^{0.6})^{\frac{1}{0.6}}\right]^{0.6} \tag{1.2}$$

where N is the number of interferers in the cable. This estimate is somewhat pessimistic since it implicitly assumes that each of the different services is using the worst pair in a binder, which is physically impossible. A newer and more accurate technique for estimating the crosstalk from mixed sources is described in [25].

1.4 Previous Methods to Mitigate NEXT

Several techniques to mitigate or cancel the NEXT in xDSL systems have appeared in the literature such as spectral shaping [19] [20] and frequency-division duplexing (FDD). Since spectral shaping relies more on the average spectral characteristics of the NEXT in a transmission line, it does not always yield optimal results. Nevertheless, spectral shaping techniques have improved the interoperability of different DSL systems by reducing the amount of NEXT between the lines. FDD has been used in asymmetric DSL (FDD-ADSL) and very-high rate DSL (FDD-VDSL) systems [21]. However, in a mixed environment with different DSL and non-DSL systems where the transmitting and receiving spectrums overlap, FDD systems are subjected to NEXT from other DSL systems which would require cancellation [23]. In other techniques, the NEXT sources in a line are first identified and

NEXT cancellation methods or spectrum management techniques are then used to supress the NEXT [24]. In a paper by Zeng et al. [23], a network maintenance center that identifies the crosstalk coupling functions among the twisted pairs in the DSL systems is discussed. These crosstalk functions can be used to improve the data rate and to facilitate provisioning, maintenance, and diagnosis of xDSL systems.

Yet another effective technique that can mitigate NEXT is to deploy adaptive filters to cancel the NEXT signals from the other lines [26]. Although this technique can result in a significant reduction in NEXT, it tends to be computationally very expensive especially when the number of twisted pairs in the bundle is large. For a bundle with N twisted pairs, $N(N-1)$ adaptive filters would be needed to cancel the $N-1$ possible NEXT signals from the other lines. At the same time, accessibility to the transmitted signals from the other twisted pairs would be required. In a central office (CO), this is not a problem. Thus, if the computational complexity can be reduced, the use of adaptive filters can lead to a workable solution in a CO where the number of twisted pairs in a bundle is generally large and the NEXT among twisted pairs is high.

1.5 Scope and Contributions of Thesis

The thesis is composed of seven chapters. Chapter 2 describes the construction of simulation models of twisted-pair and NEXT channels. These models are required in order to test the performance of the newly developed algorithms in various twisted-pair channels and NEXT-noise conditions. The construction of the models is based on two-port network theory using the ABCD-parameter representation. Chapters 3-6 constitute the main part of the thesis where four new NEXT-mitigation algorithms are proposed. Chapter 7 provides concluding remarks and suggestions for further study.

In Chapter 3, a new NEXT cancellation algorithm for DSL systems is proposed based on using adaptive filters to cancel the NEXT signals. The algorithm attempts to reduce the computational complexity involved in NEXT cancellation; it uses the fact that in a bundle

of twisted-pair lines, the NEXT that occurs on a particular line is caused by the adjacent twisted-pair lines, which constitute a small percentage of the total number of twisted-pair lines in the bundle. Hence, rather than deploying adaptive filters to cancel every possible NEXT signal on all the lines, a significant amount of computation can be saved if adaptive filters are deployed to cancel only the NEXT signals that are actually present on the lines. To achieve this, the algorithm first identifies the lines that cause NEXT and then deploys adaptive filters to cancel the significant NEXT signals detected. Since the NEXT detection process is done for every twisted-pair line in the bundle, it is important that the detection process be computationally efficient. This problem is solved by using the sign algorithm [29], which efficiently estimates the cross correlation of the transmitted and received signals; this estimate is then used to compute the magnitude of each NEXT signal present on the receiving line. By detecting the NEXT signals present on a line first and then deploying adaptive filters to cancel the significant NEXT signals, an overall computational complexity of the algorithm of order N is achieved, where N is the number of twisted-pairs in the bundle. This represents a large reduction in the computational effort relative to that in previous NEXT cancellation systems [15][26] which offer computational complexities of order N^2. This algorithm is ideally suited for NEXT cancellation in a central office where the number of twisted-pair lines in a bundles is in the hundreds, and access to the transmitted signals in the adjacent twisted-pair lines is available.

Chapter 4 is devoted to a new method of NEXT cancellation in high data-rate DSL systems. Since the sampling rate in these systems is high, the adaptive-filter length required to span the impulse response of a NEXT channel is relatively long. For DSL systems with sampling rates that exceed 1 MHz, the filter length required usually exceeds 40. It has been shown in [33][34] that when the adaptive-filter length exceeds 40, it becomes computationally more efficient to use frequency-domain instead of time-domain adaptive filters. Chapter 4 explores the use of frequency-domain least-mean-square (FDLMS) adaptive filters to cancel the significant NEXT signals that are detected. Further, an analysis of the convergence rate and tracking performance of multiple FDLMS adaptive filters is

carried out. By assuming that frequency bins in an adaptive filter are statistically independent from one another [1], the analysis is simplified to that of multiple adaptive filters with single-frequency bins. From the analysis of the convergence rate of the NEXT cancellation system, it is found that when the step size of the adaptive filter is made proportional to the magnitude of the NEXT signal that is to be cancelled, the initial convergence rate improves significantly relative to that in the case where the step sizes are all equal. In the later phases of adaptation, however, the convergence rate is improved if the step sizes of the adaptive filters are all equal. Consequently, based on these observations, an effective technique to improve the overall convergence rate of the system is to adjust the adaptive-filter step size in proportion to the magnitude of the NEXT signal during the initial phases of adaptation. Later on in the adaptation, when the error signal of the adaptive filters is reduced by more than 3 dB, the step sizes are made all equal. Further, from an analysis of the tracking performance of the NEXT cancellation system, it is observed that setting the adaptive-filter step sizes proportional to the magnitude of the NEXT signals after the adaptive filters have converged, significantly improves the tracking performance of the NEXT cancellation system. Computer simulations show that this method of adjusting the adaptive-filter step sizes significantly improves the convergence rate and the tracking performance relative to those of FDLMS adaptive filters with fixed step sizes.

For a particular twisted-pair line, the NEXT can originate from several adjacent twisted-pair lines in the bundle. For each NEXT signal, the magnitude is dependent on the amount of capacitive and inductive couplings between the twisted-pair line causing the NEXT and the line in consideration. Since the degree of coupling between any two twisted-pair lines is random, the magnitudes of the NEXT signals on a twisted-pair line are, as a result, correspondingly random. Hence, using fixed-length adaptive filters to cancel the NEXT signals is not efficient since each filter length will have to be long enough to effectively cancel the largest possible NEXT signal. However, if the filter length of each adaptive filter is varied in accordance with the magnitude of the NEXT signal that is to be cancelled, significant savings in computation can be achieved. On the basis of these principles, a NEXT cancel-

lation method is developed in Chapter 5 that uses adaptive filters where the filter lengths are varied in accordance with the magnitudes of the NEXT signals. The estimation of the adaptive-filter length is based upon the statistical distribution of energy across the length of the impulse response of the NEXT channels. Using this distribution, an optimization technique to estimate the optimum filter length is obtained, given the magnitude of the NEXT signal to be cancelled and the maximum noise tolerable by the system. In the real world scenario, however, the actual filter length required can sometimes be different from the statistically optimum filter length. Hence, to make adjustments for this difference, another algorithm that further refines the length of the adaptive filter is used. The proposed method in combination with the method described in Chapter 3 can significantly reduce the computational complexity of the NEXT cancellation system; moreover, as the number of twisted pairs in a bundle increases the advantage of using this method over existing methods [15][26] increases even more. The method described in this chapter can also be used to reduce the complexity in active noise cancellation systems where multiple adaptive filters are required to supress multiple noise components.

Chapter 6 is devoted to a new method of mitigating NEXT in which the NEXT removal is done in the wavelet-transform domain. Typically in twisted-pair lines, the spectrum of the received signal has greater energy in the low-frequency end of the spectrum whereas that of the NEXT signal has greater energy in the high-frequency end. The new method uses this difference in spectra between the NEXT and received signals to remove the NEXT from the received signal. The advantages of using the wavelet transform to remove the NEXT are threefold: First, depending upon the characteristics of the NEXT and the received signals for a particular cable type, appropriate wavelets can be designed to provide maximal removal of the NEXT from the received signal. Second, since NEXT noise is almost Gaussian [50], the threshold values for removing the NEXT noise across the various wavelet levels can be accurate estimated [55][56][57]. And third, the wavelet noise removal is performed blockwise and is, therefore, extremely efficient and well suited for NEXT removal in high data-rate DSL systems. Unlike NEXT cancellation with adaptive

filters, the new method does not require any reference signals in order to remove the NEXT signals. Hence, it can even be adopted to remove FEXT, where the corresponding reference signals are usually not available. Furthermore, from the simulation results it is found that the amount of NEXT reduction achieved is dependent upon the type of wavelet used: the Battle-Lemarie wavelet, for example, offers an improvement of around 2 dB over the Daubechies wavelet of order 10. Also, simulation comparisons of two wavelet thresholding estimates, the universal estimate and the Stein's unbias risk estimate (SURE), reveal that in low SNR conditions the universal estimate performs better, while in high SNR conditions it is the SURE estimate.

Chapter 2

Simulation Models

2.1 Introduction

Setting up a laboratory containing an actual testbed of transmission lines for a DSL system can be quite expensive. Besides, a physical testbed will probably not be flexible enough to provide the different kinds of environments that are present in the real world. A more cost-effective and versatile method is to employ accurate simulation models of the transmission lines and DSL systems. Simulation models also provide the flexibility to vary the model parameters so that different noise and channel environments can be simulated for testing the algorithms. It is important, however, for the simulation model to represent the actual system accurately. An accurate simulation model will require little or no modification of the algorithm when it is later deployed in the field.

To model a channel, extensive loop surveys are made to acquire the channel parameters of typical loop configurations. By using accurate measuring equipment, the primary parameters of the loops are obtained. These parameters are then used to simulate and derive the channel impulse responses of various loop configurations.

The simulations were done using MATLAB. The platform was a Sun Blade 2000 workstation running the Sun Solaris operating system.

2.2 Channel Modelling

One way to model a twisted-pair channel is to define the channel in terms of the primary and secondary parameters of a distributed circuit model of a line [12]. A unit of such

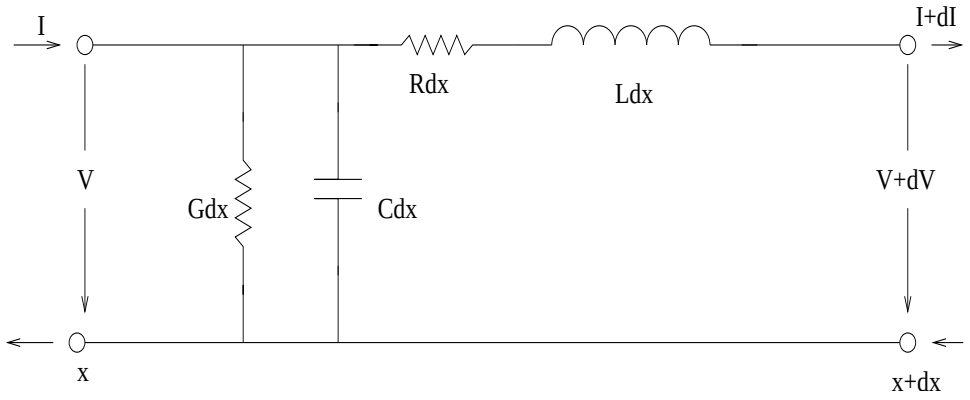

Figure 2.1. *A two-port network model of a transmission line unit.*

a model called the $RLGC$ model is shown in Fig. 2.1. The equivalent circuit for an ideal transmission line is a cascade of many such units, each with identical, frequency-dependent primary parameters. Using the primary parameters, the secondary parameters such as the impedance, attenuation, phase, and $ABCD$ chain parameters can be derived.

The primary parameters for the twisted pair line are obtained directly or indirectly using wide-bandwidth, high-precision test equipment. The ones used in the $RLGC$ models of the common AWG primary inter-exchange carrier (PIC) cables were based on careful measurements and curve fitting done in the early 1970s. They are believed to be valid up to 10 MHz and represent the typical values for such cables.

The primary parameters can be represented either as parameters to equations that have been curve fitted to measured data or as R, L, C, and G values versus frequency [13, 14]. Table 2.1 gives the values of the primary $RLGC$ parameters for a 26-AWG PIC cable at different frequencies. Using the primary parameters, the characteristic impedance $Z_o(s)$, the propagation constant $\gamma(s)$, and the transfer function $H(d, s)$ of the cable can be

Table 2.1. *Cable parameters for 26-AWG filled PIC*

MHz	R (ohm/Km)	G (μS/Km)	L (mH/Km)	C (nF/Km)
0.304	397.8	48.3	0.685	46.44
0.327	398.7	52	0.682	46.77
0.357	399.5	56	0.68	47.09
0.388	400.3	60.2	0.677	47.38
0.418	401.6	64.9	0.676	47.64
0.456	403.9	69.7	0.674	47.9
0.496	407.3	75.1	0.672	48.15
0.534	413.9	80.8	0.671	48.37
0.582	423.1	86.9	0.67	48.59
0.633	437.7	93.6	0.668	48.78
0.682	454.6	101	0.667	48.95
0.743	478.8	108	0.665	49.07
0.809	506.4	117	0.663	49.14
0.871	533.3	125	0.661	49.18
0.949	565.9	135	0.658	49.15
1.033	595.1	145	0.654	49.08
1.112	616.4	156	0.652	49.05
1.212	635.4	168	0.649	48.98
1.319	649.9	181	0.646	48.95
1.421	665	195	0.644	48.97
1.548	688.1	209	0.643	48.99
1.684	721.9	226	0.641	49
1.814	758	243	0.639	48.99
1.977	796	261	0.637	48.93
2.151	821.3	281	0.634	48.86
2.317	840	302	0.633	48.86
2.525	871.4	326	0.632	48.85
2.748	913.4	351	0.63	48.82
2.959	948.7	377	0.628	48.81
3.225	979.9	406	0.627	48.77
3.509	1018	436	0.625	48.75

MHz	R (ohm/Km)	G (μS/Km)	L (mH/Km)	C (nF/Km)
3.78	1057	471	0.624	48.75
4.119	1100	506	0.623	48.72
4.482	1153	545	0.621	48.69
4.827	1196	586	0.62	48.68
5.26	1243	630	0.619	48.66
5.724	1300	679	0.618	48.63
6.165	1347	730	0.617	48.62
6.718	1403	786	0.616	48.6
7.31	1467	846	0.614	48.57
7.874	1519	909	0.614	48.57
8.58	1581	980	0.613	48.54
9.337	1650	1054	0.612	48.52
10.06	1712	1134	0.611	48.52
10.96	1785	1222	0.61	48.5
11.92	1872	1312	0.609	48.48
12.84	1943	1415	0.608	48.48
14	2024	1522	0.608	48.46
15.23	2129	1637	0.607	48.43
16.4	2206	1763	0.606	48.44
17.87	2307	1894	0.605	48.42
19.45	2431	2042	0.605	48.4
20.95	2513	2196	0.604	48.4
22.83	2636	2363	0.603	48.38
24.84	2759	2545	0.603	48.36
26.76	2886	2734	0.603	48.37
29.16	2996	2947	0.602	48.35
31.73	3149	3170	0.601	48.33
34.17	3301	3411	0.601	48.35
37.24	3470	3673	0.6	48.33
40	3671	3946	0.6	48.34

evaluated by using the equations

$$Z_o(s) = \sqrt{\frac{R(f) + sL(f)}{G(f) + sC(f)}} \tag{2.1}$$

$$\gamma(s) = \sqrt{[G(f) + sC(f)][R(f) + sL(f)]} \tag{2.2}$$

$$H(d, s) = e^{-d\gamma(s)} \tag{2.3}$$

where d is the length of the cable which is assumed to be perfectly terminated, and $s = j2\pi f$.

2.3 $ABCD$ Two-Port Parameters

A subscriber loop is made up of sections of different wire gauges and terminated with a resistive impedance. Older loop plants may even have bridged taps. However, due to impedance mismatch, the transfer function of the telephone subscriber loop is not a simple product of the transfer functions of the twisted-pair cable sections. To accurately estimate the subscriber loop channel, the two-port $ABCD$ parameters are used.

For a standalone two-port network, the input/output voltage and current relationships are given by

$$V_1 = AV_2 + BI_2 \tag{2.4}$$

$$I_1 = CV_2 + DI_2 \tag{2.5}$$

or in matrix form by

$$\begin{bmatrix} V_1 \\ I_1 \end{bmatrix} = \begin{bmatrix} A & B \\ C & D \end{bmatrix} \begin{bmatrix} V_2 \\ I_2 \end{bmatrix} \tag{2.6}$$

where the $ABCD$ parameters are defined as

$$A = \frac{V_1}{V_2}\Big|_{I_2=0} \tag{2.7}$$

$$B = \frac{V_1}{I_2}\Big|_{V_2=0} \tag{2.8}$$

$$C = \frac{I_1}{V_2}\Big|_{I_2=0} \tag{2.9}$$

$$D = \frac{I_1}{I_2}\Big|_{V_2=0} \tag{2.10}$$

The $ABCD$ parameters for a cable are complex and frequency dependent, and are related to the characteristic impedance $Z_o(s)$, and the propagation constant $\gamma(s)$ by

$$A(s) = \cosh[\gamma(s)d] \tag{2.11}$$

$$B(s) = Z_o(s)\sinh[\gamma(s)d] \tag{2.12}$$

$$C(s) = \frac{1}{Z_o(s)}\sinh[\gamma(s)d] \tag{2.13}$$

$$D(s) = \cosh[\gamma(s)d] \tag{2.14}$$

where d is the length of the cable.

Each cable section can be described by its own $ABCD$ parameters. Since a twisted-pair telephone loop is generally made up of many cables in series, the $ABCD$ parameters for the entire subscriber loop are a simple matrix product of the $ABCD$ matrices of all the cable sections.

The input impedance and cable transfer function can also be expressed in terms of $ABCD$ parameters. For a twisted pair loop with terminal impedance $Z_t(s)$, the input

impedance $Z_i(s)$ is given by

$$Z_i(s) = \frac{A(s) + \dfrac{B(s)}{Z_t(s)}}{C(s) + \dfrac{D(s)}{Z_t(s)}} \tag{2.15}$$

and the transfer function $H(s)$ of a twisted pair loop with a source impedance $Z_s(s)$ assumes the form

$$H(s) = \frac{Z_t(s)}{Z_s(s)(C(s)Z_t(s) + D(s)) + A(s)Z_t(s) + B(s)} \tag{2.16}$$

The magnitude of the input impedance and the amplitude response of CSA test loop #6 of length 9000 ft and gauge 26 AWG are shown in Figs. 2.2 and 2.3, respectively.

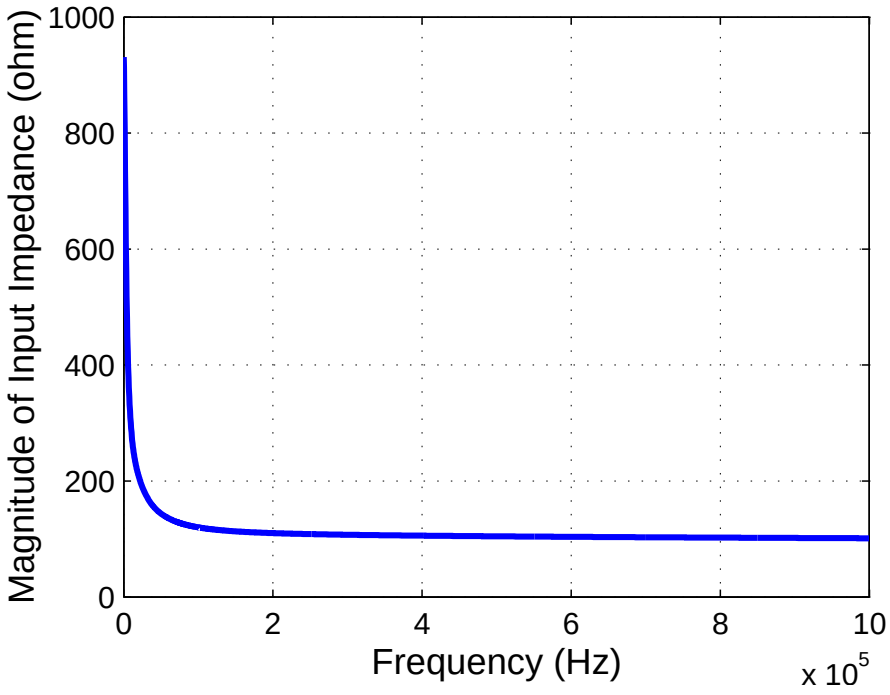

Figure 2.2. *Magnitude of the input impedance versus frequency of CSA loop 6.*

For a bridged tap, the two-port network can be considered to have only a shunt impedance. Therefore, the $ABCD$ parameters of a bridged tap can be computed using an

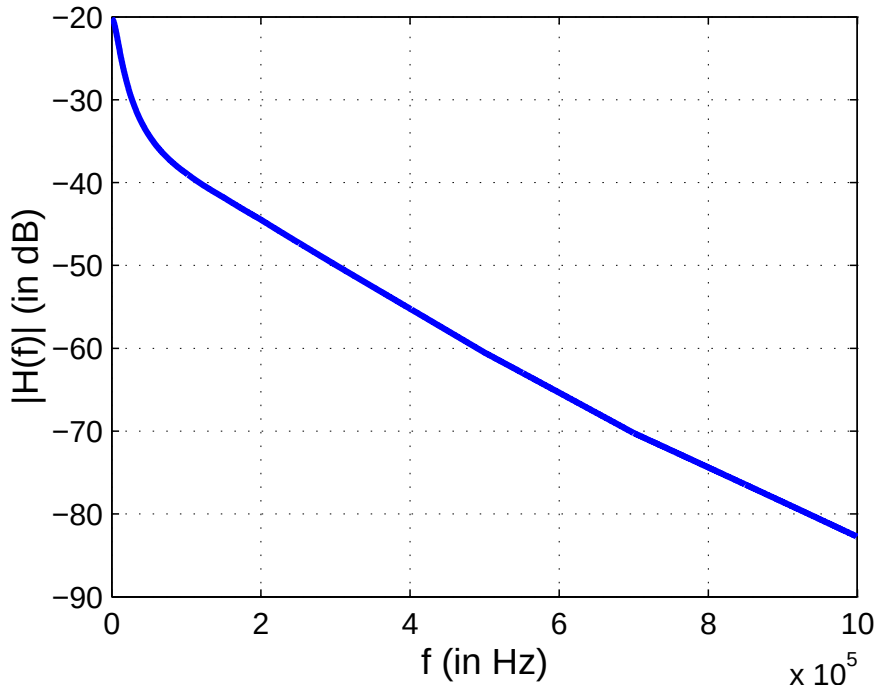

Figure 2.3. *The amplitude response of CSA loop 6.*

open-ended transmission line formula

$$\begin{bmatrix} A & B \\ C & D \end{bmatrix} = \begin{bmatrix} 1 & 0 \\ z^{-1} & 1 \end{bmatrix} \begin{bmatrix} 1 & 0 \\ \frac{C_{br}(s)}{A_{br}(s)} & 1 \end{bmatrix} \tag{2.17}$$

where $A_{br}(s)$ and $C_{br}(s)$ are the frequency-dependent $ABCD$ parameters of the section of the cable that is connected as a bridged tap.

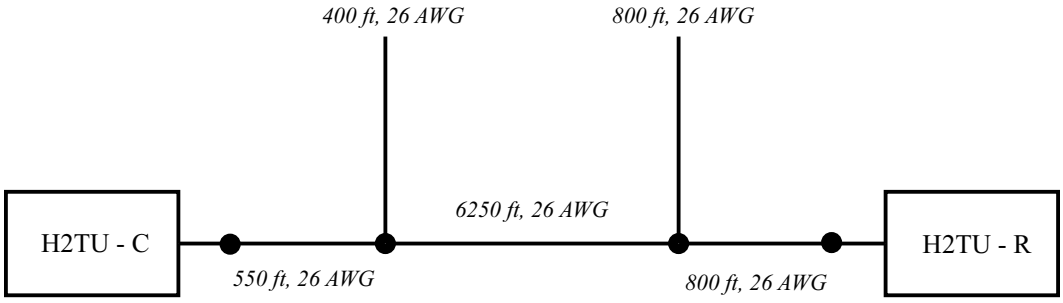

Figure 2.4. *CSA loop 4 with two bridged taps.*

The configuration of a subscriber loop with two bridged taps is shown in Fig. 2.4. The corresponding input impedance and amplitude response are shown in Figs. 2.5 and 2.6, respectively. Comparing Figs. 2.5 and 2.6 with Figs.2.2 and 2.3, respectively, we note that the presence of bridged taps in CSA loop 4 has caused more variability, with frequency, in the input impedance and amplitude response.

2.4 NEXT Model

In order to estimate the impulse response of the NEXT channel, we use the method described by Chen [15] where it is assumed that the NEXT is caused by an imbalance in coupling capacitances between the twisted pairs. In this method, the capacitive coupling between two twisted-pair loops is broken down into smaller units of length Δl. As can be seen in Fig. 2.7, the capacitive couplings in each of these units are represented by four coupling capacitances. By combining the couplings of each unit, an overall capacitive coupling

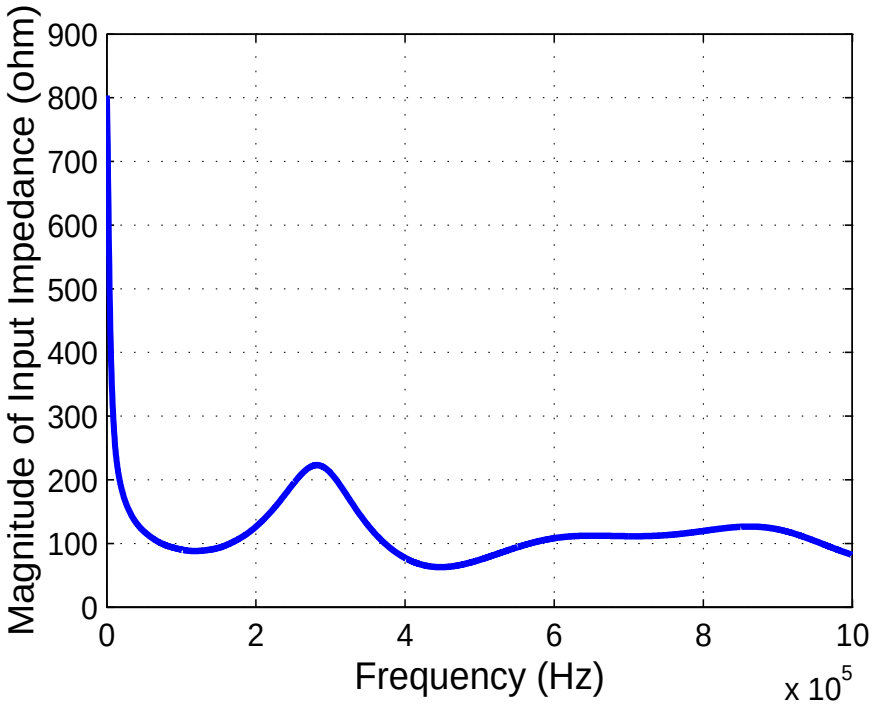

Figure 2.5. *Magnitude of the input impedance versus frequency of CSA loop 4.*

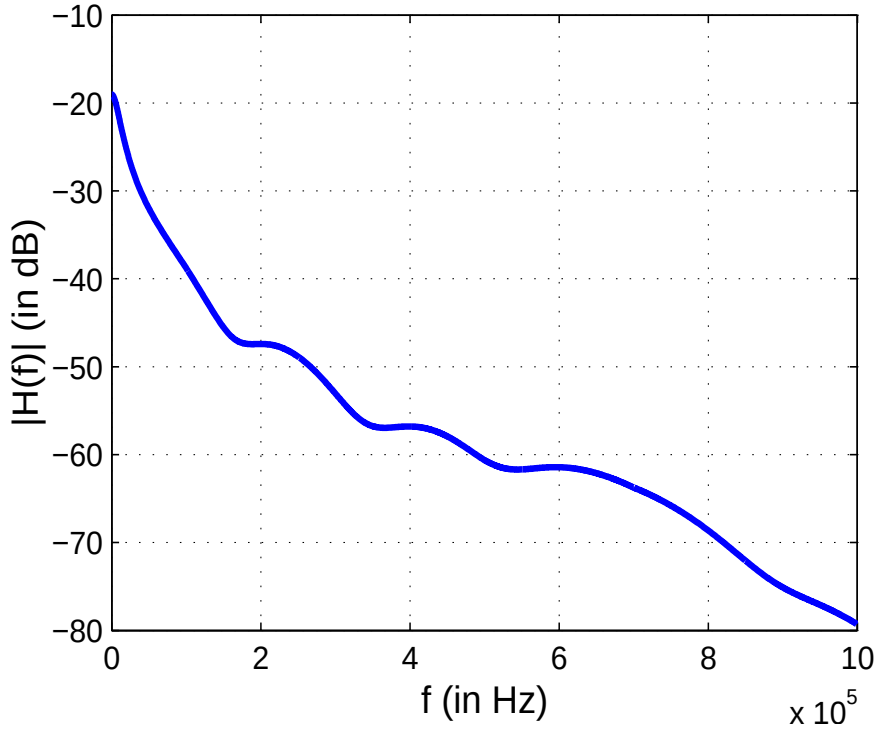

Figure 2.6. *The amplitude response of CSA loop 4.*

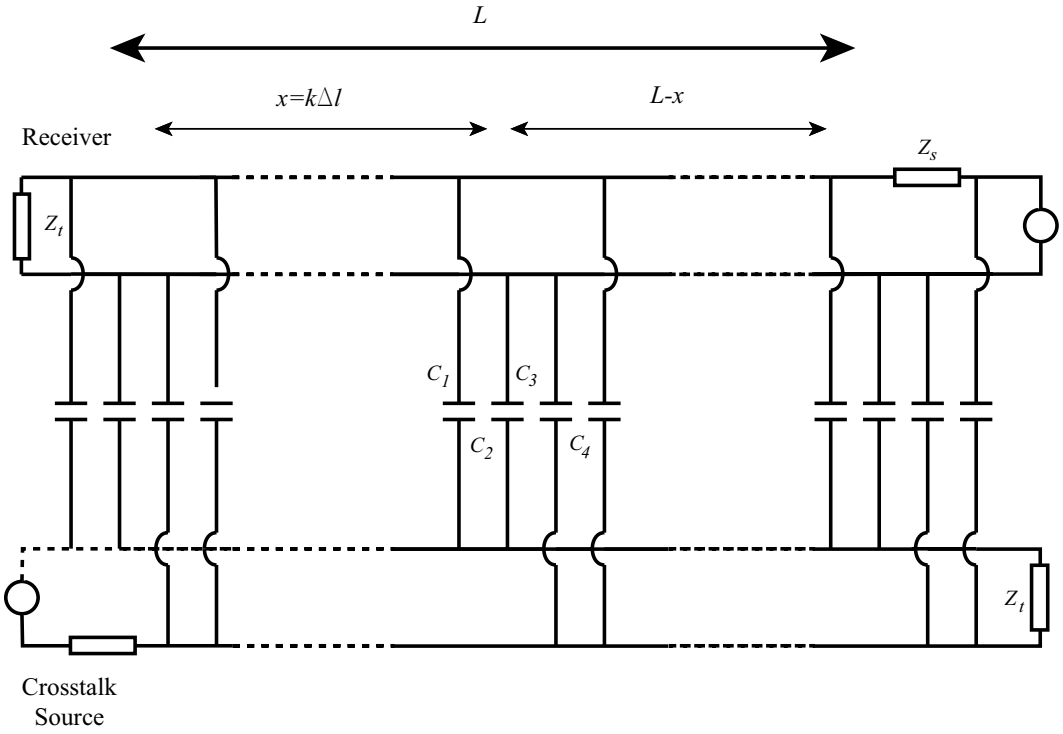

Figure 2.7. *Capacitive model of crosstalk coupling.*

between the two twisted-pair loops is obtained. A corresponding two-port network model of the individual coupling mechanism is shown in Fig. 2.8. In order to model the NEXT,

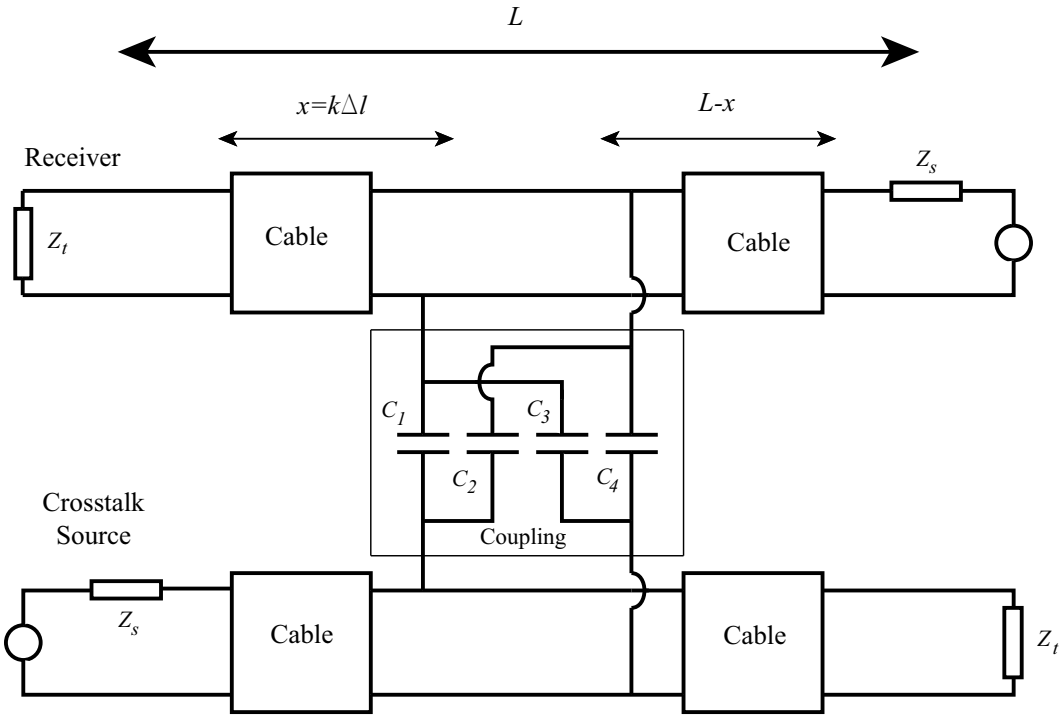

Figure 2.8. *A two-port network equivalent circuit for crosstalk coupling.*

the loop sections beyond the coupling point can be simplified by using a parallel impedance similar to a bridged tap. The complete model of the NEXT between two twisted pairs is shown in Fig. 2.9. As can be seen, it is a combination of two-port networks representing the cable sections, the capacitive coupling between the twisted pairs, and the parallel twisted pair loop impedances. The $ABCD$ parameters for the crosstalk-originating cable section are given by

$$\begin{bmatrix} A_o & B_o \\ C_o & D_o \end{bmatrix} = \begin{bmatrix} A_N & B_N \\ C_N & D_N \end{bmatrix} \begin{bmatrix} 1 & 0 \\ \dfrac{C_F Z_t + D_F}{A_F Z_t + B_F} & 1 \end{bmatrix} = \begin{bmatrix} A_N + B_N \dfrac{C_F Z_t + D_F}{A_F Z_t + B_F} & B_N \\ C_N + D_N \dfrac{C_F Z_t + D_F}{A_F Z_t + B_F} & D_N \end{bmatrix} \tag{2.18}$$

where subscript N denotes the near-end section and the subscript F denotes the far-end section of the cable with reference to the location of the crosstalk source and the receiver.

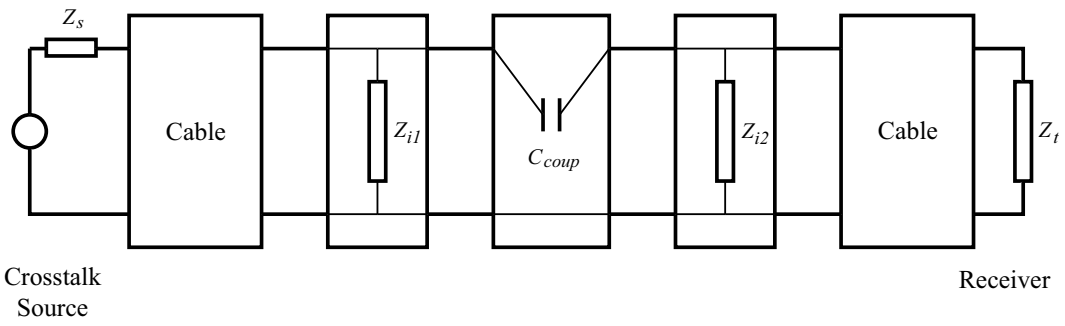

Figure 2.9. *A simplified two-port circuit for crosstalk.*

The $ABCD$ parameters for the crosstalk-receiving cable section are given by

$$\begin{aligned}\begin{bmatrix} A_R & B_R \\ C_R & D_R \end{bmatrix} &= \begin{bmatrix} 1 & 0 \\ \dfrac{C_F Z_t + D_F}{A_F Z_t + B_F} & 1 \end{bmatrix} \begin{bmatrix} A_N & B_N \\ C_N & D_N \end{bmatrix} \\ &= \begin{bmatrix} A_N & B_N \\ A_N \dfrac{C_F Z_t + D_F}{A_F Z_t + B_F} + C_N & B_N \dfrac{C_F Z_t + D_F}{A_F Z_t + B_F} + D_N \end{bmatrix} \end{aligned} \tag{2.19}$$

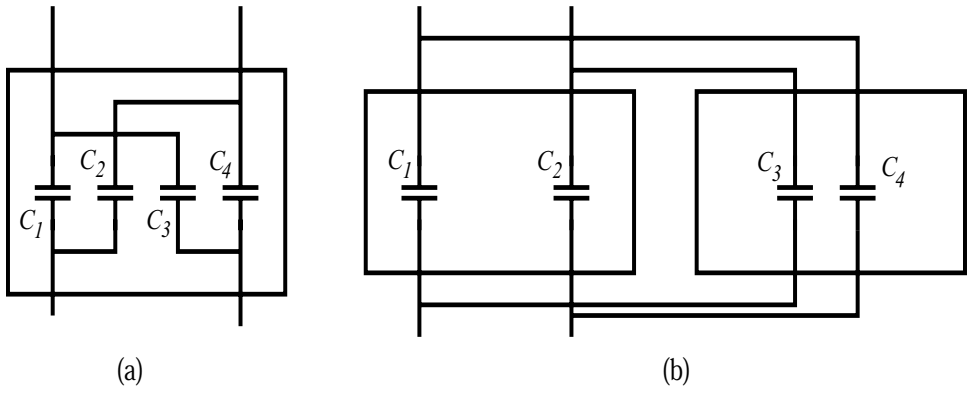

Figure 2.10. *Equivalence of the two-port coupling network.*

To obtain the $ABCD$ parameters of the capacitive couplings between the twisted pair

sections, the four coupling capacitors are split into two parallel two-port networks as depicted in Fig. 2.10. For network (a) in Fig. 2.10, the $ABCD$ parameters are given by

$$\begin{bmatrix} A_A & B_A \\ C_A & D_A \end{bmatrix} = \begin{bmatrix} 1 & \frac{1}{j\omega(C_1+C_2)} \\ 0 & 1 \end{bmatrix} \tag{2.20}$$

and for network (b) they are given by

$$\begin{bmatrix} A_B & B_B \\ C_B & D_B \end{bmatrix} = \begin{bmatrix} 1 & \frac{1}{j\omega(C_3+C_4)} \\ 0 & 1 \end{bmatrix} \tag{2.21}$$

The capacitive coupling is therefore the parallel combination of networks (a) and (b), whose $ABCD$ parameters are given by

$$\begin{bmatrix} A_C & B_C \\ C_C & D_C \end{bmatrix} = \begin{bmatrix} 1 & \frac{1}{j\omega(C_1+C_2-C_3-C_4)} \\ 0 & 1 \end{bmatrix} = \begin{bmatrix} 1 & \frac{1}{j\omega C_{coup}} \\ 0 & 1 \end{bmatrix} \tag{2.22}$$

where C_{coup} is the coupling capacitance, which may be negative. To evaluate the NEXT transfer function, the twisted pair is divided into n sections, each of length Δl. For the k-th section, the NEXT $ABCD$ parameters are evaluated by cascading the crosstalk-originating cable section, the capacitive coupling section, and the crosstalk-receiving cable section to give

$$\begin{bmatrix} A_k & B_k \\ C_k & D_k \end{bmatrix} = \begin{bmatrix} A_o & B_o \\ C_o & D_o \end{bmatrix}\Bigg|_{x=k\Delta l} \begin{bmatrix} A_C & B_C \\ C_C & D_C \end{bmatrix} \begin{bmatrix} A_R & B_R \\ C_R & D_R \end{bmatrix}\Bigg|_{x=k\Delta l} \tag{2.23}$$

where $x = k\Delta l$ represents the location on the loop. Thus the frequency response of the k-th section, in terms of the $ABCD$ parameters, is given by

$$H_k(\omega_i) = \frac{Z_t}{Z_s(C_k(\omega_i)Z_t + D_k(\omega_i)) + A_k(\omega_i)Z_t + B_k(\omega_i)} \tag{2.24}$$

By multiplying the frequency responses of the various sections, we get the overall frequency response of the NEXT channel as

$$H_{cross}(\omega_i) = \sum_{k=1}^{n} H_k(\omega_i) \tag{2.25}$$

The amplitude response of the simulated NEXT channel is obtained by taking the absolute value of $H_{cross}(\omega_i)$, and the impulse response is obtained by taking the inverse Fourier transform of $H_{cross}(\omega_i)$. The NEXT was simulated by using two twisted-pair loops of gauge 26 AWG and length 8 kft with a source and terminal impedance of 135 ohms, and an HDSL transformer. The two twisted-pair loops have uniformly distributed random coupling capacitances ranging from -10 to 10 pF with $\Delta l = 9$ feet. The simulated NEXT amplitude response is shown in Fig. 2.11 and the impulse response of the simulated NEXT channel after passing through a fourth-order Butterworth lowpass anti-aliasing filter with a -3dB cutoff frequency of 200 KHz is shown in Fig. 2.12.

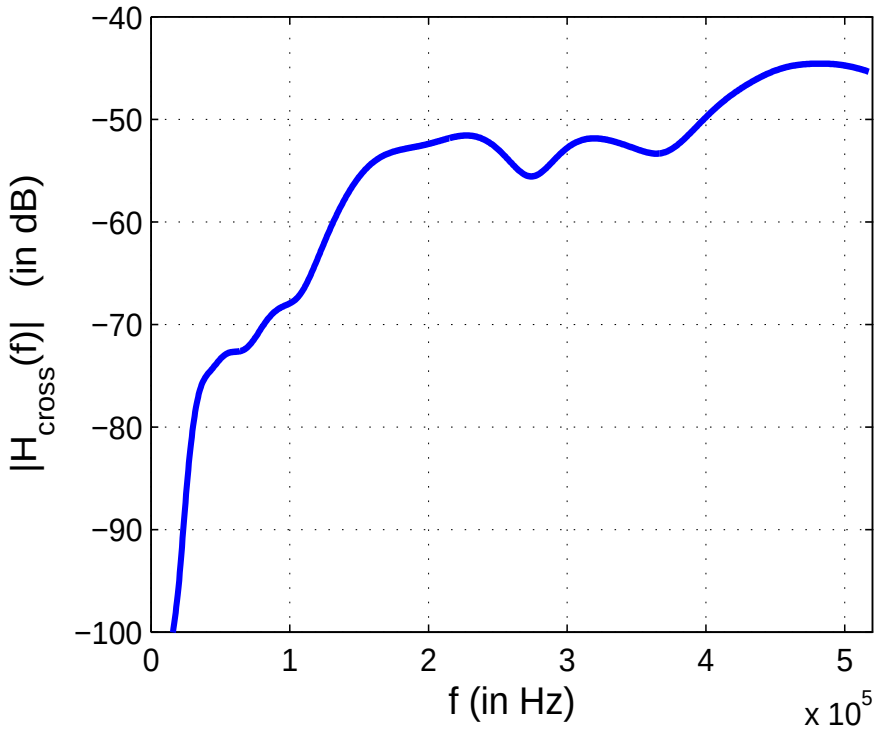

Figure 2.11. *Estimated NEXT amplitude response.*

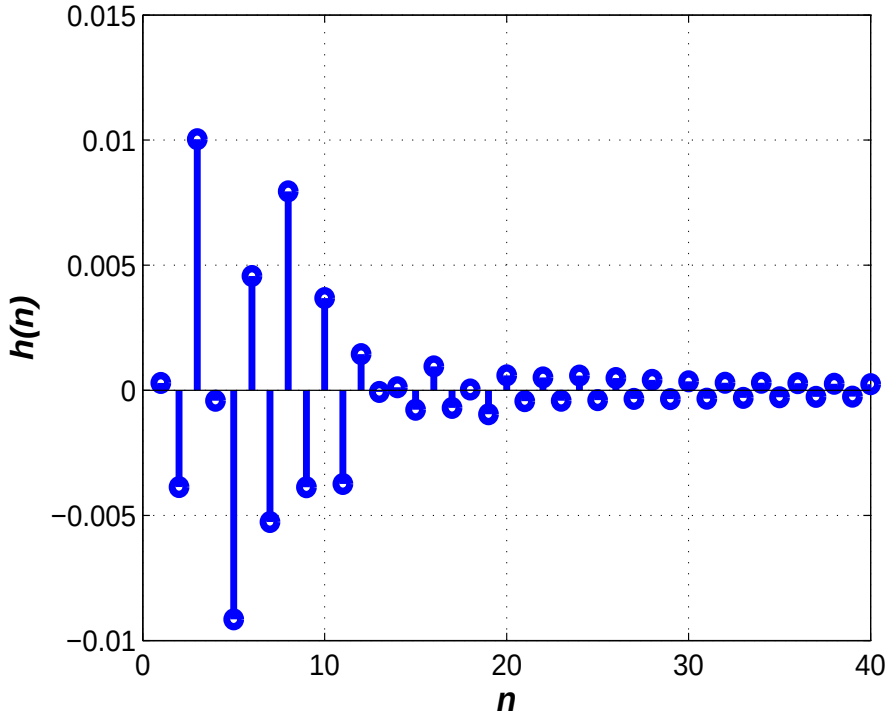

Figure 2.12. *Estimated NEXT impulse response sampled at 571.333 KHz.*

2.5 Conclusions

The simulation models described in this chapter were used to generate the crosstalk and received signals for our crosstalk cancellation experiments. To verify and to improve the accuracy of the models, the Telcordia's NEXT coupling measurements [9], which were measured from real transmission cables, were used as reference. By using the simulation models we were able to simulate various kinds of cables with different numbers of twisted pairs and different combinations of DSL systems.

Chapter 3

NEXT Cancellation System

3.1 Introduction

In this chapter, a new NEXT cancellation system is proposed that uses a fast and efficient algorithm to estimate the crosscorrelation between the transmitted and received signal. The detection and cancellation are carried out simultaneously, and are integrated in a way such that the estimation of the smaller NEXT signals becomes more and more accurate as the larger NEXT signals are cancelled. The chapter is organized as follows: Section 3.2 describes a fast and efficient algorithm to estimate the crosscorrelation for detecting the NEXT signals. Section 3.3 presents a NEXT cancellation system that detects and cancels the NEXT signals. Simulation results are presented and discussed in section 3.4 while in section **??** a comparison is made between time- and frequency-domain adaptive filters for use as NEXT cancellers. Conclusions are drawn in section 3.5.

3.2 Estimation of Crosscorrelation

For xDSL systems in which there is an overlap between the transmit and receive spectra, the signal received on a single twisted pair in a bundle typically contains an echo component in addition to NEXT. For the purpose of crosstalk detection and cancellation, we assume that the echo at the hybrid has been cancelled by an echo canceller before detection is

performed. The echo-cancelled signal can be expressed as

$$y_r(n) = r(n) + \eta_b(n) + \sum_i h_i(n) * d_i(n) \tag{3.1}$$

where $y_r(n)$ is the noisy observation, $r(n)$ is the received message signal, $\eta_b(n)$ is additive background noise, $d_i(n)$ is the signal transmitted on pair i, and $h_i(n)$ is the impulse response of the crosstalk coupling between pair i and the considered pair.

Usually, the impulse response of the channel can be readily estimated [28]. Hence, the received signal can be removed leaving only the crosstalk signals. With the echoes from the received signal and the transmitted signal removed, the received signal $y_r(n)$ can be expressed as

$$y(n) = \eta_b(n) + \sum_i h_i(n) * d_i(n) \tag{3.2}$$

where $d_i(n)$ is the transmitted signal. Assuming that $y(n)$ and $d_i(n)$ are widesense stationary, and that $d_i(n)$ is a random process of energy σ_d^2, which is made up of random variables that are statistically independent and have the same probability distribution, the crosscorrelation between the two signals is given by

$$R_{yd_i}(l) = E[y(n+l)d_i(n)] = \sigma_d^2 h_i(l) \tag{3.3}$$

This shows that if signal $d_i(n)$ is uncorrelated, the crosscorrelation is proportional to the impulse response of the crosstalk coupling function. However, in a mixed environment where several DSL systems may interfere with one another, the reference input samples from the other DSL system types will first need to be resampled if the sampling rate is different from the line where the NEXT is to be cancelled. In that case, the resampled reference input signal is given by

$$\widehat{d}_i(n) = \sum_{l=0}^{N-1} d_i(l)\text{sinc}\left(n - \frac{lT}{T'}\right) \tag{3.4}$$

where $1/T$ is the sampling rate of the transmitted signal $d_i(n)$, and $1/T'$ is the sampling rate of the resampled signal $\widehat{d}_i(n)$. To make the crosscorrelation $R_{y\widehat{d}_i}(l)$ proportional to

the NEXT impulse response $h_i(n)$, a deconvolution function $\Delta_{d_i}(n)$ can be found for each DSL system type such that $R_{y\hat{d_i}}(n) * \Delta_{d_i}(n) = \sigma_d^2 h_i(l)$.

Assuming that the transmitted and received signals are ergodic, the crosscorrelation R_{yd_i} can be approximated as

$$R_{yd_i}(l) = \frac{1}{N}\sum_{n=1}^{N} y(n+l)d_i(n) \tag{3.5}$$

where N is the number of data samples.

Assuming $d_i(n)$ to be a zero-mean stationary Gaussian process, the crosscorrelation can be efficiently estimated as [30] [31]

$$R_{yd_i}(l) = \frac{1}{N}\sum_{n=1}^{N} y(n+l)\ \text{sign}[d_i(n)] \tag{3.6}$$

where

$$\text{sign}(x) = \begin{bmatrix} -1 & \text{for } x < 0 \\ 1 & \text{for } x \geq 0 \end{bmatrix}$$

It can be shown that the crosscorrelation in (3.6) can be computed using only additions. This makes it computationally simple and well suited for hardware implementation.

3.3 NEXT Cancellation System

The NEXT cancellation system of interest is illustrated in Fig. 3.1. To achieve efficiency, adaptation is used only for lines in a bundle that require removal of NEXT from the received signal. As can be seen in Fig. 3.1, the cancellation system for a certain twisted pair consists of two parts, one for NEXT detection and one for NEXT cancellation. Using the crosscorrelation technique described in section 3.2 the NEXT signals are detected in the first part. Once the significant NEXT signals are detected, they are assigned time-domain adaptive filters for cancellation.

The received signal $y(n)$ in (3.2) can be written as

$$y(n) = \sum_i y_i(n) + \eta_b(n) \tag{3.7}$$

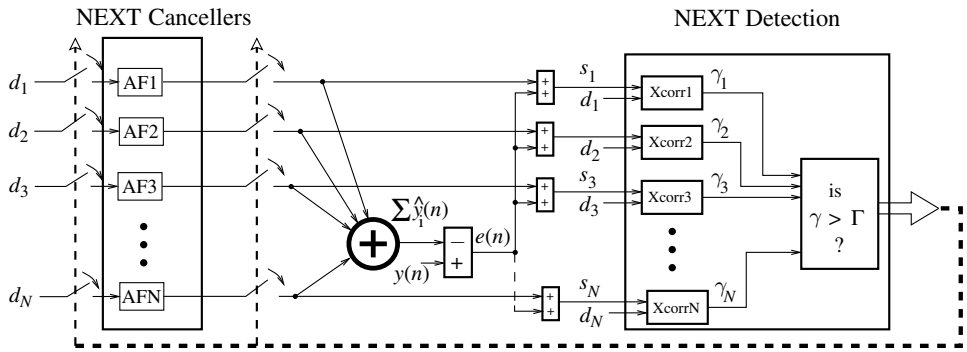

Figure 3.1. *NEXT cancellation system.*

where $y_i(n) = h_i(n) * d_i(n)$. Hence, if we assume that $d_i(n)$ is widesense stationary and i.i.d, then from (3.3) $R_{yd_i}(l) = \sigma_d^2 h_i(l)$. However, the presence of other crosstalk signals and background noise can make the estimate of $R_{yd_i}(l)$ rather noisy and inaccurate. The degree of variation in the estimate of $R_{yd_i}(l)$ can be found by taking the variance of $R_{yd_i}(l)$, which is given by

$$\begin{aligned} \text{Var}[R_{yd_i}(l)] &= E[|y(n+l)d_i(n)|^2] - E[y(n+l)d_i(n)]^2 \\ &= \sigma_d^4 \sum_{i=1}^{N} \sum_{k} h_i^2(k) + \sigma_d^2 \sigma_{\eta_b}^2 - \sigma_d^4 h_i^2(l) \end{aligned} \tag{3.8}$$

where $\sigma_{\eta_b}^2$ is the magnitude of the background noise $\eta_b(n)$. Equation (3.8) shows that the overall crosstalk noise, including the background noise, causes the estimate of $R_{yd_i}(l)$ to be noisy. On the other hand, the presence of the negative term $-\sigma_d^4 h_i^2(l)$ implies that the variance of the estimate decreases as the magnitude of $h_i(l)$ increases. This also implies that if the NEXT signal is small, the estimate of $R_{yd_i}(l)$ would be noisy and inaccurate.

In order to obtain a more accurate estimate of $R_{yd_i}(l)$, especially for smaller NEXT signals, the adaptive filter estimates of the NEXT signals that have already been detected and assigned adaptive filters for cancellation should first be subtracted from the received signal before estimating $R_{yd_i}(l)$. This is achieved by using the error signal $e(n)$, instead of $y(n)$, and then adding it to the adaptive-filter estimate $\hat{y}_i(n)$, if it has already been assigned

an adaptive filter. The resulting signal $s_i(n)$ is given by

$$s_i(n) = e(n) + a\hat{y}_i(n) \tag{3.9}$$

where a is either 1 or 0, depending upon whether or not an adaptive filter has been assigned for cancelling the NEXT signal on line i. From Fig. 3.1, the error $e(n)$ can be expressed as

$$\begin{aligned} e(n) &= y(n) - \sum_i \hat{y}_i(n) \\ &= \sum_i y_i(n) - \sum_i \hat{y}_i(n) + \eta_b(n) \end{aligned} \tag{3.10}$$

Using (3.9) and (3.10), $s_i(n)$ can be expressed as

$$s_i(n) = \sum_{j,j\neq i} (y_j(n) - \hat{y}_j(n)) + y_i(n) + \eta_b(n) \tag{3.11}$$

Now taking the crosscorrelation of $s_i(n)$ with $d_i(n)$, we get

$$R_{s_i d_i}(l) = E[s_i(n+l)d_i(n)] = \sigma_d^2 h_i(l) \tag{3.12}$$

It can be observed from (3.3) and (3.12) that the value of $R_{s_i d_i}(l)$ is the same as that of $R_{y d_i}(l)$. The variance of $R_{s_i d_i}(l)$ is evaluated as

$$\text{Var}[R_{s_i d_i}(l)] = E[|s_i(n+l)d_i(n)|^2] - E[s_i(n+l)d_i(n)]^2 \tag{3.13}$$

For LMS adaptive filters, we can assume that $\hat{y}_j(n)$ is independent of $d_i(n)$, for $i \neq j$ as $\mu \to 0$ [33]. Thus (3.13) can be simplified to

$$\text{Var}[R_{s_i d_i}(l)] = \underbrace{\sigma_d^2 \sum_{j,j\neq i} \sigma_{e_j}^2(n) + \sigma_d^4 \sum_k h_i^2(k) + \sigma_d^2 \sigma_{\eta_b}}_{\sigma_T^4(n)} - \sigma_d^4 h_i^2(l) \tag{3.14}$$

where $\sigma_{e_j}^2(n)$ is the magnitude of the estimation error between the adaptive filter estimate and the NEXT signal on line j after iteration n. Equation (3.14) shows that as the adaptation progresses and the estimation error $e_j(n)$ in each line decreases, the variance of $R_{s_i d_i}(l)$ also decreases thereby making the crosscorrelation more accurate.

Because the estimated error $e_j(n)$ decreases as the adaptation progresses, the crosscorrelation $R_{s_i d_i}(l)$ can be expressed in a time-varying form as

$$R_{s_i d_i}(l, n) = \sigma_d^2 h_i(l) + \alpha_l(n) \tag{3.15}$$

where $\alpha_l(n)$ is a zero-mean random sequence with variance $[\sigma_T^4(n) - \sigma_d^4 h_i^2(l)]$.

The term $\alpha_l(n)$ in (3.15) can cause random fluctuations in the estimate of $R_{s_i d_i}(l, n)$ but a smoother estimate can be obtained by lowpass filtering $R_{s_i d_i}(l, n)$ first. A lowpass filtered estimate of the crosscorrelation $\hat{R}_{s_i d_i}(l, n)$ can be obtained by using the first-order recursive equation

$$\hat{R}_{s_i d_i}(l, n) = (1 - \lambda)\hat{R}_{s_i d_i}(l, n - 1) + \lambda R_{s_i d_i}(l, n) \tag{3.16}$$

where λ is a positive constant less than unity that controls the shape of the amplitude response of the lowpass filter.

The NEXT detection block computes the crosscorrelation $R_{s_i d_i}(l, n)$ using (3.6) to estimate the magnitude of the NEXT signals. The NEXT cancellation block, consists of adaptive filters that are used to cancel the significant NEXT signals detected by the first block. To decide whether a particular crosstalk signal is large enough to require cancellation by an adaptive filter, a threshold value Γ can be set such that if

$$\gamma_i(n) = \sum_{l=k_1}^{k_2} \hat{R}_{s_i d_i}(l, n)^2 > \Gamma \tag{3.17}$$

where k_1 and k_2 are the filter-tap indices between which the maximum energy is concentrated, the NEXT signal is considered large enough for cancellation. The threshold Γ is empirically selected depending on the maximum amount of NEXT the DSL system can tolerate.

As can be seen in Fig. 3.1, the NEXT cancellers are coupled with the NEXT detectors so that $s_i(n)$ can be evaluated first and then used to estimate $R_{s_i d_i}(l)$. As the adaptation progresses and the adaptive filter estimation-error of the larger NEXT signals becomes less and less, $\gamma_i(n)$ for the smaller NEXT signals becomes more accurate.

The adaptive filter can be an LMS filter, one of its variations, or even an RLS filter. The LMS filter is preferred because of its low computational complexity and good stability characteristics even in noisy environments [33]. Since the reference signal to the adaptive filter is taken after the scrambler in a DSL system, it has a low eigenvalue spread which improves the good convergence rate for LMS-type adaptive filters [33]. However, in a mixed environment, the resampled signals tend to have a higher eigenvalue spread, and would need to be pre-whitened if a faster convergence rate is desired.

The computational complexity in a NEXT cancellation system is dependent on the percentage of twisted pairs causing NEXT in a line, which, in turn, is dependent on the type of cable used, the number of twisted pairs in each cable, the power of the transmitted signals, the noise tolerance of the xDSL system, and so on. However, in a bundle where the number of twisted pairs is large (larger than 20), the average number of twisted pairs causing significant NEXT in a particular twisted pair is fairly constant and does not increase if the number of twisted pairs in the bundle is increased. This is because the NEXT is usually caused by the surrounding adjacent twisted pairs whose number is fixed (typically around seven for the innermost twisted pair layer [17]). Hence if, on the average, the NEXT on a particular twisted pair is caused by p twisted pairs, the total number of adaptive filters that would be required to cancel the NEXT in all the lines would be Np where N is the total number of twisted pairs in the bundle. Since the method first detects the NEXT signals present on a line before assigning adaptive filters, the number of adaptive filters required would also be Np. In the proposed implementation, the detection process utilizes the sign algorithm which entails only additions and thus the amount of computation required for the detection process is negligible relative to that required by an adaptive filter. For this reason, the computational complexity of the proposed implementation typically increases linearly with N as opposed to that in existing NEXT cancellation systems [26] [15] which increases in proportion to N^2.

3.4 Simulations Results

The NEXT cancellation system was simulated for the case of the second generation high bit-rate DSL (HDSL2) environment using NLMS adaptive filters. The transmission bundle was assumed to comprise 7 twisted pairs of 26 AWG wire of length 7600 feet as specified in the T1E1.4 draft for HDSL2 system standard [36]. The length of the adaptive filters was 30, which is adequate for the sampling rate of an HDSL2 system. The NLMS coefficient update equation is given by

$$\mathbf{w}_i(n+1) = \mathbf{w}_i(n) + \frac{\mu}{||\mathbf{d}_i(n)||}\mathbf{d}_i(n)e^*(n) \tag{3.18}$$

where $\mathbf{w}_i^H(n)$ is the Hermitian transpose of a vector whose elements are the coefficients of the ith adaptive filter and μ is the adaptation constant. The length of the crosscorrelation $R_{s_i d_i}(l,n)$ was fixed at 20 and was lowpass filtered using (3.16) with $\lambda = 0.1$ before evaluating $\gamma_i(n)$ for each line using (3.17). The sampling rate was set to twice the symbol rate and the check whether $\gamma_i(n)$ exceeds the threshold Γ was carried out after every 200 samples.

The crosscorrelation $R_{s_i d_i}(l)$ was calculated by using the sign algorithm in (3.6) which has been shown to be very fast and sufficiently accurate [27] [29]. A comparison between the sign algorithm and the standard method for calculating $R_{s_i d_i}(l)$ in Figs. 3.2 and 3.3, respectively, confirms the accuracy of the sign algorithm in estimating $R_{s_i d_i}(l)$. Fig. 3.4 shows the power spectral densities (PSDs) of the simulated NEXT signals and the associated noise floor. As can be seen, the PSDs are of varying magnitudes similar to what would occur in the received signal of a real twisted pair. Fig. 3.5 shows plots of $\gamma_i(n)$ for the various NEXT signals versus the number of iterations. The numbers within square brackets in the legend of the figure represent the magnitudes of the NEXT signals. The threshold Γ used in the simulation was set to 0.2×10^{-10} and is represented by the horizontal dashed line in the figure. As can be seen, the estimated magnitudes of the first five NEXT signals, i.e., $\gamma_i(n)$ for $n = 1, \ldots, 5$, exceed the threshold value and by focusing the computational effort on eliminating these signals, increased computational efficiency can be achieved.

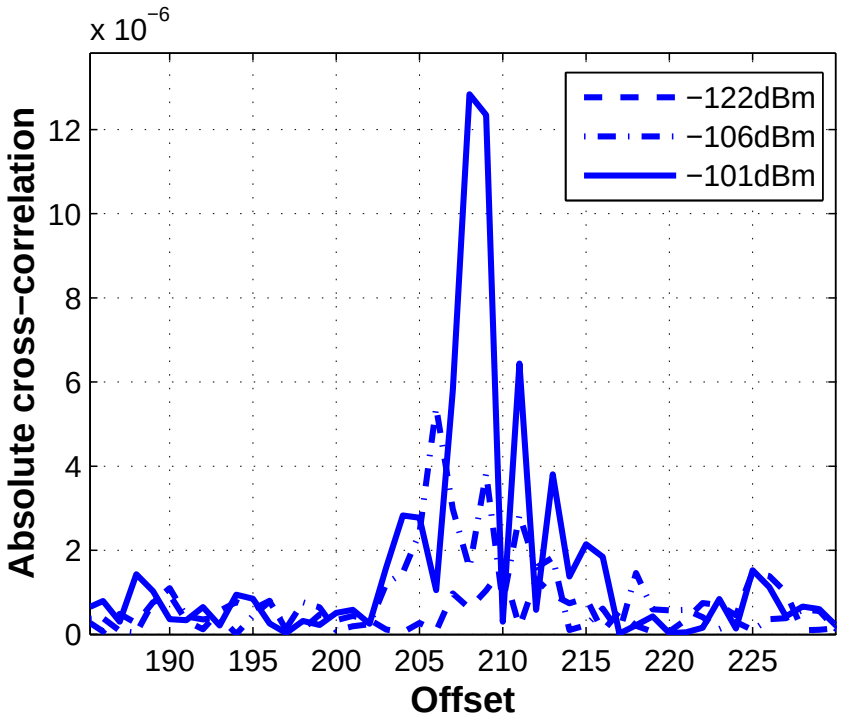

Figure 3.2. *NEXT crosscorrelation using the sign algorithm.*

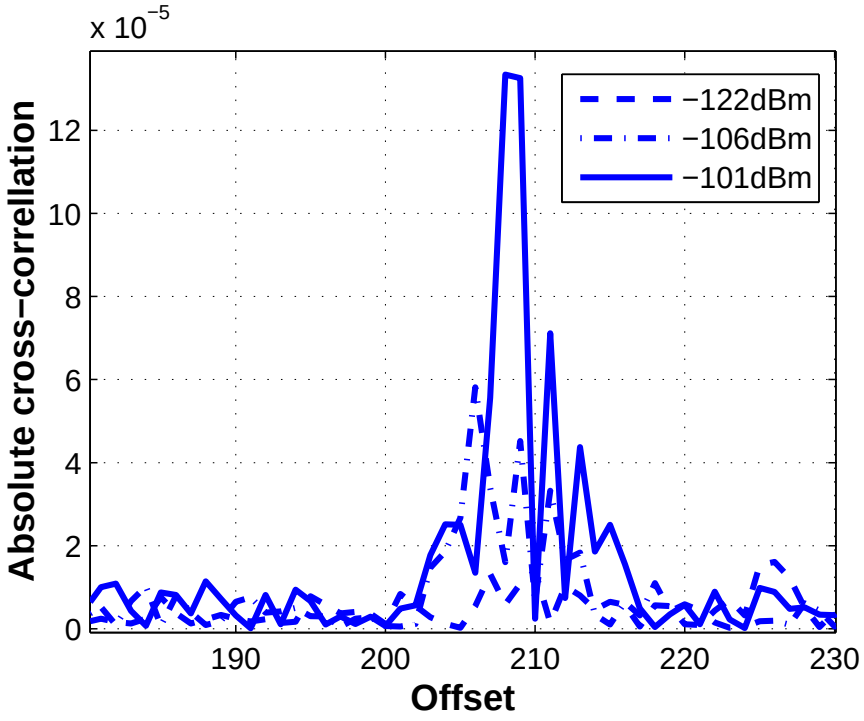

Figure 3.3. *NEXT crosscorrelation using the standard formula*

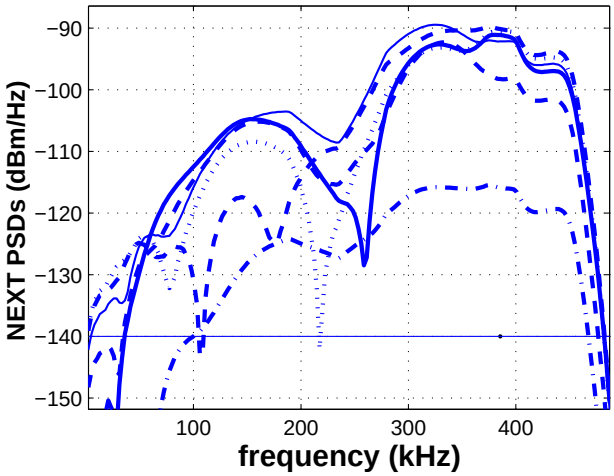

Figure 3.4. *PSDs of six simulated NEXT signals in a twisted pair (Horizontal line represents the noise floor).*

This is because the estimated magnitude of the sixth signal is below the threshold value and can thus be ignored. Although there was a savings of only one adaptive filter in this simulation, the amount of savings increases tremendously as the number of twisted pairs in the bundle increases. This is because, as mentioned in the previous section, most of the NEXT originates from a small number of surrounding adjacent twisted pairs in the bundle.

Fig. 3.6 shows a plot of the absolute value of the error signal where each displayed point represents the average absolute sum of 200 error-signal values. As can be seen, the estimated magnitudes in Fig. 3.5 become steady and more accurate as the error in Fig. 3.6 reduces especially for the smallest NEXT signal. The error in Fig. 3.6 converges to a mean residual error value of around -121 dBm most of which is contributed by the sixth NEXT signal of magnitude -122 dBm, which was not cancelled.

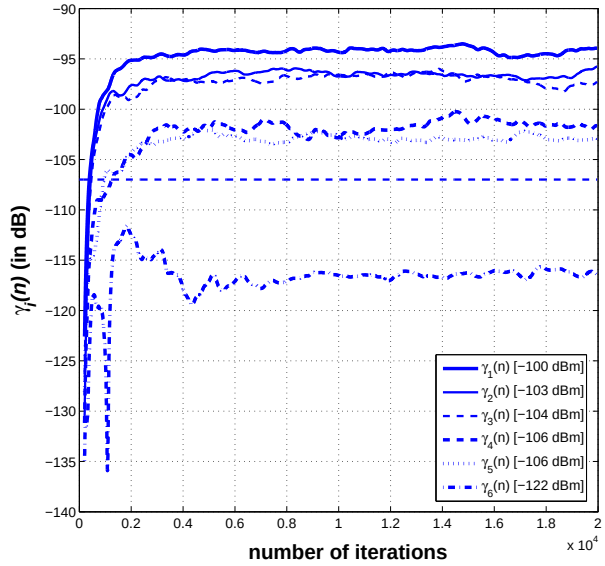

Figure 3.5. *Plot of $\gamma_i(n)$ for NEXT of different magnitude.*

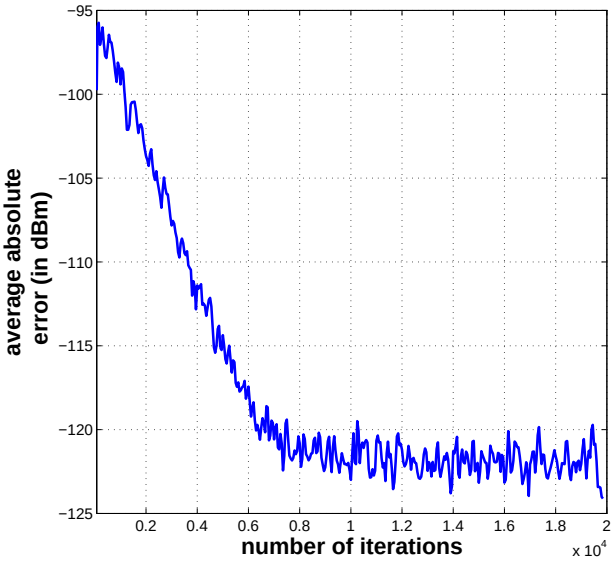

Figure 3.6. *Plot of the error versus no of iterations.*

3.5 Conclusions

An efficient NEXT cancellation system has been proposed. The new system first detects the NEXT signals present in the received signal and then assigns adaptive filters to cancel the most significant NEXT signals detected. The detection process is carried out by using a fast and efficient algorithm that estimates the crosscorrelation between the transmitted and received signal. By subtracting the adaptive filter estimates of the NEXT signals that have been detected and assigned adaptive filters for cancellation, the magnitude of smaller NEXT signals can be estimated more accurately during the NEXT detection stage. The proposed system offers overall computational complexity of order N where N is the number of twisted pairs in the bundle. This represents a large reduction in the computational effort relative to that in previous NEXT cancellation systems which offer computational complexities of order N^2.

Chapter 4

NEXT Cancellation Using FDLMS Adaptive Filters

4.1 Introduction

As the sampling rate increases, the filter length required for NEXT cancellation also increases since more samples are required to span the impulse response of the crosstalk coupling function. By using a frequency-domain least-mean-squares (FDLMS) algorithm instead of a time-domain least-mean-squares (TDLMS) algorithm, the amount of computation can be greatly reduced especially when the length of the adaptive canceller is large [34] [33]. If the environment is nonstationary, the mean-square error (MSE) will increase resulting in increased noise in the system. This increase in MSE can be lowered by improving the tracking performance of the NEXT cancellers.

In this chapter, a new NEXT cancellation system that uses FDLMS adaptive filters is proposed. In this system, the NEXT signals are first detected using a low-computational-complexity technique similar to the one discussed in section 3.2. Once the NEXT is detected, FDLMS adaptive filters are assigned to cancel only the significant NEXT signals. Various schemes of assigning step sizes are also explored that lead to improved convergence rate and tracking performance.

The chapter is organized as follows: In section 4.2, the convergence rate and tracking performance of the proposed NEXT cancellation system are studied and ways to improve

the convergence rate and tracking performance are proposed. In section 4.3 simulation results are presented while in section 4.4 a comparison is made between time- and frequency-domain adaptive filters. Conclusions are drawn in section 4.5.

4.2 Improved Convergence Rate & Tracking Performance

The model of the frequency-domain adaptive-filter algorithm for NEXT cancellation is shown in Fig. 4.1 where the DFT-FFT blocks compute the discrete Fourier transform (DFT) using a fast Fourier transform (FFT) (see Chap. 7 of [22]). This is an extension of a model used by Bershad et al. [38], which incorporates multiple adaptive filters [4]. The input signals $d_i(n)$ to the DFT-FFT blocks are assumed to be statistically independent, joint Gaussian, and widesense stationary thereby making the disjoint spectral outputs uncorrelated. Under these circumstances, the outputs of each of the DFT-FFT blocks in the different disjoint frequency bins are statistically independent of one another. Thus, the analysis can be simplified by considering only one frequency bin [39]. Since the DFT operations are linear with respect to the joint Gaussian input sequences, the DFT outputs are jointly complex Gaussian sequences.

The weight update equation for adaptive filter i for each frequency bin is given by

$$w_i(k+1) = w_i(k) + \mu_i \varepsilon(k) x_i^*(k) \tag{4.1}$$

where $w_i(k)$ is the complex scalar weight at the kth iteration of adaptive filter i, $k = n/L$ where L is the length of the DFT block, $x_i(k)$ is the ith frequency-domain input data sequence, μ_i is the ith feedback coefficient, and

$$\begin{aligned} \varepsilon(k) &= z(k) - \sum_{i=1}^{N} \hat{z}_i(k) + \eta(k) \\ &= \sum_{i=1}^{N} z_i(k) - \sum_{i=1}^{N} \hat{z}_i(k) + \eta(k) \end{aligned} \tag{4.2}$$

is the error for each frequency bin where $z_i(k)$ is the NEXT from line i for a particular frequency bin and $\hat{z}_i(k) = w_i(k) x_i(k)$ is the output from the ith adaptive filter.

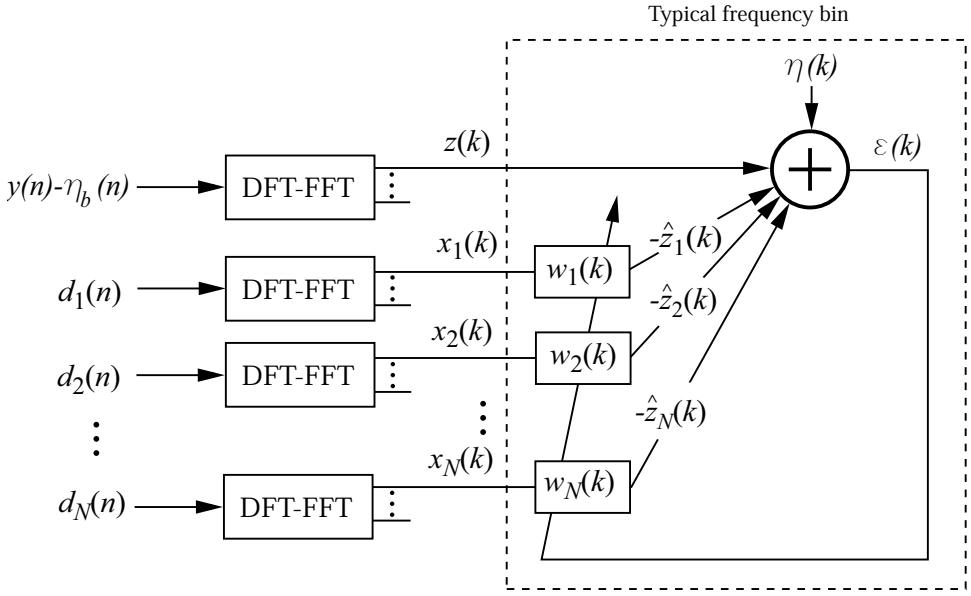

Figure 4.1. *Model for the FDLMS algorithm for each frequency bin.*

If an additive Gaussian noise $\eta(k)$ which is statistically independent relative to the input and the received NEXT signals is added to the error $\varepsilon(k)$, then the relevant statistics of $z_i(k)$ and $x_i(k)$ are

$$\begin{aligned} E[x_i(k)] &= E[z_i(k)] = 0 \\ E[|x_i(k)|^2] &= \sigma_x^2 \\ E[|z_i(k)|^2] &= |\alpha_i|^2\sigma_x^2 \\ E[z_i(k)x_i^*(k)] &= \alpha_i\sigma_\eta^2 \\ E[|\eta(k)|^2] &= \sigma_\eta^2 \\ E[x_i(k)x_j(k)] &= 0 \quad \text{for } i \neq j \end{aligned} \tag{4.3}$$

where α_i is the complex correlation coefficient of the desired signal $z_i(k)$ when $E[|\varepsilon(k)|^2]$ is minimized.

Subtracting α_i from both sides of (4.1) so that $\nu_i(k) = w_i(k) - \alpha_i$ yields

$$\nu_i(k+1) = \nu_i(k) + \mu_i \left[\sum_{j=1}^{N} z_j(k) + \eta(k) - \sum_{j=1}^{N} w_j(k)x_j(k) \right] x_i^*(k) \tag{4.4}$$

Squaring the magnitude on both sides in (4.4), taking the expectation, and then evaluating each of the terms yields a first-order linear difference equation for $E[|\nu_i(k)|^2]$ of the form

$$\begin{aligned} E[|\nu_i(k+1)|^2] &= (1-2\mu_i\sigma_x^2+2\sigma_x^4\mu_i^2)E[|\nu_i(k)|^2] \\ &\quad +\mu_i^2\sigma_x^4\sum_{j=1,j\neq i}^{N}E[|\nu_j(k)|^2]+\mu_i^2\sigma_x^2\sigma_\eta^2 \end{aligned} \tag{4.5}$$

If $\mu_{oi}=\mu_i\sigma_x^2$, (4.5) can be written as

$$\begin{aligned} E[|\nu_i(k+1)|^2] &= (1-2\mu_{oi}+2\mu_{oi}^2)E[|\nu_i(k)|^2] \\ &\quad +\mu_{oi}^2\sum_{j=1,j\neq i}^{N}E[|\nu_j(k)|^2]+\mu_{oi}^2\left(\frac{\sigma_\eta^2}{\sigma_x^2}\right) \end{aligned} \tag{4.6}$$

Expressing (4.6) in matrix form, we have

$$\mathbf{v}(k+1)=\mathbf{A}\mathbf{v}(k)+\mathbf{b} \tag{4.7}$$

where

$$\mathbf{v}(k)^T=\begin{bmatrix}E[|\nu_1(k)|^2] & E[|\nu_2(k)|^2] & \cdots & E[|\nu_N(k)|^2]\end{bmatrix} \tag{4.8}$$

$$\mathbf{A}=\begin{bmatrix}(1-2\mu_{o1}+2\mu_{o1}^2) & \mu_{o1}^2 & \cdots & \mu_{o1}^2 \\ \mu_{o2}^2 & (1-2\mu_{o2}+2\mu_{o2}^2) & \cdots & \mu_{o2}^2 \\ \vdots & \vdots & \vdots & \vdots \\ \mu_{oN}^2 & \mu_{oN}^2 & \cdots & (1-2\mu_{oN}+2\mu_{oN}^2)\end{bmatrix} \tag{4.9}$$

and

$$\mathbf{b}^T=\frac{\sigma_\eta^2}{\sigma_x^2}\begin{bmatrix}\mu_{o1}^2 & \mu_{o2}^2 & \cdots & \mu_{oN}^2\end{bmatrix} \tag{4.10}$$

Assuming that the system is stable, the solution of the difference equation in (4.7) can be obtained as

$$\mathbf{v}(k)=\mathbf{A}^k\mathbf{v}(0)+(\mathbf{A}^{k-1}+\mathbf{A}^{k-2}+\cdots+\mathbf{I})\mathbf{b} \tag{4.11}$$

or more compactly as

$$\mathbf{v}(k) = \mathbf{A}^k\mathbf{v}(0) + (\mathbf{I} - \mathbf{A})^{-1}(\mathbf{I} - \mathbf{A}^k)\mathbf{b} \tag{4.12}$$

4.2.1 Stability

For stability, the norm of matrix $\mathbf{A}$ for the system in (4.12) must be less than unity; that is

$$||\mathbf{A}||_2 < 1 \tag{4.13}$$

Matrix $\mathbf{A}$ given in (4.9) can be expanded into a sum of two matrices as

$$\mathbf{A} = \begin{bmatrix} (1-\mu_{o1})^2 & 0 & \cdots & 0 \\ 0 & (1-\mu_{o2})^2 & \cdots & 0 \\ \vdots & \vdots & \vdots & \vdots \\ 0 & 0 & \cdots & (1-\mu_{oN})^2 \end{bmatrix} + \begin{bmatrix} \mu_{o1}^2 \\ \mu_{o2}^2 \\ \vdots \\ \mu_{oN}^2 \end{bmatrix} \begin{bmatrix} 1 \\ 1 \\ \vdots \\ 1 \end{bmatrix}^T \tag{4.14}$$

Now for any two matrices or vectors $\mathbf{X}$ and $\mathbf{Y}$, we have

$$||\mathbf{X} + \mathbf{Y}|| \;\leq\; ||\mathbf{X}|| + ||\mathbf{Y}|| \tag{4.15}$$

$$||\mathbf{XY}|| \;\leq\; ||\mathbf{X}||\;\;||\mathbf{Y}|| \tag{4.16}$$

and if we apply the properties in (4.15) and (4.16) to (4.14), we obtain

$$||\mathbf{A}||_2 \leq \max\{(1-\mu_{oi})^2\} + \sqrt{N\sum_{i=1}^{N}\mu_{oi}^4} \tag{4.17}$$

The system described by (4.7) can always be made stable by making the right-hand side of (4.17) less than unity. Hence in practical applications, stability can be achieved by ensuring that the condition

$$\max\{(1-\mu_{oi})^2\} + \sqrt{N\sum_{i=1}^{N}\mu_{oi}^4} \;<\; 1 \tag{4.18}$$

is satisfied.

4.2.2 Convergence rate

The MSE for the proposed system is given by

$$E[|\varepsilon(k)|^2] = \sigma_x^2 \sum_{i=1}^{N} E[|\nu_i(k)|^2] + \sigma_\eta^2 \tag{4.19}$$

In real-world echo cancellers, the adaptation step size μ is typically significantly smaller than the speed-optimal gain or the stability-limit gain [40]. The same is true for NEXT cancellers especially when the number of adaptive filters in the system is large. The value μ_{oi} is generally much smaller than the stability-limit gain which is always less than 1. It is, therefore, safe to assume that μ_{oi} is significantly larger than μ_{oi}^2. With this assumption, matrix $\mathbf{A}$ can be approximated as

$$\mathbf{A} \approx \hat{\mathbf{A}} = \begin{bmatrix} (1-2\mu_{o1}) & 0 & \cdots & 0 \\ 0 & (1-2\mu_{o2}) & \cdots & 0 \\ \vdots & \vdots & \vdots & \vdots \\ 0 & 0 & \cdots & (1-2\mu_{oN}) \end{bmatrix} \tag{4.20}$$

Thus, (4.12) can be simplified as

$$\mathbf{v}(k) = \hat{\mathbf{A}}^k \mathbf{v}(0) + (\mathbf{I} - \hat{\mathbf{A}})^{-1}(\mathbf{I} - \hat{\mathbf{A}}^k)\mathbf{b} \tag{4.21}$$

where

$$\hat{\mathbf{A}}^k = \begin{bmatrix} (1-2\mu_{o1})^k & 0 & \cdots & 0 \\ 0 & (1-2\mu_{o2})^k & \cdots & 0 \\ \vdots & \vdots & \vdots & \vdots \\ 0 & 0 & \cdots & (1-2\mu_{oN})^k \end{bmatrix} \tag{4.22}$$

and

$$(\mathbf{I} - \hat{\mathbf{A}})^{-1}(\mathbf{I} - \hat{\mathbf{A}}^k) = \begin{bmatrix} \dfrac{1-(1-2\mu_{o1})^k}{2\mu_{o1}} & 0 & \cdots & 0 \\ 0 & \dfrac{1-(1-2\mu_{o2})^k}{2\mu_{o2}} & \cdots & 0 \\ \vdots & \vdots & \vdots & \vdots \\ 0 & 0 & \cdots & \dfrac{1-(1-2\mu_{oN})^k}{2\mu_{oN}} \end{bmatrix} \tag{4.23}$$

In NEXT cancellation, the NEXT originating from the other lines is variable and, assuming that the initial weight, $w_i(0)$, of each adaptive canceller is zero, we have $\nu_i(0) = -\alpha_i$; thus

$$\mathbf{v}(0) = \begin{bmatrix} E[|\nu_1(0)|^2] \\ E[|\nu_2(0)|^2] \\ \vdots \\ E[|\nu_N(0)|^2] \end{bmatrix} = \begin{bmatrix} |\alpha_1|^2 \\ |\alpha_2|^2 \\ \vdots \\ |\alpha_N|^2 \end{bmatrix} \tag{4.24}$$

Using (4.21) and (4.24), the MSE in (4.19) can be expressed as

$$\begin{aligned} E[|\varepsilon(k)|^2] &= \frac{\sigma_x^2}{2} \sum_{i=1}^{N} \Bigg\{ 2(1-2\mu_{oi})^k |\alpha_i|^2 \\ &\quad + \mu_{oi}[1-(1-2\mu_{oi})^k] \frac{\sigma_\eta^2}{\sigma_x^2} \Bigg\} + \sigma_\eta^2 \end{aligned} \tag{4.25}$$

The minimum MSE can be estimated by letting $k \to \infty$ in (4.25) so that

$$\text{MSE}_{min} \approx E[|\varepsilon(\infty)|^2] = \frac{\sigma_\eta^2}{2} \sum_{i=1}^{N} \mu_{oi} + \sigma_\eta^2 \tag{4.26}$$

Simplifying (4.25) and neglecting the squared and higher terms of μ_{oi}, we get an approximate value for $E[|\varepsilon(k)|^2]$ as

$$E[|\varepsilon(k)|^2] \approx \sigma_x^2 \sum_{i=1}^{N} |\alpha_i|^2 - 2\sigma_x^2 \sum_{i=1}^{N} k|\alpha_i|^2 \mu_{oi} + \sigma_\eta^2 \tag{4.27}$$

For $\mu_{oi} \ll 1$, (4.27) would be reasonably accurate during early iterations (small values of k) since the contributions of higher-order terms are insignificant. Hence, from (4.26) and (4.27), we see that for $\sum_{i=1}^{N} \mu_{oi} =$ constant, the MSE will be subjected to a greater initial reduction per iteration if

$$\mu_{oi} = K|\alpha_i|^2 \tag{4.28}$$

where K is a constant, rather than making all of the μ_{oi} equal.

In an FDLMS adaptive filter, $|\alpha_i|$ is generally not known until the adaptive filter has fully converged. Also, $|\alpha_i|$ tends to vary for each frequency bin depending on the spectrum of the NEXT channel transfer function. However, a good estimate of the average value of

$|\alpha_i|$ over the entire NEXT frequency range is the maximum value of $|R_{yd_i}(l)|^2$ defined in (3.6), that is,

$$|\alpha_i|^2_{average} \approx c\left[\max_l\{|R_{yd_i}(l)|^2\}\right] \tag{4.29}$$

where $|\alpha_i|_{average}$ is the average value of $|\alpha_i|$ for each frequency bin, and c is some constant. Since $R_{yd_i}(l)$ is calculated when estimating γ_i in (3.17), it can be reused without additional computation. Thus, a good approximation for (4.28) for practical purposes for all the frequency bins of the ith adaptive filter is given by

$$\mu_{oi} = \kappa\left[\max_l\{|R_{yd_i}(l)|^2\}\right] \tag{4.30}$$

where κ is an appropriate constant chosen such that the minimum MSE in (4.26) is below a prescribed threshold.

4.2.3 Tracking Performance

The tracking performance of the proposed FDLMS NEXT cancellation system can be investigated by extending the time-domain adaptive-filter model described in [41] to the frequency domain [5]. The model for a single frequency bin is illustrated in Fig. 4.2. Coefficients $\alpha_1(k), \alpha_2(k), \ldots, \alpha_N(k)$ are used to model N unknown NEXT channels and $\eta(k)$ is a complex additive Gaussian noise. The unknown NEXT channels can be made nonstationary by making each coefficient $\alpha_i(k)$ time-varying. The parameters $w_1(k), w_2(k), \ldots, w_N(k)$ are the frequency-domain complex scalar weights of the adaptive filters for the frequency bin under consideration. From Fig. 4.2, the nonstationary signal $z(k)$ can be written as

$$z(k) = \sum_{i=1}^{N} z_i(k) \quad \text{where } z_i(k) = \alpha_i(k)x_i(k) \tag{4.31}$$

In order to model the ith unknown channel as a first-order Markov process [33, 44], a recursive, first-order, lowpass digital filter with transfer function $1/(z-a)$ was used with a zero-mean white noise signal $\beta_i(k)$ as input. The difference equation of such a filter is given by

$$\alpha_i(k+1) = a\alpha_i(k) + \beta_i(k) \tag{4.32}$$

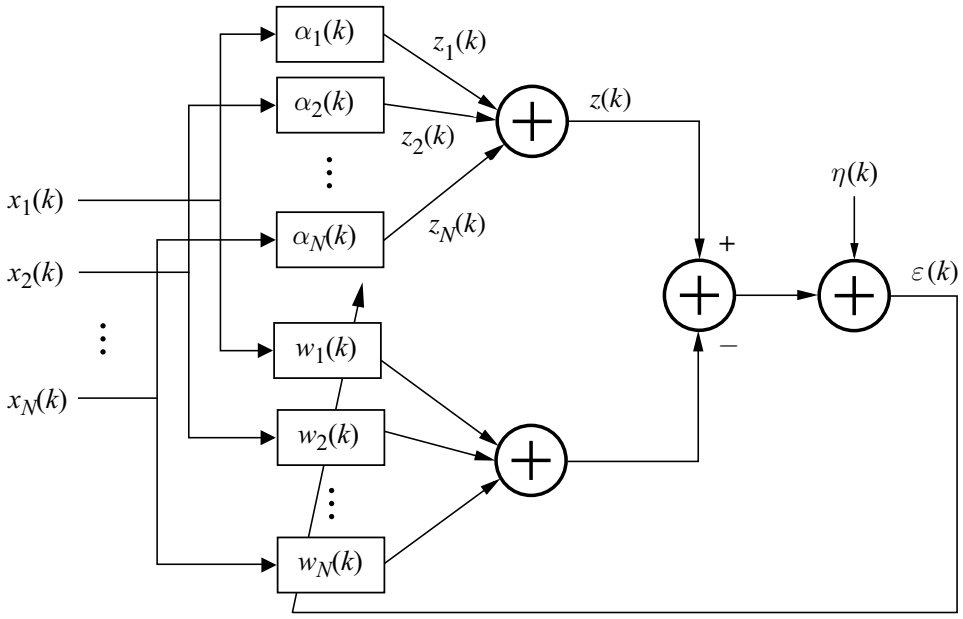

Figure 4.2. *Time-varying model of the frequency domain adaptive filter for a single frequency bin.*

In the analysis to follow, it is assumed that the nonstationary environment is a slowly changing one. Such an environment can be simulated by setting the parameter a in (4.32) very close to unity. This ensures that the filter has a passband width which is much smaller than the bandwidth of the incoming signal. A consequence of this assumption is that many iterations of the Markov model would be required to produce a significant change in the tap weight $\alpha_i(k)$. Since the coefficient $\alpha_i(k)$ is time varying, the weight error is given by

$$\nu_i(k) = w_i(k) - \alpha_i(k) \tag{4.33}$$

Using (4.1), (4.31), (4.32), and (4.33), we get

$$\begin{aligned} \nu_i(k+1) &= w_i(k+1) - \alpha_i(k+1) \\ &= \nu_i(k) - \mu_i|x_i(k)|^2 \sum_{i=1}^{N} \nu_i(k) + \mu_i \eta(k) x_i^*(k) - \beta_i(k) \end{aligned} \tag{4.34}$$

Squaring the magnitude of both sides in (4.34), taking the expectation, and evaluating the terms yields

$$\begin{aligned} E[|\nu_i(k+1)|^2] &= E[|\nu_i(k)|^2](1-2\mu_i\sigma_x^2) + \mu_i^2\sigma_x^4 \sum_{j=1}^{N} |\nu_j(k)|^2 \\ &\quad +\mu_i\sigma_\eta(k)^2\sigma_x^2 + \sigma_{\beta_i}^2 \end{aligned} \tag{4.35}$$

Upon convergence, we have

$$E[|\nu_i(k+1)|^2] = E[|\nu_i(k)|^2] \tag{4.36}$$

Substituting (4.36) in (4.35) and replacing $\mu_i\sigma_x^2$ by μ_{oi} yields

$$E[|\nu_i(k)|^2] = \frac{\mu_{oi}\sigma_\eta^2}{2\sigma_x^2} + \frac{\sigma_{\beta_i}^2}{2\mu_{oi}} + \frac{\mu_{oi}}{2}\sum_{j=1}^{N} E[|\nu_j(k)|^2] \tag{4.37}$$

Summing (4.37) with respect to i and rearranging terms gives

$$\sum_{i=1}^{N} E[|\nu_i(k)|^2] = \frac{\frac{\sigma_\eta^2}{2\sigma_x^2}\sum_{i=1}^{N}\mu_{oi} + \frac{1}{2}\sum_{i=1}^{N}\frac{\sigma_{\beta_i}^2}{\mu_{oi}}}{1-\frac{1}{2}\sum_{i=1}^{N}\mu_{oi}} \tag{4.38}$$

In a wireline environment, the magnitude of NEXT depends on the amount of capacitive (inductive) coupling between the twisted pairs causing the NEXT and the twisted pair receiving the NEXT. In a nonstationary xDSL environment, these couplings tend to vary over time due to variations in temperature, mechanical vibration, displacement, etc. For a nonstationary environment where the couplings vary slowly over time, it is reasonable to assume that variation in the coupling capacitance (inductance) is proportional to the magnitude of the coupling capacitance (inductance). Hence, considering $C_p(k)$ to be a random variable denoting the NEXT capacitive coupling, we can assume that at a certain time instant k, the variation is such that

$$E[\{C_p(k)-\lambda(k)\}^2] \propto \lambda(k)^2 \tag{4.39}$$

where $\lambda(k) = E[C_p(k)]$, so that

$$\frac{E[C_p(k)^2] - E[C_p(k)]^2}{E[C_p(k)]^2} \approx \text{constant} \tag{4.40}$$

In an xDSL environment, if the attenuation is considered to be approximately proportional to $\sqrt{f}$ where f is the frequency in Hz, then the crosstalk power spectrum can be expressed as [21]

$$|H_{NEXT}(f,l)|^2 \approx \frac{(2\pi CR)^2}{4\varsigma} f^{1.5}(1 - e^{-4l\varsigma\sqrt{f}}) \tag{4.41}$$

where C is the cross-coupling capacitance, R is the load impedance, l is the length of the loop, and ς is the real part of the propagation constant [21]. In (4.41), the inductive coupling is ignored altogether. For the differential mode, it is typically smaller than the capacitive coupling but it is not insignificant [21]. From (4.41) it is observed that the power of the NEXT for a particular frequency is dependent on the magnitude of the capacitive coupling. On the basis of (4.40), it follows that the relative degree of variation in the complex coefficient $\alpha_i(k)$ will be approximately the same for every frequency bin. Thus we get

$$\frac{E[|\beta_i(k)|^2]}{|\alpha_i(k)|^2} \approx \text{constant} = \delta \qquad \text{for } i = 1, \ldots, N \tag{4.42}$$

where δ represents the degree of variation. Now upon using (4.42) in (4.38), we have

$$\sum_{i=1}^{N} E[|\nu_i(k)|^2] = \frac{\frac{\sigma_\eta^2}{2\sigma_x^2} \sum_{i=1}^{N} \mu_{oi} + \frac{1}{2}\delta \sum_{i=1}^{N} \frac{|\alpha_i(k)|^2}{\mu_{oi}}}{1 - \frac{1}{2}\sum_{i=1}^{N} \mu_{oi}} \tag{4.43}$$

This equation shows that for a fixed value of $\sum_{i=1}^{N} \mu_{oi}$, $\sum_{i=1}^{N} E[|\nu_i(k)|^2]$ will be a minimum if μ_{oi} is made proportional to $|\alpha_i(k)|^2$, that is

$$\mu_{oi} = K|\alpha_i(k)|^2 \tag{4.44}$$

where K is a constant. Equation (4.44) is, however, identical to (4.28). Hence, as explained in section 4.2.2, a good approximation to realizing the benefits of (4.28) and, therefore, to (4.44) is to vary the step sizes as in (4.30).

4.3 Simulation Results

Extensive simulations were undertaken to study the convergence rate and tracking performance of the proposed system in an HDSL2 environment [36]. Two different methods of assigning step sizes, referred to as methods A and B, were investigated. For both methods, the term $\sum_{i=1}^{N} E[|\nu_i(k)|^2]$ in (4.19) was evaluated using (4.11). For method A all μ_{oi} were made equal whereas for method B they were made proportional to $|\alpha_i|^2$ as in (4.28).

4.3.1 Convergence rate

To study the convergence rate, simulations were carried out using each of methods A and B for assigning the step sizes assuming six different NEXT signals. The random values 0.9, 0.8, 0.2, 0.1, 0.3, and 0.2 were assigned to the magnitudes of the six NEXT signals, i.e., the weight vector $\mathbf{v}(0)$ assumed the form

$$\mathbf{v}(\mathbf{0}) = [0.9 \;\; 0.8 \;\; 0.2 \;\; 0.1 \;\; 0.3 \;\; 0.2]^{\mathrm{T}}$$

and σ_x^2 and σ_η^2 were set to 1.0 and 0.1, respectively. The convergence rate was evaluated for five different values of K (0.0096, 0.019, 0.028, 0.038, 0.048) and the results obtained are plotted in Fig. 4.3. As can be seen, method B offers an improved rate of convergence (steeper MSE curve) during the initial phase of convergence whereas method A offers a better rate of convergence later on when the MSE has reduced to a value below about -5 dB. Therefore, an effective strategy to achieve an improved rate of convergence would be to use method B initially and then switch over to method A when the MSE has been reduced to a value less than -5 dB.

The convergence rate of the NEXT cancellation system of Fig. 3.1 was then studied. Six NEXT signals were assumed, having magnitudes of 0.0064, 0.28, 0.07, 1, 0.02, and 0.58. The simulations were carried out in an HDSL2 environment using FDLMS adaptive filters each of length 100 to cancel the NEXT signals. Methods A and B were used for updating the step sizes as described above except that in method B μ_{oi} was set using (4.30). A third

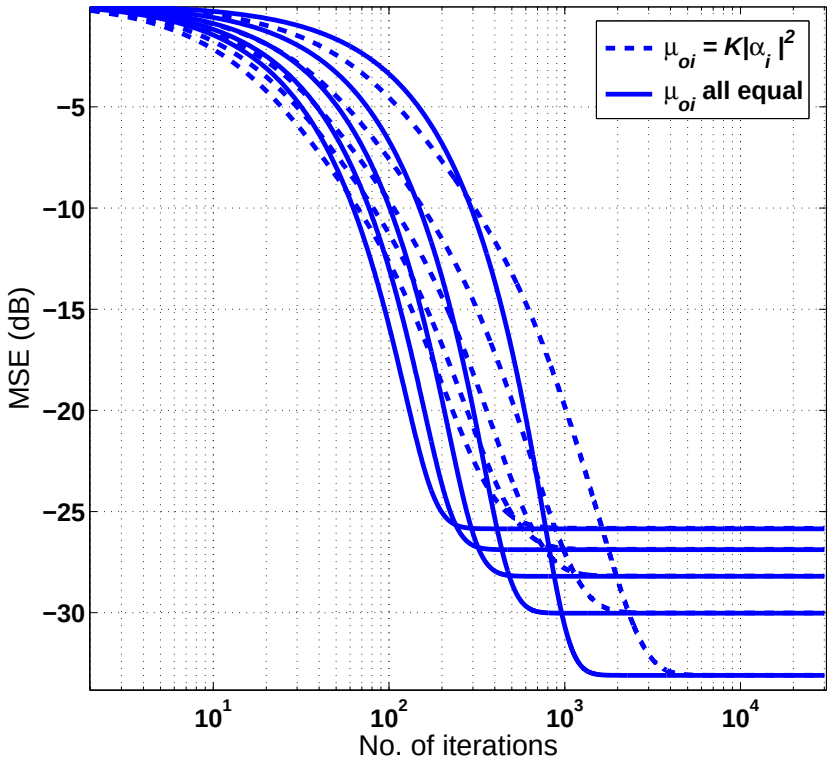

Figure 4.3. *Plot of the MSE for μ_{oi} all equal and μ_{oi} proportional to $|\alpha_i|^2$.*

method was also explored, referred to here as method C, whereby the step sizes were set according to method B during the initial phases of convergence and when the MSE was reduced by 5 dB, the step sizes were estimated as per method A. The results obtained are plotted in Fig. 4.4. As can be seen, method C combines the advantages of methods A and B.

4.3.2 Tracking performance

The tracking performance of the proposed system was investigated by carrying out simulations in a nonstationary environment. The coefficients $\alpha_i(k)$ of the unknown NEXT channels were made time-varying by updating them using (4.32). The initial magnitudes of the six NEXT signals used in the simulations were 0.0005, 0.0996, 0.0009, 10, 0.0003, and

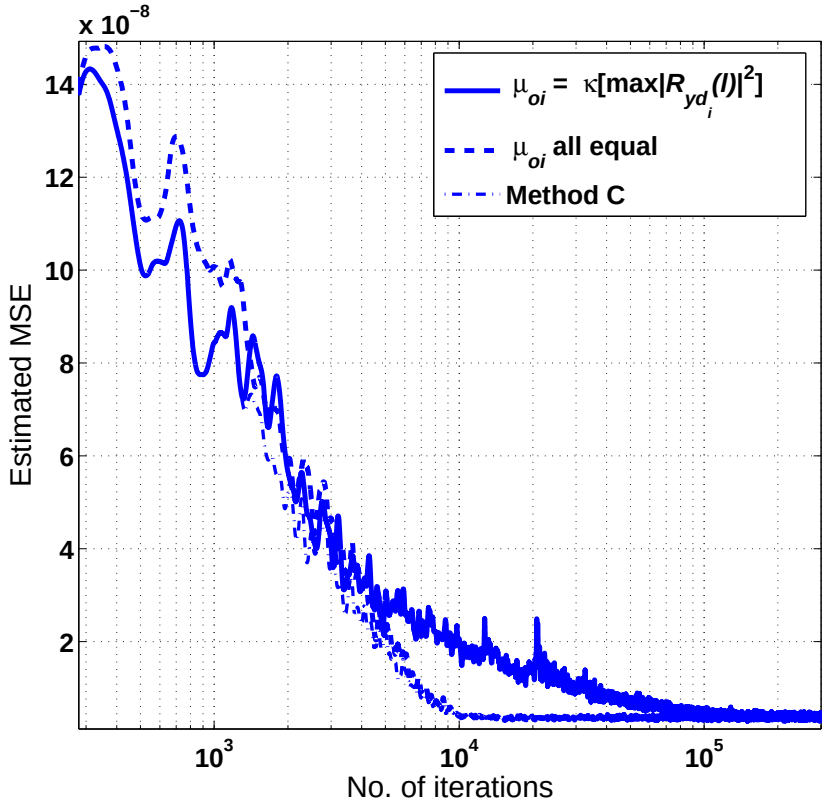

Figure 4.4. *Plot of the estimated MSE for (a) μ_{oi} all equal (b) μ_{oi} proportional to max$_l\{|R_{yd_i}(l)|^2\}$ and (c) method C.*

8.3774. The variance of the process noise for each NEXT channel was made proportional to the squared magnitude of the coefficient of the unknown channel on the basis of equation (4.42), i.e.,

$$\sigma^2_{\beta_i} = E[|\beta_i(k)|^2] = \delta|\alpha_i(k)|^2$$

and the nonstationary parameter δ was set to -45 dB. Two tracking tests were carried out using the same set of data. In the first test, the system was simulated over 50,000 iterations using method A for assigning the step sizes. In the second test, the system was again simulated with method A and when convergence had been achieved at 30,000 iterations method A was replaced by method B. The same $\sum_{i=1}^{N} \mu_{oi}$ was used for the two methods to ensure that both methods converge to the same MSE in a stationary environment. The results ob-

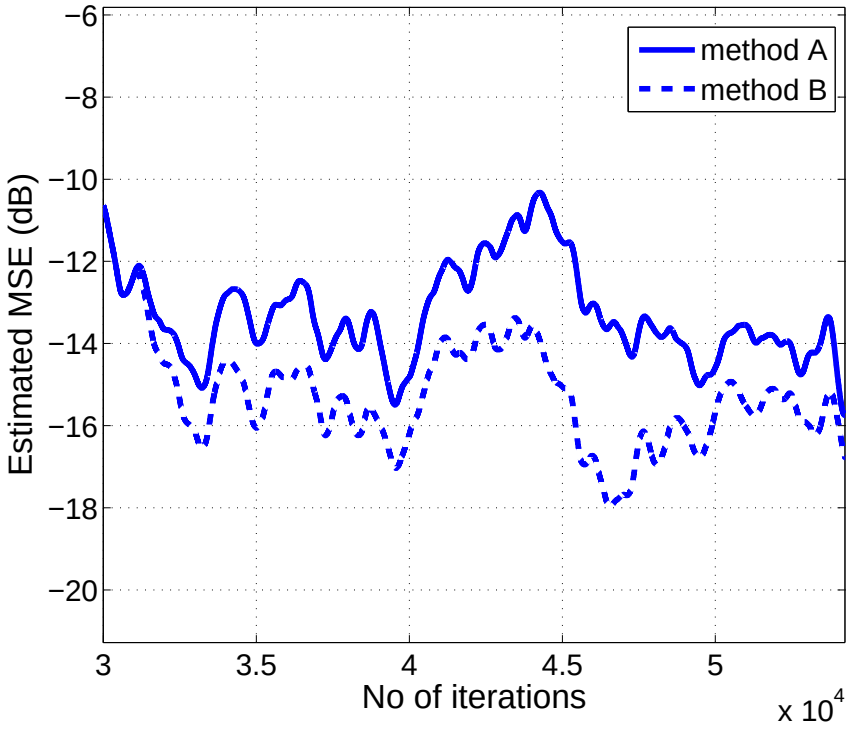

Figure 4.5. *Plot of the estimated MSE in a nonstationary environment with δ equal to -45 dB.*

tained are shown in Fig. 4.5. As can be seen, the use of method B after initial convergence to the minimum reduces the MSE by another 3 dB when compared with method A.

The investigation of convergence has shown that an improved convergence rate can be achieved by using method C for assigning the step sizes, i.e., method B followed by method A. The investigation of tracking has shown that a much better tracking performance can be achieved by using method B. Therefore, by using method C to start with and switching over to method B when convergence is achieved, the convergence rate as well as the tracking performance can both be improved.

For a stationary environment, the minimum MSE upon convergence given by (4.26) can be expressed as

$$\text{MSE}_{min} \approx E[|\varepsilon(\infty)|^2] = \frac{\sigma_\eta^2}{2} \sum_{i=1}^{N} \mu_{oi} + \sigma_\eta^2 \tag{4.45}$$

and if μ_{oi} is much less than unity, then both methods will have the same minimum MSE in a stationary environment if $\sum_{i=1}^{N} \mu_{oi}$ is the same for methods A and B. This fact is confirmed by Fig. 4.6 which depicts the results of simulations.

In subsection 4.2.3, it was assumed that the nonstationary environment is a slow time-varying one. For environments where the NEXT channel can undergo sudden changes, though unlikely in an xDSL environment, it would be preferable to use method A for assigning the step sizes.

4.4 Comparison of time- and frequency-domain implementations

Two alternative NEXT cancellation implementations have been explored in Chapter 3 and Sections 4.1-4.3, namely, through the use of time- and frequency-domain adaptive filters. In this section, we compare the two implementations with respect to computational efficiency and latency.

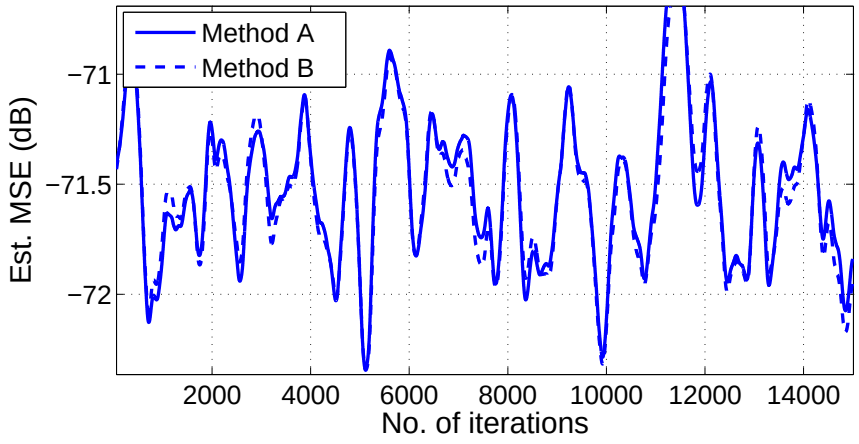

Figure 4.6. *Plot of the estimated MSE upon convergence in a stationary environment.*

The computational complexities of the NLMS and FDLMS algorithms are estimated as follows: a) For the NLMS algorithm with M tap weights operating on real data, M multiplications are performed to compute the output and a further M multiplications are performed to update the tap weights for a total of $2M$ multiplications per iteration. The normalizing factor requires 1 multiplication per iteration. Consequently, for a block of M output samples, the total number of multiplications is $2M^2 + M$.

b) For the FDLMS algorithm, each N-point FFT (and IFFT) requires approximately $N \log_2 N$ real multiplications where $N = 2M$ [34]. As per the structure in [34], five frequency transformations are performed, which account for $5N \log_2 N$ multiplications. Moreover, the computation of the frequency-domain output vector requires $4N$ multiplications and that of the cross-correlations relating to the gradient vector estimation requires another $4N$ multiplications. Consequently, the total number of multiplications performed in the FDLMS algorithm for a block of M samples is $10M \log_2 M + 26M$ [34].

Based on the above estimates, the computational complexity ratio of the FDLMS relative to the NLMS algorithm can be defined as

$$\delta(M) = \frac{2M + 1}{10 \log_2 M + 26} \tag{4.46}$$

Using this formula, the computational complexity can be plotted as shown in Fig. 4.7. From the plot it can be seen that using NLMS adaptive filters would be more efficient when the required adaptive filter length is less than 40.

In most existing DSL systems, the sampling rate is less than 1 MHz and the impulse response duration of the NEXT channel is less than 20 μs [15]. For such systems, a length of 30 for the adaptive filters would be quite adequate and, therefore, the time-domain implementation would be preferred. On the other hand, for systems that require a filter length larger than 40, the frequency-domain implementation discussed in this chapter would offer improved computational efficiency. In effect, the time- and frequency-domain are complementary with respect to computational efficiency.

Another difference between the time- and frequency-domain implementations has to

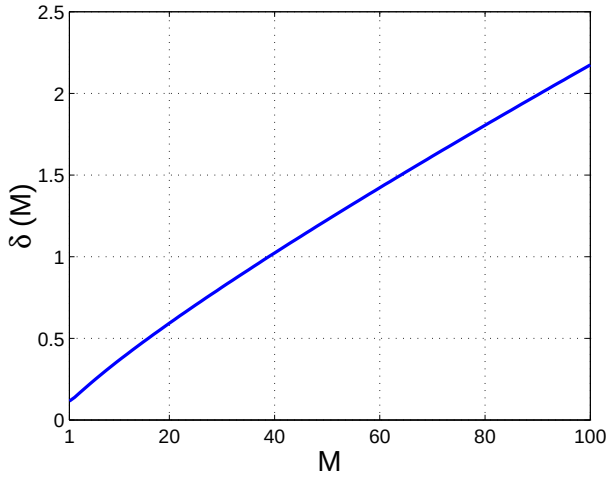

Figure 4.7. *Plot of the complexity ratio $\delta(M)$ of FDLMS to NLMS adaptive filters versus the filter length.*

do with latency. The time-domain implementation processes the data sample by sample unlike the frequency-domain implementation which processes the data block by block. Consequently, the frequency-domain implementation introduces latency which can be a problem in real-time applications where the delay introduced by the block exceeds the maximum-delay tolerance of the application.

4.5 Conclusions

A new NEXT cancellation system for high data-rate xDSL systems was proposed. The new system is equipped with a mechanism whereby the NEXT signals are detected and then FDLMS adaptive filters are assigned to cancel only the significant NEXT signals. By this means, the computational load can be significantly reduced. Three methods for assigning the step sizes in the adaptive filters were investigated. By making the step size for each adaptive filter proportional to the magnitude of the NEXT signal during the initial phases of adaptation and then making them all equal during the later phases, i.e., by using method C for assigning the step sizes, the convergence rate can be significantly improved.

And by returning after convergence to step sizes that are proportional to the magnitudes of the NEXT signals, a much better tracking performance can also be achieved.

The time-domain and frequency-domain implementations have been compared with respect to computational complexity. The choice between the two depends critically on the required filter length. For applications where a filter length less than 40 is acceptable, reduced computational complexity can be achieved by using the time-domain implementation. On the other hand, if a larger filter length is required, the frequency-domain implementation would be preferable.

Chapter 5

NEXT Cancellation Using Variable-Length Cancellers

5.1 Introduction

In Chapter 3 the computational complexity is reduced by detecting the major NEXT sources using a low-complexity crosscorrelation algorithm along with fixed-length adaptive filters [31] [1]. If the filter length of each adaptive filter is allowed to vary with the magnitude of the NEXT signals, significant savings can be achieved in terms of the total filter length of the adaptive filters. This reduction in the total filter length results in improved usage of hardware which also translates into significant savings in computations.

In this chapter, an algorithm that adjusts the lengths of the adaptive filters according to the magnitudes of the NEXT signals is proposed. By normalizing and then combining many NEXT impulse responses for a particular cable, a normalized NEXT profile is created [2]. Using this profile, the starting and ending tap positions of the adaptive filter for a certain maximum noise threshold are computed. The algorithm starts the NEXT cancellation by using adaptive filters with minimal filter lengths. The filter taps are positioned along the locations where the maximum absolute value of the NEXT impulse responses typically occur. As the adaptation progresses, the tap positions for each adaptive filter are periodically adjusted based on the absolute peak value of each adaptive filter. When all the adaptive filters have fully converged, another algorithm is used to readjust the length of

those adaptive filters with filter lengths that may be too long or too short.

The chapter is organized as follows: In section 5.2 the conditions for optimizing the filter length of each adaptive filter are derived. In section 5.3 an algorithm that minimizes the number of filter taps under the constraint that the maximum crosstalk noise is below a given threshold is described. Simulation results are presented in section 5.4 and conclusions are drawn in section 5.5.

5.2 Filter-tap minimization

Suppose an adaptive filter of length L_i is used to cancel the near-end crosstalk from line i. Using (3.10) the instantaneous error $e(n)$ due to all the NEXT sources in the bundle upon convergence can be written as

$$e(n) = y(n) - \sum_{i=1}^{N} \sum_{k=0}^{L_i-1} \hat{h}_i(k) d_i(n-k) \tag{5.1}$$

where $\hat{h}_i(k)$ is the estimated NEXT impulse response of the ith adaptive filter and N is the number of adaptive filters used to cancel the NEXT signals.

Assuming that the transmitted data are statistically independent and wide-sense stationary with zero mean, the mean-square-error upon convergence can be expressed as

$$\begin{aligned} E[|e(n)|^2] &= \sum_{i=1}^{N} \sigma_{d_i}^2 \sum_{k=0}^{L_i-1} |h_i(k) - \hat{h}_i(k)|^2 \\ &\quad + \sum_{i=1}^{N} \sigma_{d_i}^2 \sum_{k=L_i}^{\infty} |h_i(k)|^2 + \sigma_\eta^2 \end{aligned} \tag{5.2}$$

where $h_i(n)$ is the near-end crosstalk impulse response from the ith line, $\hat{h}_i(n)$ is the estimated NEXT impulse response of the ith adaptive canceller of length L_i, $\sigma_{d_i}^2$ is the variance of the transmitted data, and σ_η^2 is the variance of the additive noise in the system.

Assuming that all of the lines have the same DSL type, the variance of the transmitted

data in each of the lines can be considered to be equal. This simplifies (5.2) to

$$\begin{aligned} E[|e(n)|^2] &= \sigma_d^2 \sum_{i=1}^{N} \sum_{k=0}^{L_i-1} |h_i(k) - \hat{h}_i(k)|^2 \\ &\quad + \sigma_d^2 \sum_{i=1}^{N} \sum_{k=L_i}^{\infty} |h_i(k)|^2 + \sigma_\eta^2 \end{aligned} \tag{5.3}$$

where $\sigma_d = \sigma_{d_1} = \cdots = \sigma_{d_i} = \cdots = \sigma_{d_N}$. Upon convergence, the first term in (5.3) is much smaller than the background noise σ_η^2 and hence

$$E[|e(n)|^2] \approx \sigma_d^2 \sum_{i=1}^{N} \sum_{k=L_i}^{\infty} |h_i(k)|^2 + \sigma_\eta^2 \tag{5.4}$$

Suppose that $E[|e(n)|^2]$ is fixed at λ_{max} which is the maximum noise that is tolerable by the system, we can minimize $\sum_{i=1}^{N} L_i$ subject to the constraint

$$\lambda_{max} = \sigma_d^2 \sum_{i=1}^{N} \sum_{k=L_i}^{\infty} |h_i(k)|^2 + \sigma_\eta^2 \tag{5.5}$$

This is an optimization problem of finding the minimum total filter length of the adaptive filters for a given maximum tolerable NEXT noise.

Suppose, however, that the total number of taps of all the NEXT cancellers is fixed, that is, $\sum_{i=1}^{N} L_i =$ constant, then a length L_i can be found for each NEXT canceller such that $E[|e(n)|^2]$ is minimized, that is, we solve the optimization problem

$$\min_{L_i} E[|e(n)|^2] \tag{5.6}$$

$$\text{subject to: } \sum_{i=1}^{N} L_i = \text{ constant} \tag{5.7}$$

Using (5.4) and neglecting the constant terms σ_d and σ_η, we can state the problem as

$$\begin{aligned} &\min_{L_i} \sum_{i=1}^{N} \sum_{k=L_i}^{\infty} |h_i(k)|^2 \\ &\text{subject to: } \sum_{i=1}^{N} L_i = \text{ constant} \end{aligned} \tag{5.8}$$

or

$$\max_{L_i} \sum_{i=1}^{N} \sum_{k=0}^{L_i-1} |h_i(k)|^2$$
$$\text{subject to:} \sum_{i=1}^{N} L_i = \quad \text{constant} \tag{5.9}$$

5.3 Optimizing the filter lengths

In order to estimate the length L_i for adaptive filter i, we create a NEXT impulse-response profile for a given cable type, defined by

$$C_p(k) = \max \left[\frac{|h_1(k)|}{h_{\text{MAX}_1}}, \frac{|h_2(k)|}{h_{\text{MAX}_2}}, ..., \frac{|h_n(k)|}{h_{\text{MAX}_n}} \right] \tag{5.10}$$

where h_{MAX_i} is the normalizing factor given by

$$h_{\text{MAX}_i} = \max[|h_i(1)|, |h_i(2)|, ..., |h_i(\infty)|] \tag{5.11}$$

and $h_i(n)$ denotes the NEXT impulse response inclusive of the transmit and receive filters. The NEXT impulse responses used for generating $C_p(k)$ can be obtained either through crosstalk impulse-response measurements for the particular cable type, or can be generated through simulations [15].

For a cable of certain specifications, the envelopes of the NEXT impulse responses are similar to one another although of varying magnitudes. The maximum NEXT between any two twisted pairs occurs in the initial portion of the cable [21]; hence, the maximum absolute values of the NEXT impulse responses will each have a small delay that is localized around some small value on the time scale. From the NEXT profile $C_p(k)$, the peak value of the NEXT impulse responses can be found to localize around k_{max} where

$$C_p(k_{max}) = \max_i [C_p(i)] \tag{5.12}$$

Since the peak values of all the crosstalk impulse responses occur around k_{max}, we can start with adaptive filters that have filter taps positioned around k_{max}. Assuming that all the peak

values occur between $(k_{max} - M/2)$ and $(k_{max} + M/2)$, we can have NEXT cancellers with filter taps positioned between $(k_{max} - M/2)$ and $(k_{max} + M/2)$. Thus the minimum number of filter taps that each of the NEXT cancellers can have is $M + 1$.

For the ith filter, the maximum absolute value α_i of the $M + 1$ filter taps is defined as

$$\alpha_i = \max_i[|h_i(k_{max} - \frac{M}{2})|, \ldots, |h_i(k_{max})|, \ldots, |h_i(k_{max} + \frac{M}{2})|] \tag{5.13}$$

The NEXT profile in (5.10) gives the maximum possible absolute value of a normalized NEXT impulse response at each filter-tap position. As will be seen, the profile is used for obtaining the filter tap starting and ending positions of minimum length for a given maximum noise tolerance.

An adaptive canceller with filter taps starting from $(n_{start} + 1)$ and terminating at $(n_{stop} - 1)$, will not be able to cancel the NEXT impulse response before $(n_{start} + 1)$ and after $(n_{stop} - 1)$. Thus, if the NEXT impulse response is normalized so that its peak absolute value is unity then the maximum possible NEXT power that is not cancelled is given by

$$\eta_{max} = \sum_{k=0}^{n_{start}} C_p^2(k) + \sum_{k=n_{stop}}^{\infty} C_p^2(k) \tag{5.14}$$

Similarly, the maximum power η_l that is not cancelled before n_{start} is given by

$$\eta_l(n_{start}) = \sum_{k=0}^{n_{start}} C_p^2(k) \tag{5.15}$$

and the maximum power η_h that is not cancelled after n_{stop} is

$$\eta_h(n_{stop}) = \sum_{k=n_{stop}}^{\infty} C_p^2(k) \tag{5.16}$$

Using (5.15) and (5.16), we can write (5.14) as

$$\eta_{max}(n_{start}, n_{stop}) = \eta_l(n_{start}) + \eta_h(n_{stop}) \tag{5.17}$$

From (5.15), we can get a plot of η_l versus n_{start}. Since η_l is monotonically increasing with n_{start}, a unique inverse function $g_l(\eta_l)$ that gives the starting tap position n_{start} for a

maximum power η_l can be obtained from the plot, that is

$$n_{start} = g_l(\eta_l) \tag{5.18}$$

Similarly, (5.16) gives the plot of η_h versus n_{stop}, from which an inverse function $g_h(\eta_l)$ that gives the ending tap position n_{stop} is obtained; that is

$$n_{stop} = g_h(\eta_h) \tag{5.19}$$

Using (5.18) and (5.19), the filter length can be obtained as

$$n_{stop} - n_{start} = g_h(\eta_h) - g_l(\eta_l) \tag{5.20}$$

For a fixed uncancelled power λ that lies before n_{start} and after n_{stop}, finding the tap positions n_{start} and n_{stop} such that (5.20) is minimized is the optimization problem [45] of minimizing (5.20) subject to the constraint

$$\eta_l + \eta_h = \lambda \tag{5.21}$$

Assuming that the impulse response has been normalized to have its peak value at unity, the solution of the optimization problem gives the starting and ending tap positions of the minimum filter length for a maximum tolerable noise λ.

We let the solution of the optimization problem in (5.20) and (5.21) be two functions $f_{start}(\lambda_i)$ and $f_{stop}(\lambda_i)$ such that

$$n_{start,i} = f_{start}(\lambda_i) \tag{5.22}$$

and

$$n_{stop,i} = f_{stop}(\lambda_i) \tag{5.23}$$

where $n_{start,i}$ and $n_{stop,i}$ are the optimum starting and ending tap positions for adaptive filter i, and λ_i is a rescaled value of λ and defined by

$$\lambda_i = \frac{\lambda}{\alpha_i^2} \tag{5.24}$$

where α_i is given in (5.13).

Rescaling λ is necessary because $f_{start}(\lambda_i)$ and $f_{stop}(\lambda_i)$ are obtained from the crosstalk profile $C_p(k)$ which has been normalized so that its absolute peak value is unity. Therefore, in order to find the tap limits of an impulse response with a peak absolute value of α_i, we need to rescale λ according to (5.24).

We start the NEXT cancellation with each adaptive filter having $M+1$ taps positioned between $(k_{max} - M/2)$ and $(k_{max} + M/2)$. The maximum uncancelled NEXT impulse power that can be tolerated is fixed at λ for each line. To find the maximum uncancelled power from all of the lines, we first define a_i and $\bar{a}_i$ such that

$$a_i = \begin{cases} 1 & \text{if } \alpha_i^2[\sum_k C_p^2(k) - M - 1] > \lambda \\ 0 & \text{otherwise} \end{cases} \tag{5.25}$$

$$\bar{a}_i = \text{complement of } a_i \tag{5.26}$$

The expression $a_i = 1$ implies that the maximum power of the NEXT impulse response at all but the $M+1$ tap positions is greater than λ. Thus, in order to bring down the maximum uncancelled NEXT power to λ, the filter length of the adaptive filter has to be increased beyond $M+1$. This is done by using (5.22) and (5.23) which gives the starting and ending tap positions for adaptive filter i for a given value of λ and α_i.

When $a_i = 0$, the maximum uncancelled NEXT impulse response power for an adaptive filter with $M+1$ taps is less than λ and therefore the filter length is not increased but fixed at $M+1$. Thus, the maximum uncancelled power when $a_i = 0$ is given by $\alpha_i^2[\sum_k C_p^2(k) - M]$.

The total uncancelled NEXT impulse power Γ_{max} from all the lines is therefore

$$\Gamma_{max} = \sum_{i=1}^{N} a_i\lambda + \sum_{i=1}^{N} \bar{a}_i\alpha_i^2 \left[\sum_k C_p^2(k) - M - 1\right] \tag{5.27}$$

Solving (5.27) for λ can be complicated since a_i and $\bar{a}_i$ are also dependent on λ. The solution can be simplified if a_i and $\bar{a}_i$ are approximated by b_i and $\bar{b}_i$ such that

$$b_i = \begin{cases} 1 & \text{if } \alpha_i^2[\sum_k C_p^2(k) - M - 1] > \frac{\Gamma_{max}}{N} \\ 0 & \text{otherwise} \end{cases} \tag{5.28}$$

$$\bar{b}_i = \text{complement of } b_i \tag{5.29}$$

Hence,

$$\Gamma_{max} \approx \sum_{i=1}^{N} b_i \lambda + \sum_{i=1}^{N} \bar{b}_i \alpha_i^2 \left[\sum_k C_p^2(k) - M - 1 \right] \tag{5.30}$$

Solving for λ, we get

$$\lambda = \frac{\Gamma_{max} - \sum_{i=1}^{N} \bar{b}_i \alpha_i^2 \left[\sum_k C_p^2(k) - M - 1 \right]}{\sum_{i=1}^{N} b_i} \tag{5.31}$$

where

$$\sum_{i=1}^{N} b_i \neq 0 \tag{5.32}$$

Thus by knowing α_i for each adaptive filter, we use (5.31) to find λ for a given value of Γ_{max}. Once λ is obtained, we can use (5.24) to find λ_i for each adaptive filter. Knowing λ_i, we then use (5.22) and (5.23) to get the starting and ending tap positions for adaptive filter i.

5.3.1 Adjusting the tap weights on convergence

Once all the adaptive cancellers have fully converged, the tap limits can be adjusted further to reduce the mean residual error while keeping the total of all filter lengths fixed. An algorithm that minimizes $E(|e(n)|^2)$ in (5.4) by adjusting the filter lengths while keeping the total of all the filter lengths fixed is used. The algorithm scans the sum of squares of the last n filter taps on all the adaptive filters, and compares the maximum value with the minimum. Parameter n can be varied from 1 to the minimum filter length $M + 1$. If the ratio of the maximum to the minimum exceeds a certain threshold value, the adaptive filter having the minimum value is reduced in length by one tap, and the one having the maximum value is increased by one tap. It is assumed that with the new filter length the minimum mean-square error value upon convergence will be smaller than the previous value, thereby maximizing $\sum_{i=1}^{N} \sum_{k=1}^{L_i} |h_i(k)|^2$, which is also the same as solving the maximization problem in (5.9). The same procedure is repeated each time the adjusted filter taps have converged. It stops when the ratio of the maximum to the minimum value is below a prescribed threshold.

5.4 Simulation Results

In the simulations, the crosstalk impulse-response measurements were taken from measurements performed on a University of Ottawa cable [47]. After removing the d.c. component, the impulse responses were convolved with the transmit and receive filters of an HDSL2 system [36]. A total of 50 crosstalk impulse responses were used to generate the crosstalk profile defined in (5.10). A plot of the generated profile is shown in Fig. 5.1. From

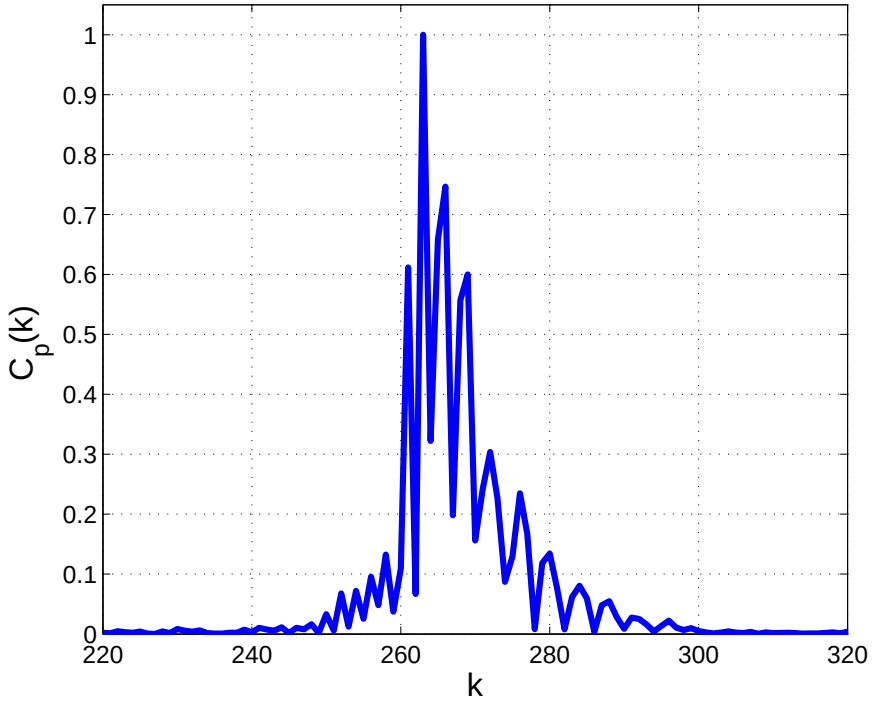

Figure 5.1. *Near-end crosstalk profile generated from 50 NEXT impulse responses.*

the crosstalk profile $C_p(k)$ defined in (5.10), functions $g_l(\eta_l)$ and $g_h(\eta_h)$ were found using (5.18) and (5.19), respectively; their plots are given in Figs. 5.2 and 5.3. Function $g_l(\eta_l)$ gives the starting tap position n_{start} for a given η_l while function $g_h(\eta_h)$ gives the ending tap position n_{stop} for a given η_h.

Once functions $g_l(\eta_l)$ and $g_h(\eta_h)$ were known, equation (5.20) was minimized with re-

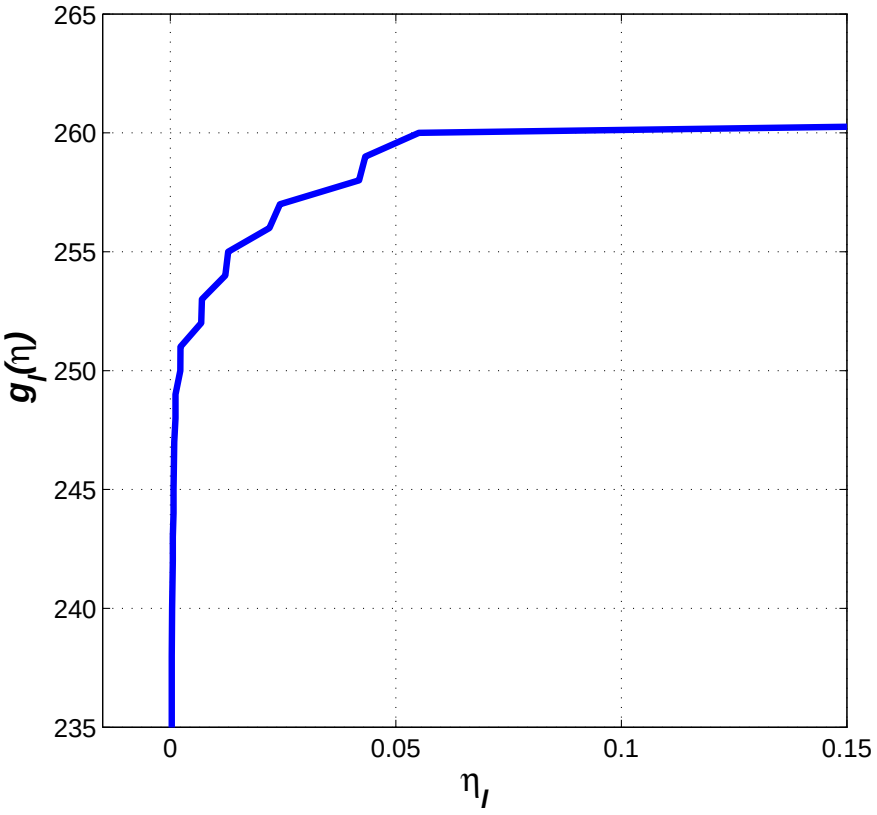

Figure 5.2. *Plot of $g_l(\eta)$ versus η_l.*

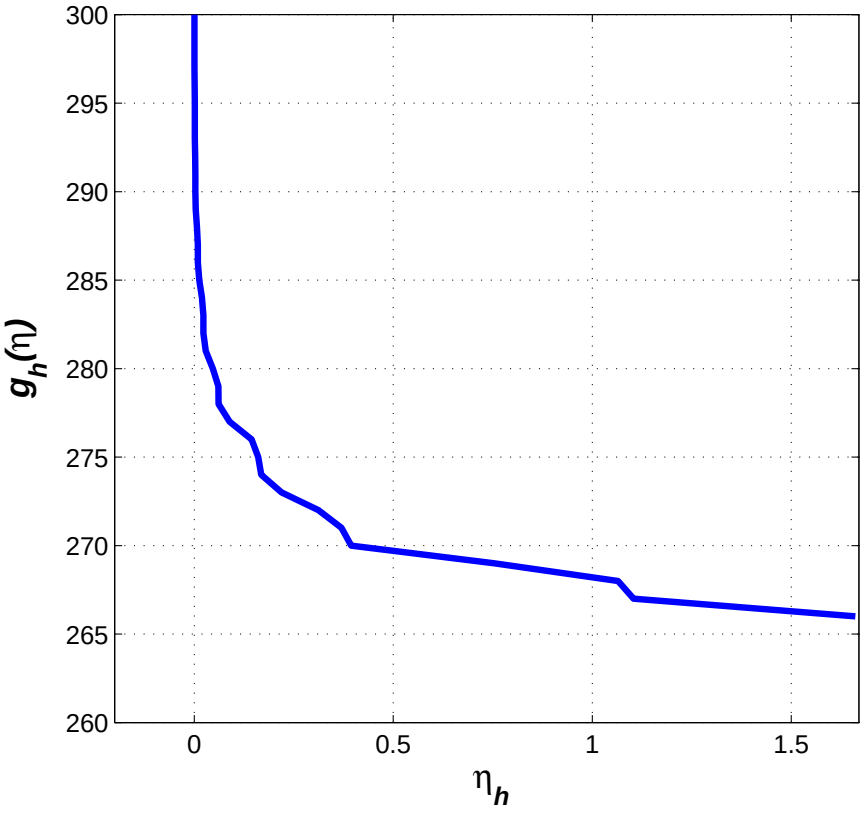

Figure 5.3. *Plot of* $g_h(\eta)$ *versus* η_h.

spect to λ where λ is defined in (5.21). This is an optimization problem whose solution are two functions $f_{start}(\lambda_i)$ and $f_{stop}(\lambda_i)$ as defined in (5.22) and (5.23), respectively. Functions $f_{start}(\lambda_i)$ and $f_{stop}(\lambda_i)$ give the starting and ending tap positions for a given λ_i. Their plots are shown in Figs. 5.4 and 5.5.

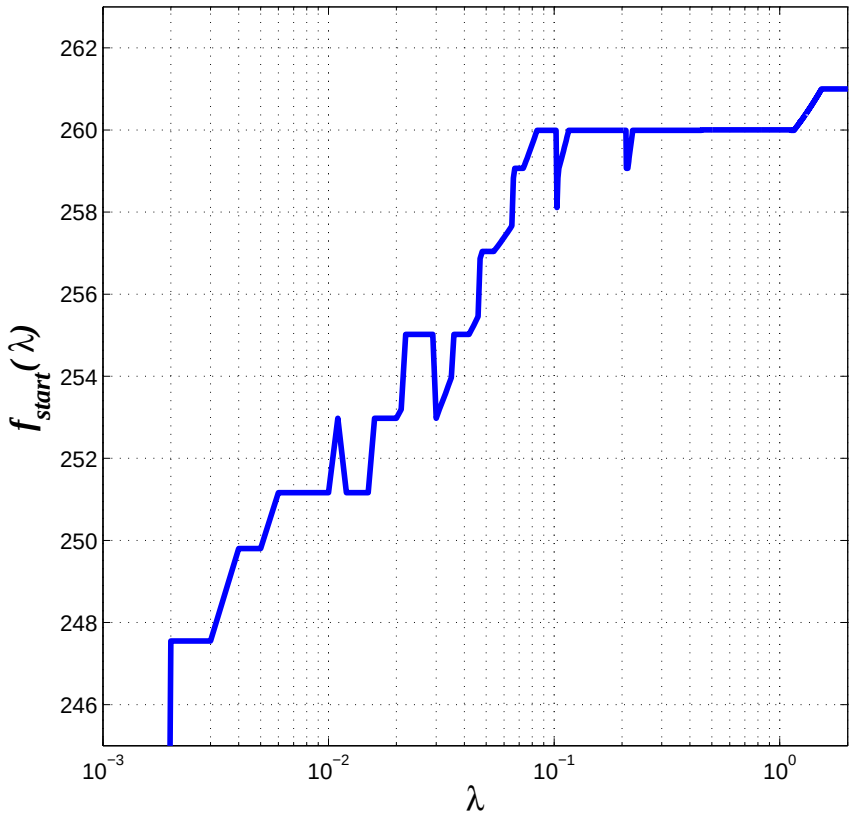

Figure 5.4. *Plot of $f_{start}(\lambda)$ versus λ.*

During the NEXT cancellation process, we can use $f_{start}(\lambda_i)$ and $f_{stop}(\lambda_i)$ to find the starting and ending tap positions for each adaptive filter. By taking the difference between the ending and starting tap positions the required filter length is obtained. A plot of this difference versus λ is shown in Fig. 5.6. Equation (5.13) gives α_i for each adaptive filter and (5.31) gives the value of λ. Using (5.24), we use the values of α_i and λ obtained to estimate λ_i for each adaptive filter. The NEXT cancellers used in the simulations were

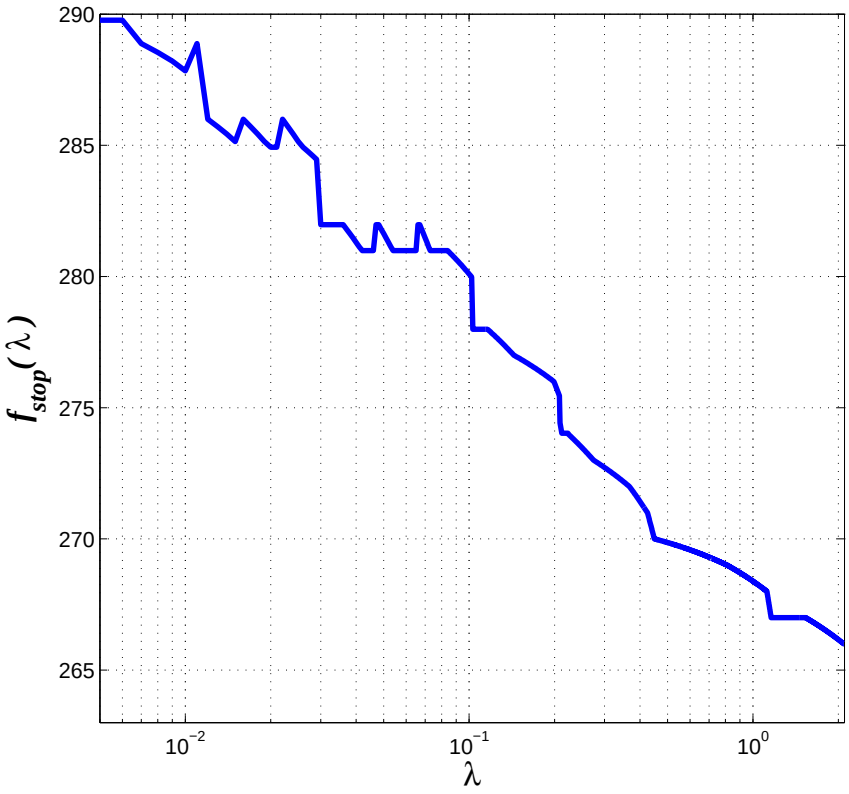

Figure 5.5. *Plot of $f_{stop}(\lambda)$ versus λ.*

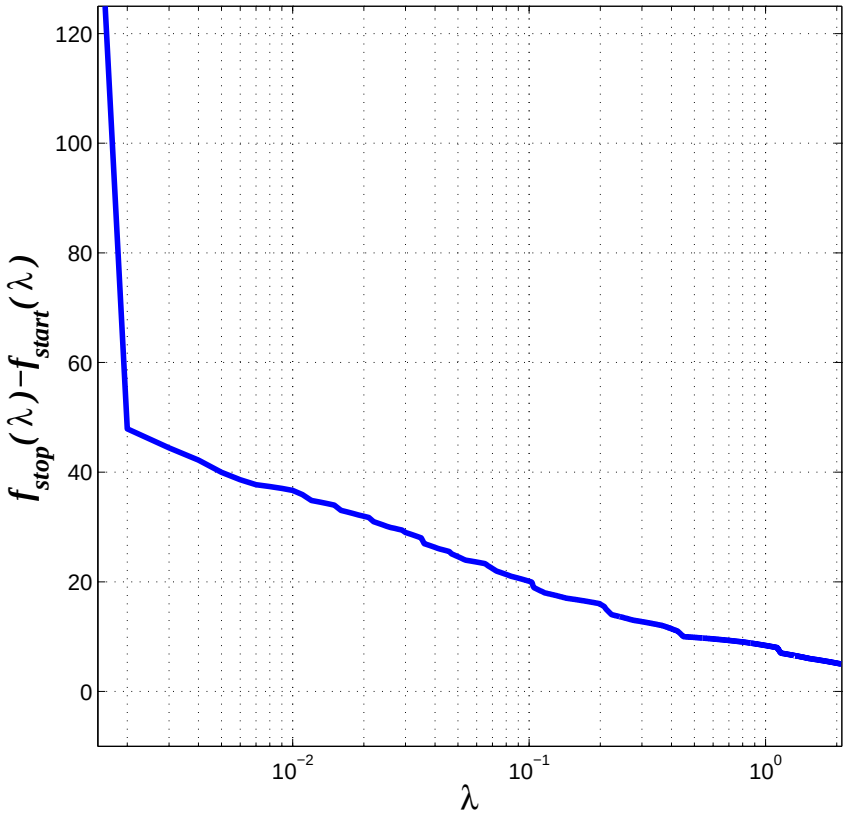

Figure 5.6. *Plot of $f_{stop}(\lambda) - f_{start}(\lambda)$ versus λ.*

normalized least mean-square (NLMS) adaptive filters [33] with the initial number of taps $M+1$ set to 3. Filter length adjustments were done after every 500 iterations of the adaptive filters. After 2000 iterations, the adaptive filters were assumed to have attained convergence and the second algorithm described in section 5.3.1 was then used; this algorithm is used to readjust the filter length of each adaptive filter while keeping the total length of all the adaptive filters fixed.

5.5 Conclusions

A new method that adjusts the length of each adaptive filter according to the magnitude of the near-end crosstalk signal has been proposed. Since the NEXT signals are typically of varying magnitudes, using the method can result in a reduction of the total filter length relative to that achieved with fixed-length adaptive filters. The NEXT cancellation is started by using adaptive filters with minimum filter lengths. As the adaptation progressed, the filter length of each adaptive filter is adjusted according to the magnitude of the NEXT signal. Upon convergence, another algorithm is initiated that readjusts the filter lengths of those adaptive filters that may be too long or too short.

Chapter 6

NEXT Mitigation using Wavelets

6.1 Introduction

The techniques presented in Chapters 3, 4, and 5 for the cancellation of NEXT require that the transmitted signals of the crosstalk sources be available to the adaptive filters cancelling the NEXT signals and if this is not the case the techniques would not be suitable.

In this chapter, a new crosstalk mitigation technique that does not require the transmitted signals from the crosstalk sources to be available is proposed. In the new technique, the noisy signal is first transformed to the wavelet domain and then an appropriate threshold technique is applied to reduce the crosstalk noise. Crosstalk noise, i.e., NEXT or FEXT, has spectral power that is typically confined to the higher end of the signal frequency band while the received signal is more concentrated at the lower end. The new threshold method takes advantage of the difference in spectral-power distribution to significantly improve the signal-to-crosstalk-noise ratio (SCNR) of the signal. Therefore, it is appropriate for reducing FEXT as well as background noise in addition to NEXT. FEXT and background noise cannot be cancelled by adaptive filters since the reference signals for these sources are generally not available. Moreover, unlike the computational complexity in NEXT cancellation with adaptive filters, the computational complexity in the wavelet technique is independent of the number of crosstalk sources (or equivalently, the number of lines in the bundle) thereby making it very efficient for bundles with a large number of twisted pairs. Another attractive feature of this technique is that unlike optimal linear estimators, such

as the Wiener filter, where prior knowledge of the magnitude and exact statistics of the crosstalk is required for optimal performance, the proposed method does not require any prior knowledge about the crosstalk magnitude but estimates it as the algorithm progresses. Furthermore, since the processing is done blockwise rather than sample-by-sample, the technique has a low computational complexity. And with the use of new fast wavelet transform algorithms such as those in [48] [49], which have complexity of the order of $L \log L$ where L is the length of a block of data, the technique can be very efficient and fast.

This chapter is organized as follows: Section 6.2 describes the characteristics of NEXT and FEXT, namely, their frequency distributions, and their Gaussian nature. Section 6.3 presents the various wavelet denoising techniques for NEXT reduction. Simulation results are presented and discussed in section 6.4 while conclusions are drawn in section 6.5.

6.2 Gaussian Nature of Crosstalk

In a transmission cable, the communication channel is subjected to crosstalk interference from multiple twisted pairs. Due to the presence of multiple crosstalk interferers, the NEXT tends to be a Gaussian random process [50]. Assuming that the transmitted signals in all the interfering pairs have the same power density spectrum, the NEXT PSD $S_N(f)$ for sufficiently long loops of 1000 feet or more can be expressed as

$$S_N(f) \approx \chi S(f) f^{\frac{3}{2}} \tag{6.1}$$

where χ is a Gaussian random variable which is a function of the disturbed pair under consideration and $S(f)$ is the PSD of the input voltage of the interfering pairs. Expression (6.1) has been found to be quite accurate for the kind of multi-interference NEXT that is observed in practice [17]. Similarly, a corresponding expression for FEXT is given by

$$S_F(f) = \psi S(f) f^2 d e^{-2\zeta\sqrt{f}d} \tag{6.2}$$

where ψ is a Gaussian random variable which is a function of the disturbed pair under consideration, d is the cable length, and ζ is the proportionality constant. As such, the filters

defined by (6.1) and (6.2) can be used to simulate NEXT and FEXT signals, respectively, by using white Gaussian noise as the input signal.

Since NEXT is more dominant than FEXT, the focus in this chapter is on NEXT reduction. However, the proposed technique can also be used to mitigate FEXT in environments where the crosstalk interference is predominantly FEXT, for example, in an ADSL environment.

Unlike the power in NEXT signals, that of the received signal is more attenuated in the higher frequency regions of the transmission band. This is because the amplitude response of a twisted-pair channel usually decreases with frequency. Typically, the attenuation is approximately proportional to $\sqrt{f}$ [17].

6.3 Crosstalk Mitigation Using Wavelets

Since the paper of Donoho et al. on wavelet denoising in 1993 [51], the use of wavelet techniques for the removal of noise from a signal has become increasingly popular. One reason is that it provides a quasi-optimal minmax estimate of a noisy piecewise-smooth signal on a wavelet basis, which for certain classes of signals even outperforms linear estimators [52]. Another reason is the flexibility in choosing the wavelets. Depending upon the nature of the signal, the most appropriate wavelet that minimizes the number of coefficients can be selected and used for removing the noise [53].

When denoising a signal, it is important to have a knowledge of the nature of the noise. Consider a noise-corrupted signal $x(n)$ which can be modelled as

$$x(n) = s(n) + w(n) \tag{6.3}$$

where $s(n)$ is the noise-free signal and $w(n)$ is the noise. If $w(n)$ is an additive white Gaussian noise, the wavelet transform of $w(n)$ will also be white Gaussian with the same magnitude across all levels. Hence, (6.3) can be expressed in the wavelet domain as

$$\kappa(n) = \delta(n) + \gamma(n) \tag{6.4}$$

where $\kappa(n)$ is the wavelet transform of $x(n)$, $\delta(n)$ is the wavelet transform of $s(n)$, and $\gamma(n)$ is the wavelet transform of $w(n)$. It should be noted that $\gamma(n)$, like $w(n)$, will also be white Gaussian with the same variance.

In order to reconstruct $s(n)$ from measures of $x(n)$, it is necessary to remove the noise contribution from $\kappa(n)$. Donoho and Johnstone have proposed two types of shrinkage functions for a given threshold λ [54]:

- Soft thresholding, which is defined by

$$y_S(n) = \begin{cases} \text{sgn}[y(n)](|y(n)| - \lambda) & \text{if } |y(n)| > \lambda \\ 0 & \text{if } |y(n)| \leq \lambda \end{cases} \tag{6.5}$$

- Hard thresholding, which is defined by

$$y_H(n) = \begin{cases} y(n) & \text{if } |y(n)| > \lambda \\ 0 & \text{if } |y(n)| \leq \lambda \end{cases} \tag{6.6}$$

In order to determine the threshold λ, we use the so called universal threshold proposed by Donoho and Johnstone, which is given by [55]

$$\lambda_{univ} = \sigma\sqrt{2\log_{10} N} \tag{6.7}$$

where

$$\sigma = \frac{\text{MAD}(\boldsymbol{\kappa}_L)}{0.6745} \tag{6.8}$$

N is the length of the signal, L is the finest wavelet scale, $\boldsymbol{\kappa}_L$ is a vector whose elements are the wavelet coefficients of the finest scale, and MAD is the median absolute deviation of the coefficients. Equation (6.8) follows from the fact that the wavelet coefficients are Gaussian random variables and thus the MAD is proportional to the standard deviation σ.

If the noise disturbance is correlated, the noise level across the different levels would be different and, as such, the threshold defined in (6.7) would not be effective. Instead, a level-dependent threshold is used. A popular level-dependent threshold method proposed by Johnstone and Silverman [56], which assumes that the noise is Gaussian distributed, is given by

$$\lambda_{i_{univ}} = \sigma_i\sqrt{2\log n_i} \tag{6.9}$$

where

$$\sigma_i = \frac{\text{MAD}(\boldsymbol{\kappa}_i)}{0.6745} \tag{6.10}$$

and $\boldsymbol{\kappa}_i$ is a vector whose elements are the wavelet coefficients for level i.

Another method of estimating λ_i is to apply Stein's unbiased risk estimate (SURE) threshold method. As described in [57], the SURE estimate, although first investigated for white Gaussian noise settings [58], remains unbiased even with correlated Gaussian noise; it is given by

$$\lambda_{i_{SURE}} = \sigma_i t(\frac{w_i}{\sigma_i}) \tag{6.11}$$

where

$$t(x) = \text{argmin}_{\ 0 \le t \le \sqrt{2\log d}}\ U(t) \tag{6.12}$$

and

$$U(t) = n_i + \sum_k \left\{\min(x_k^2, t^2) - 2I(|x| \le t)\right\} \tag{6.13}$$

where I is the indicator function ($I(\cdot) = 1$ if $|x_k| \le t$ and $I(\cdot) = 0$ if $|x_k| > t$), and n_i is the number of coefficients at level i.

6.3.1 Estimate of the crosstalk noise across the wavelet levels

Since the NEXT noise has greater power towards the higher end of the frequency spectrum, the magnitude of the wavelet coefficients at the higher wavelet levels will be predominantly due to NEXT. However, there are instances where the magnitude of the NEXT noise in a twisted pair is small or the received signal is large. In such cases, the magnitude of the wavelet coefficients at the higher levels will also have significant contributions from the received signal. As such, using the lowest level wavelet coefficients to estimate the NEXT noise will not always be accurate, especially, when the SCNR of the received signal is high.

In order to get a fairly accurate estimate of the magnitude of the NEXT noise in each wavelet level, we take advantage of the fact that the spectral power of the NEXT signal is confined to the higher end of the frequency spectrum while the power of the received signal

is confined to the lower end. Hence, first, the typical distributions of the NEXT magnitudes across the different wavelet levels are estimated. This is done by passing white Gaussian noise through a filter with NEXT PSD as given in (6.1), taking its wavelet transform, and then using the wavelet-transformed signal to evaluate the NEXT distribution ratio α_i, given by

$$\alpha_i = \frac{\text{MAD}(\boldsymbol{\gamma}_i)}{\text{MAD}(\boldsymbol{\gamma}_L)} \tag{6.14}$$

where $\boldsymbol{\gamma}_i$ is a vector whose elements are the wavelet coefficients of the wavelet-transformed crosstalk noise for level i, and L the finest (highest) level. Next, the distributions of the magnitude of the received signal across the wavelet levels are estimated. This is done by taking the wavelet transform of the received signal and evaluating the ratio β_i given by

$$\beta_i = \frac{\text{MAD}(\boldsymbol{\delta}_i)}{\text{MAD}(\boldsymbol{\delta}_L)} \tag{6.15}$$

where $\boldsymbol{\delta}_i$ is a vector whose elements are the wavelet coefficients of the wavelet-transformed received signal for level i. Thus, by using the ratios α_i and β_i it is possible to estimate the powers of the NEXT signal and the received signal at a particular wavelet level.

Suppose a received signal $x(n)$ corrupted by NEXT noise is transformed such that the wavelet coefficients for level i are represented by vector $\boldsymbol{\kappa}_i$; in such a case, the MAD estimate σ_{xi} is given by

$$\sigma_{xi}^2 = \text{MAD}(\boldsymbol{\kappa}_i) \tag{6.16}$$

If σ_{Ni}^2 and σ_{Si}^2 are the NEXT signal power and the received signal power, respectively, for level i, then σ_{xi}^2 will be the sum of σ_{Ni}^2 and σ_{Si}^2, i.e.,

$$\sigma_{xi}^2 = \sigma_{Ni}^2 + \sigma_{Si}^2 \tag{6.17}$$

By using (6.14), (6.15), and (6.17), we have the following two equations for the ith and Lth levels:

$$\sigma_{NL}^2 + \sigma_{SL}^2 = \sigma_{xL}^2 \tag{6.18}$$

$$\alpha_i^2\sigma_{NL}^2 + \beta_i^2\sigma_{SL}^2 = \sigma_{xi}^2 \tag{6.19}$$

Solving (6.18) and (6.19), the crosstalk noise power estimate for level i is given by

$$\sigma_{Ni}^2 = \alpha_i^2 \sigma_{NL}^2 = \alpha_i^2 \frac{\beta_i^2 \sigma_{xi}^2 - \sigma_{xL}^2}{\beta_i^2 - \alpha_i^2} \tag{6.20}$$

Once the powers of the crosstalk noise at the different levels have been estimated, the threshold values for the various levels are computed. Both the universal and the SURE threshold estimates, given in (6.9) and (6.11), respectively, can be used. However, in situations of extreme sparcity in the wavelet coefficients of the desired signal, which happens when the SNR of the received signal is low, the SURE principle described in (6.11) has a serious drawback [58]: the noise contributed to the SURE profile by the many coordinates at which the signal is zero swamps the information contributed to the SURE profile by the few coordinates where the signal is nonzero. Hence, in such cases the universal threshold given in (6.9) would be a more accurate threshold estimate. Consequently, a hybrid scheme similar to the one proposed in [58] can be adopted; that is, when the SNR of the signal is below a certain threshold the universal threshold estimate is used, and when the SNR is above the threshold the SURE estimate is used. In equation form, this is given by

$$\lambda_i = \begin{cases} \lambda_{i_{SURE}} & \text{if SNR} > \Gamma \\ \lambda_{i_{univ}} & \text{if SNR} \leq \Gamma \end{cases} \tag{6.21}$$

where Γ is an appropriately selected threshold. Since the SNR of the received signal is not readily available, an approximate estimate can be obtained by solving equations (6.18) and (6.19) for σ_{Ni}^2 and σ_{Si}^2, respectively, and taking their ratios; that is,

$$\text{SNR} \approx k \frac{\sigma_{SL}^2}{\sigma_{NL}^2} \tag{6.22}$$

where k is some constant which can be determined empirically.

6.4 Simulation Results

The NEXT-corrupted received signal for the simulations was generated as shown in Fig. 6.1. As can be seen in the figure, the received signal was generated by passing a zero-mean uniformly distributed random sequence through a channel filter. The channel filter was used

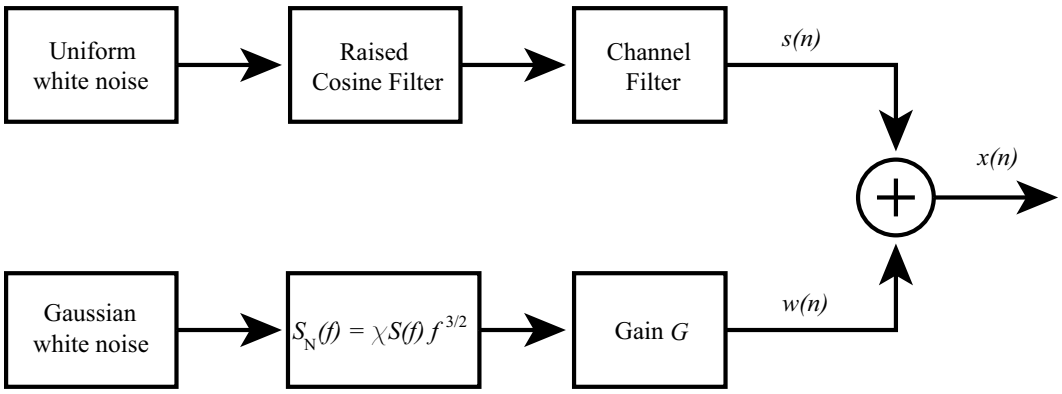

Figure 6.1. *Block diagram for generating NEXT-interfered received signals.*

to model a twisted pair channel of length 7600 feet and gauge 26 AWG. The NEXT signal was generated by passing white Gaussian noise through a filter with PSD as given in (6.1). The term $S(f)$ in (6.1) represents the combined PSD of the HDSL2 mask, the transmit filter, and the receive filter. The NEXT-interfered received signal was obtained by adding the NEXT noise $w(n)$ with the clean signal $s(n)$. By adjusting the gain G, the magnitude of the NEXT noise (or correspondingly the SNR of the received signal) can be adjusted.

The NEXT noise distribution ratio α_i and the received signal distribution ratio β_i were evaluated for a particular wavelet using (6.14) and (6.15), respectively. The two ratios were evaluated beforehand, and were required in order to estimate the crosstalk noise power at the various wavelet levels.

In order to study the wavelet technique, two simulation experiments, Experiments A and B, were conducted as detailed below.

Experiment A

In Experiment A, two threshold methods, namely, the universal and SURE threshold methods were tested. The setup used is shown in Fig. 6.2. In both methods, the noisy signal was divided into blocks, each of length 2048, and by using WAVELAB[1] the discrete wavelet

[1] Available from the Stanford Statistics Department, courtesy of D. L. Donoho and I. M. Johnstone

transform was applied on each block. The NEXT-noise powers for levels 7, 8, 9 and 10 were then estimated using (6.20). Once the NEXT-noise powers at the different levels were estimated, the threshold values were next evaluated using two threshold methods, namely, the universal and SURE threshold methods. To reduce (or shrink) the wavelet coefficients the soft thresholding method in (2.4) was used. Tables 6.1 and 6.2 show a comparison of the two threshold methods for the Battle-Lemarie wavelet and the Daubechies wavelet of order 10, respectively. On comparing the SNRs in Tables 6.1 and 6.2, it can be seen that the Battle-Lemarie wavelet gives better SNR improvement (by a few dBs) than the Daubechies wavelet of order 10. It is also observed that at high SNRs, the SURE threshold method gives better SNR improvement whereas at very low SNRs the universal threshold method outperforms the SURE method. Hence, by adopting the hybrid technique in (6.21), the best of the two threshold methods can be utilized.

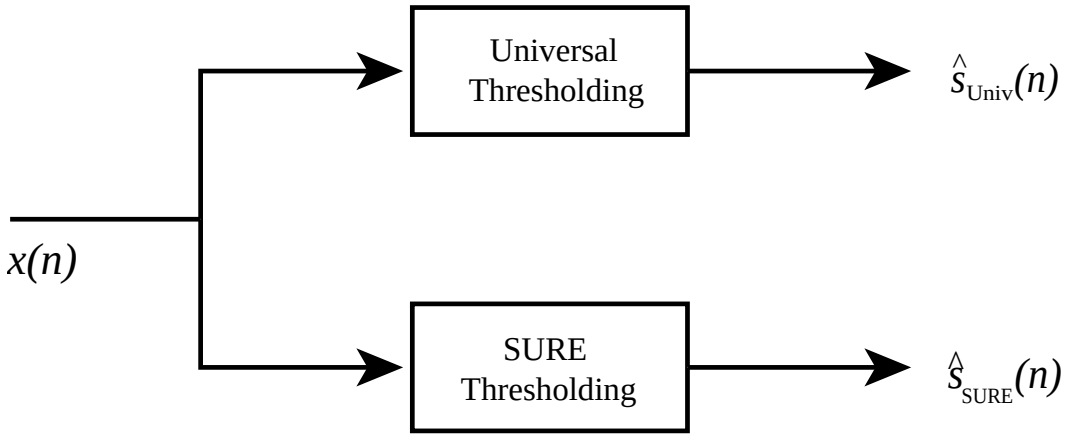

Figure 6.2. *Simulation setup for comparing the performance between the universal and SURE estimates in reducing NEXT.*

Experiment B

In Experiment B, the SNR was evaluated by passing both the noisy and denoised signals through a matched filter, that is, a filter that maximizes the SNR of the received signal. A block diagram of the simulation setup used is shown in Fig. 6.3. In our simulations, the

Table 6.1. *Comparison between the universal and SURE estimates, using the Battle-Lemarie wavelet.*

$\text{SNR}_{x(n)}$ (dB)	$\text{SNR}_{\hat{s}_{univ}(n)}$ (dB)	$\text{SNR}_{\hat{s}_{SURE}(n)}$ (dB)
-25	13.9	-3
-5	19.8	15.8
0.03	21.2	19.36
10	23.36	24.3
20	26.2	31.8

Table 6.2. *Comparison between the universal and SURE estimates, using the Daubechies wavelet of order 10.*

$\text{SNR}_{x(n)}$ (dB)	$\text{SNR}_{\hat{s}_{univ}(n)}$ (dB)	$\text{SNR}_{\hat{s}_{SURE}(n)}$ (dB)
-25	14.02	-3.3
-5	18.8	15.29
0.03	20.37	18.48
10	22.53	23.95
20	25	28.68

causal matched filter was realized by using the expression

$$f(t) = h(C - t) \tag{6.23}$$

where C is some constant and $h(t)$ is the received pulse shape of finite length of a single data symbol. To select the threshold, the hybrid estimate as given in (6.21) was used. The

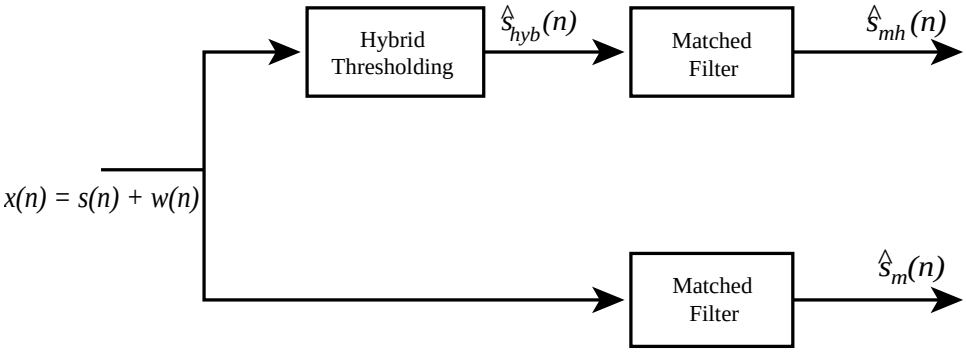

Figure 6.3. *Block diagram of the simulation setup for comparing the SNR performance between the noisy signal and the denoised signal (the Battle-Lemarie wavelet was used).*

measured SNRs of the received signal are given in Table 6.3. From the table, it can be seen that for low SNRs, the wavelet-denoised signal $\hat{s}_{mh}(n)$ has significantly better SNR than the noisy signal $\hat{s}_m(n)$. However, as the SNR of the received signal increases, the SNR improvement obtained by using the wavelet-denoising method decreases. And when the SNR becomes relatively high as in row 5 of Table 6.3, the denoised signal has a much lower SNR than the noisy signal. The power spectra of $\hat{s}_m(n)$ and $\hat{s}_{mh}(n)$ are compared in Figs. 6.4 and 6.5 for two SNRs of the noisy signal $x(n)$; the power spectra of a clean (NEXT-free) received signal is also shown in both the figures to serve as a reference. The SNR of $x(n)$ in Fig. 6.4 is -5 dB while in Fig. 6.5 it is 10 dB. From the two figures, it can be seen that at a low SNR of -5 dB there is greater spectral improvement in using the wavelet technique than at a higher SNR of 10 dB, in agreement with the results in Table 6.3.

Table 6.3. *Effectiveness of the wavelet denoising technique in reducing NEXT.*

$\text{SNR}_{x(n)}$ (dB)	$\text{SNR}_{\hat{s}_{hyb}(n)}$ (dB)	$\text{SNR}_{\hat{s}_{mh}}(n)$ (dB)	$\text{SNR}_{\hat{s}_m}(n)$ (dB)
-25	13.9	27.37	17
-5	15.8	43.7	37
0.03	19.36	46.53	42.03
10	24.3	52.41	52.04
20	31.8	57.47	62

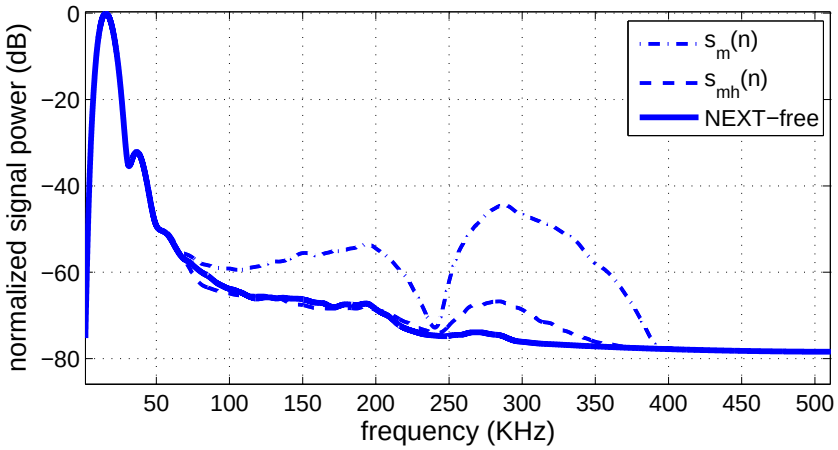

Figure 6.4. *PSD of the noisy signal, denoised signal, and crosstalk-free signal after both are passed through the matched filters (the SNR of the noisy signal was* -5 *dB).*

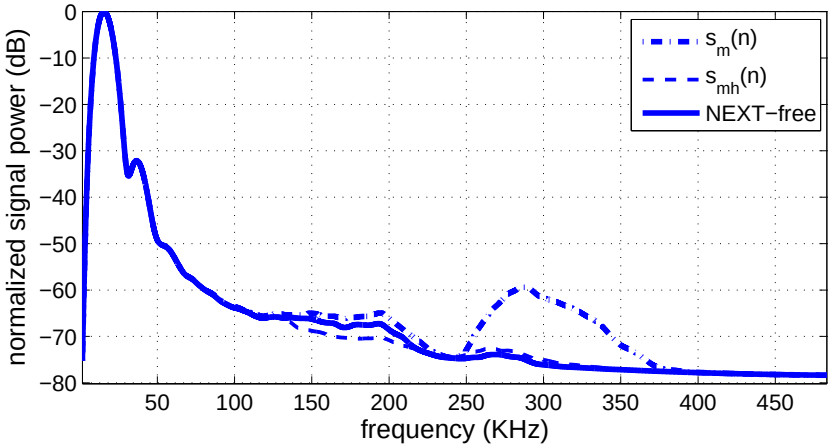

Figure 6.5. *PSD of the noisy signal, denoised signal, and crosstalk-free signal after they are passed through the matched filter (the SNR of the noisy signal was* 10 *dB).*

6.5 Conclusions

A new method to mitigate near-end crosstalk noise in xDSL systems was proposed. The method entails using wavelet denoising techniques to reduce the crosstalk noise in the received signal. Unlike the received signal, which has greater spectral power in the lower end of the frequency spectrum, NEXT power typically increases with frequency; the proposed method uses a wavelet denoising technique that takes advantage of this difference in spectral power distribution to mitigate the crosstalk noise. Furthermore, the wavelet technique has a low computational complexity which makes it efficient, fast, and well suited for high data-rate applications. Simulation results confirmed the effectiveness of the proposed method in reducing the NEXT noise, especially, in low SNR conditions where NEXT mitigation is critical. As the SNR of the received signal increases, the effectiveness of the proposed method decreases; however, in high SNR conditions NEXT mitigation is not as critical and is usually not required.

Chapter 7

Conclusions

Various NEXT cancellation techniques that reduce the computational complexity, increase the convergence rate, and improve the tracking performance were developed. The various techniques are

A) Cancellation using adaptive filters

B) Cancellation using FDLMS adaptive filters

C) Cancellation using variable-length cancellers

D) Mitigation using wavelets

Technique A is an efficient NEXT cancellation technique. The new system first detects the NEXT present in the received signal and then assigns adaptive filters to cancel the most significant NEXT signals detected. The detection of the NEXT signals is done by using a low computational complexity crosscorrelation technique. By subtracting the adaptive filter estimates of the NEXT signals that have been detected and assigned adaptive filters for cancellation, the magnitude of smaller NEXT signals can be estimated more accurately during the NEXT detection stage. The new system offers an overall computational complexity of order N where N is the number of twisted pairs in the bundle. This represents a large reduction in the computational effort relative to that in previous NEXT cancellation system which offered computational complexities of order N^2.

Technique B is based on the same NEXT cancellation system as Technique A but uses frequency-domain instead of time-domain adaptive filters to cancel the NEXT signals. The technique is suitable for NEXT cancellation in high data-rate DSL systems where the re-

quired adaptive filter length easily exceeds 40. Also, several schemes of assigning the adaptive filter step sizes were explored. It was found that by making the step sizes proportional to the magnitude of the NEXT signals during the initial phases of adaptation and equal later on, the convergence rate is significantly improved. And by returning after convergence to step sizes that are proportional to the magnitudes of the NEXT signals, a much better tracking performance is achieved. Adaptive filters with variable step sizes can become unstable and finding the conditions that will assure the stability of the NEXT cancellation system is of importance. This problem was solved by deriving the stability bounds for the adaptive filter step sizes.

Technique C reduces the computational load in a NEXT cancellation system. It entails adjusting the filter length of each adaptive filter according to the strength of the NEXT signal, thereby resulting in a minimum usage of filter taps. To estimate the adaptive filter length required, a normalized NEXT profile is created by normalizing and then combining many NEXT impulse responses for a particular cable. The NEXT profile is used for computing the start and end tap positions for a given maximum NEXT noise threshold. The algorithm starts the NEXT cancellation by using adaptive filters with minimum filter lengths. As the adaptation progresses, the algorithm adjusts the filter length of each adaptive filter according to the magnitude of the NEXT signal, based on the NEXT profile. And when all the adaptive filters have fully converged, another algorithm is used to readjust the filter length of those adaptive filters that are too long or too short.

Technique D entails using wavelet denoising techniques to reduce the crosstalk noise in the received signal. Unlike the received signal which has greater power in the lower end of the frequency spectrum, NEXT signals typically have greater power in the higher end. The proposed method uses a wavelet denoising technique that takes advantage of this difference in frequency spectra to mitigate the crosstalk noise. The performance of the technique is very much dependent on the type of wavelet used; that is, wavelets that are more correlated with the received signal and less correlated with the NEXT signals give better performance. Unlike the previous three techniques, Technique D is a blind technique,

which does not require the transmitted signals of the crosstalk sources to be available. Furthermore, the technique has a low computational complexity that is independent of the number of crosstalk sources, which makes it efficient, fast, and well suited for high data-rate applications.

7.1 Suggestions for Future Research

Due to the high numerical complexity associated with NEXT cancellation, more work needs to be done to reduce the required computational effort further. Infinite impulse response (IIR) adaptive filters present a better alternative to FIR adaptive filters due to their capability to accurately model the NEXT transfer function with a much lower filter order. For example, in high data rate systems where the required FIR adaptive filter length easily exceeds 100, using an IIR adaptive filter of order less than 20 will, in most cases, provide the same level of NEXT reduction, if not more. One major drawback of IIR adaptive filters, however, is the possible existance of multiple local minima or when the reference signal to the adaptive filter is colored [60][61]. Another drawback is the potential instability associated with IIR adaptive filters which would necessitate computationally expensive stability checks at every iteration [62]. Further research should consider ways to ensure that the IIR adaptive filters always converge to the global minimum and if this is not possible to a good suboptimal minimum. Also, new ways to reduce the computational effort required to assure filter stability should be explored.

Another area for further research is crosstalk mitigation using wavelet techniques. From the simulation results presented in section 6.4, it is observed that using the Battle-Lemarie wavelet resulted in better NEXT removal than using the Daubechies wavelet of order 10. These observations indicate that by using wavelet bases that take into consideration the nature of the NEXT and received signals, improved SNR performance can be obtained. In effect, future work should explore wavelet bases that are more specific to crosstalk mitigation. One approach is to refine the current best basis selection techniques [63][53] to take

into account the nature of both the crosstalk and the received signal.

References

[1] ITU, “Overview of digital subscriber line (DSL) recommendations,” *ITU-T Recommendation G.995.1*, Jun. 1999.

[2] ITU, “Digital transmission system on metallic local lines for ISDN basic rate access,” *ITU-T Recommendation G.961*, Mar. 1993.

[3] ITU, “High bit rate digital subscriber line transceivers,” *ITU-T Recommendation G.991.1*, Oct. 1998.

[4] M. Tomlinson, “New automatic equalizer employing modulo arithmetic,” *Electron. Lett.*, vol. 7, nos. 5 and 6, pp. 138-139, Mar. 1971.

[5] A. J. Viterbi, “Convolutional codes and their performance in communication systems,” *IEEE Trans. Commun.*, vol. COM-19, pp. 751-772, Oct. 1971.

[6] G. H. Im and J. J. Werner, “Bandwidth-efficient digital transmission over unshielded twisted-pair wiring,” *IEEE J. Select. Areas Commun.*, vol. 13, pp. 1643-1655, Dec. 1995.

[7] G. Ungerboeck, “Trellis-coded modulation with redundant signal sets. I. Introduction,” *IEEE Commun. Mag.*, vol. 25, pp. 5-11, Feb. 1987.

[8] I. Kalet, “The multitone channel,” *IEEE Trans. Commun.*, vol. 37, pp. 119-124, Feb. 1989.

[9] “Telcordia’s 26-gauge pair-to-pair NEXT coupling magnitude and phase measurements,” Weblink: http://net3.argreenhouse.com:8080/dsl-test/Help/helpterms.htm

[10] A. Ruiz, J. M. Cioffi, and S. Kasturia, “Discrete multiple tone modulation with coset coding for the spectrally shaped channel,” *IEEE Trans. Commun.*, vol. 40, pp. 1012-1029, Jun. 1992.

[11] ANSI, “Spectrum management for loop transmission systems,” *T1E1.4/99-002R6.*

[12] W. Y. Chen, “Twisted-pair channel models for VDSL,” *IEEE Texas Instruments T1E1 Contribution - T1E1.4/96-134*, Apr. 1996.

[13] IBM, “Some transmission characteristics of telephone cables used in the loop plant,” *IBM T1D1 Contribution - T1D1.3/86-003*, Jan. 1986.

[14] Bellcore, “ISDN basic access digital subscriber lines,” *Bellcore Technical Reference - TR-TSY-000393*, Issue 1, May 1998.

[15] W. Y. Chen, *Simulation Techniques and Standards Development for Digital Subscriber Lines*, Macmillan Technical Publishing 1998.

[16] W. Henkel, S. Olcer, K. S. Jacobsen, and B. R. Saltzberg, "Twisted pair transmission - ever increasing performance on ancient telephone wires," *IEEE J. Select. Areas Commun.*, vol. 20, no. 5, pp. 877-880, Jun. 2002.

[17] J-J Werner, "The HDSL Environment," *IEEE J. Select. Areas Commun.*, vol. 9, no. 6, pp. 785-800, Aug. 1991.

[18] J. T. Aslanis and J. M. Cioffi, "Achievable information rates on digital subscriber loops: limiting information rates with crosstalk noise," *IEEE Trans. Commun.*, vol. 40, no. 2, pp. 361-372, Feb. 1992.

[19] H. Takatori, "Spectrum compatibility from HDSL2 to T1," *Level One - T1E1.4/96-345*, Nov. 1996.

[20] G. A. Zimmerman, "HDSL2 Tutorial: Spectral compatibality and real-world performance advances," Pairgain Technologies, Jun. 1998.

[21] J. A. Bingham, *ADSL, VDSL, and Multicarrier Modulation*, Wiley, 1999.

[22] A. Antoniou, *Digital Signal Processing: Signals, Systems, and Filters*, McGraw-Hill, 2005 (in press).

[23] C. Zeng and J. M. Cioffi, "Near-end crosstalk mitigation in xDSL systems," *IEEE J. Select. Areas Commun.*, vol. 20, no. 5, pp. 949-958, Jun. 2002.

[24] S. Galli, C. Valenti, and K. J. Kerpez, "A frequency-domain approach to crosstalk identification in xDSL systems," *IEEE J. Select. Areas Commun.*, vol. 19, no. 8, pp. 1497-1506, Aug. 2001.

[25] S. Galli and K. J. Kerpez, "Methods of summing crosstalk from mixed sources - Part 1: Theoretical Analysis," *IEEE Trans. Commun.*, vol. 50, no. 3, pp. 453-461, Mar. 2002.

[26] M. L. Honig, K. Steiglitz, and B. Gopinath, "Multichannel signal processing for data communication in the presence of crosstalk," *IEEE Trans. Commun.*, vol. 38, no. 4, pp. 551-558, April 1990.

[27] R. C. Nongpiur, D. J. Shpak, and A. Antoniou, "NEXT cancellation in xDSL systems," *Proc. 36th Asilomar Conference on Signals, Systems and Computers*, Pacific Grove, CA., vol. 1, pp. 393-397, Nov. 3-6, 2002.

[28] C. Zeng, C. Aldana, A. A. Salvekar, and J. M. Cioffi, "Crosstalk identification in xDSL systems," *IEEE J. Select. Areas Commun.*, vol. 19, no. 8, pp. 1488-1496, Aug. 2001.

[29] D. Hertz, "A fast digital method of estimating the autocorrealtion of a Gaussian sta-

tionary process," *IEEE Trans. Acoust., Speech, Signal Processing*, vol. ASSP-30, no. 2, Apr. 1982.

[30] G. Jacovitti, A. Neri, and R. Cusani, "On a fast digital method of estimating the autocorrelation of Gaussian stationary process," *IEEE Trans. Acoust., Speech, Signal Processing*, vol. ASSP-32, no. 5, Oct. 1984.

[31] T. J. Shan and T. Kailath, "Adaptive algorithms with an automatic gain control feature," *IEEE Trans. Circuits Syst.*, vol. 35, no. 1, pp. 122-127, Jan. 1988.

[32] R. C. Nongpiur, D. J. Shpak, and A. Antoniou, "Near-end crosstalk cancellation using variable-length cancellers," *2003 IEEE Int. Symp. on Circuit and Systems (ISCAS)*, Bangkok, Thailand, pp. IV-345 - IV-348, vol. 4, May 25-28, 2003.

[33] S. Haykin, *Adaptive Filter Theory*, Third Edition, Prentice Hall, 1996.

[34] J. J. Shynk, "Frequency-domain and multirate adaptive filtering," *IEEE Signal Processing Mag.*, vol. 9, no. 1, pp. 14-37, 1997.

[35] R. C. Nongpiur, D. J. Shpak, and A. Antoniou, "NEXT cancellers using FDLMS filters with improved convergence rate," *Proc. 37th Asilomar Conference on Signals, Systems and Computers*, Pacific Grove, CA., Nov 9-12, 2003.

[36] "Draft for HDSL2 Standard," *T1E1.4/99-006R5*.

[37] R. C. Nongpiur, D. J. Shpak, and A. Antoniou, "NEXT cancellation in xDSL systems," *Proc. 36th Asilomar Conference on Signals, Systems and Computers*, Pacific Grove, CA., Nov. 3-6, 2000.

[38] N. J. Bershad and P. L. Feintuch, "A normalized frequency domain LMS adaptive algorithm," *IEEE Trans. Acoust., Speech, Signal Processing*, vol. ASSP-34, no. 3, Jun. 1986.

[39] N. J. Bershad and P. L. Feintuch, "Analysis of the frequency domain adaptive filter," *Proc. IEEE*, vol. 67, no. 12, Dec. 1979.

[40] D. L. Duttweiler, "Proportionate normalized least-mean-squares adaptation in echo cancellers," *IEEE Trans. Speech Audio Processing*, vol. 8, no. 5, Sep. 2000.

[41] B. Widrow, J. McCool, and M. Ball, "Stationary and nonstationary learning characteristics of the LMS adaptive filter," *Proc. IEEE*, vol. 64, pp. 1151-1162, 1976.

[42] R. C. Nongpiur, D. J. Shpak, and A. Antoniou, "NEXT cancellation system with improved convergence rate and tracking performance," *IEE Proc.-Commun.*, Vol. 152, No. 3, June 2005.

[43] R. C. Nongpiur, D. J. Shpak, and A. Antoniou, "Tracking Performance for the FDLMS near-end crosstalk canceller for xDSL Systems," *2004 IEEE Intl. Symp. on Circuit and Systems (ISCAS)*, Vancouver, Canada, vol. 3, pp. 23-26, May 2004.

[44] O. Macchi, "Optimization of adaptive identification for time-varying filters," *IEEE Trans. Automat. Contr.*, vol. AC-31, no. 3, pp. 283-287, Mar. 1986.

[45] A. Antoniou, *Optimization: Theory and Practice*, University of Victoria, Mar. 2000.

[46] A. Papoulis and S. U. Pillai, *Probability, Random Variables and Stochastic Processes*, Fourth Edition, McGraw Hill, 2002.

[47] "The University of Ottawa Cable," *http://www.ee.unb.ca/petersen/lib/data/cable_1989/description.html*

[48] O. Rioul and P. Duhamel, "Fast algorithms for discrete and continuous wavelet transforms," *IEEE Trans. Inform. Theory*, vol. 38, no. 2, pp. 569-586, Mar 1992.

[49] M. Holschneider, R. Kronland-Martinet, J. Morlet, and P. Tchamitchain, *Wavelets, Time-Frequency Methods and Phase Space*, chapter: A Real-Time Algorithm for Signal Analysis with the Help of the Wavelet transform, pp. 289-297, Springer-Verlag, Berlin, 1989.

[50] K. J. Kerpez, "Near-end crosstalk is almost Gaussian," *IEEE Trans. Commun.*, vol. 41, no. 1, pp. 670-672, Jan 1993.

[51] D. L. Donoho, I. M. Johnstone, G. Kerkyacharian, and B. Picard, "Wavelet shrinkage: Asymptopia?," *IEEE Tech. Rept., Statistics*, Stanford, 1993.

[52] S. Mallat, *A Wavelet Tour of Signal Processing*, Boston, MA: Academic, 1998.

[53] H. Krim, D. Tucker, S. Mallat, and D. Donoho, "On denoising and best signal representation," *IEEE Trans. Inform. Theory*, vol. 45, pp. 2225-2238, Nov 1999.

[54] D. Donoho, *Wavelet Shrinkage and WVD: A 10-Minute Tour*, Stanford Univ., Stanford, CA, Tech. Rep., 1992.

[55] D. Donoho, "De-noising by soft-thresholding," *IEEE Trans. Inform. Theory*, vol. 41, no. 3, pp. 613-627, 1995.

[56] I. M. Johnstone and B. W. Silverman, "Wavelet threshold estimators for data with correlated noise," *J. Roy. Statist. Soc. Ser. B*, 1997.

[57] C. Stein, "Estimation of the mean of a multivariate normal distribution," *Ann. Statist.*, 9, pp. 1135-1151, 1981.

[58] D. L. Donoho and I. M. Johnstone, "Adapting to unknown smoothness via wavelet shrinkage," *J. Am. Statist. Ass.*, 90, pp. 1200-1224, 1995.

[59] E. A. Lee and D. G. Messerschmitt, *Digital Communications*, Kluwer Academic Publishers, Boston, 1993.

[60] P. A. Regalia, *Adaptive IIR Filtering in Signal Processing and Control*, Marcel Dekker Inc., 1994.

[61] H. Fan and M. Doroslovacki, "On 'global convergence' of Steiglitz-McBride adaptive algorithm," *IEEE Trans. Circuits Syst. II*, vol. 40, no. 2, pp. 73-85, Feb. 1993.

[62] J. J. Shynk, "Adaptive IIR filtering," *IEEE ASSP Mag.*, Apr. 1989.

[63] R. R. Coifman and M. V. Wickerhauser, "Entropy-based algorithms for best basis selection," *IEEE Trans. Inform. Theory*, vol. 38, no. 2, pp. 713-718, 1992.

VITA

Surname: Nongpiur ***Given Names:*** Rajeev Conrad

Place of Birth: Shillong, India

Educational Institutions Attended

Indian Institute of Technology - Kharagpur	1994 to 1998
University of Victoria	2000 to 2005

Degrees Awarded

BTech.	Indian Institute of Technology	1998

Journal Publications

1. R. C. Nongpiur, D. J. Shpak, and A. Antoniou, "NEXT cancellation system with improved convergence rate and tracking performance," *IEE Proc.-Commun.*, Vol. 152, No. 3, June 2005.

Conference Publications

1. R. C. Nongpiur, D. J. Shpak, and A. Antoniou, "NEXT cancellation in xDSL systems," *Proc. 36th Asilomar Conference on Signals, Systems and Computers*, Pacific Grove, CA., Nov. 3-6, 2000.

2. R. C. Nongpiur, D. J. Shpak, and A. Antoniou, "Near-end crosstalk cancellation using variable-length cancellers," *2003 IEEE Int. Symp. on Circuits and Systems (ISCAS)*, Bangkok, Thailand, pp. IV-345 - IV-348, vol. 4, May 25-28, 2003.

3. R. C. Nongpiur, D. J. Shpak, and A. Antoniou, "Application of NLMS, PNLMS, and i-PNLMS algorithms for NEXT cancellation in xDSL systems," *2003 Proc. of IEEE PACRIM*, Victoria, B.C., vol.1, pp. 418-421, Aug. 2003.

4. R. C. Nongpiur, D. J. Shpak, and A. Antoniou, "NEXT cancellers using FDLMS filters with improved convergence rate," *Proc. 37th Asilomar Conference on Signals, Systems and Computers*, Pacific Grove, CA., Nov 9-12, 2003.

5. R. C. Nongpiur, D. J. Shpak, and A. Antoniou, "Tracking Performance for the FDLMS near-end crosstalk canceller for xDSL Systems," *2004 IEEE Intl. Symp. on Circuits*

and Systems (ISCAS), Vancouver, Canada, vol. 3, pp. 23-26, May 2004.

Work Submitted for Publication

1. R. C. Nongpiur, D. J. Shpak, and A. Antoniou, "Average pwoer sum of the NEXT couplings after NEXT cancellation," *2006 IEEE Int. Symp. on Circuits and Systems (ISCAS 2006)*, Kos, Greece.
2. R. C. Nongpiur, D. J. Shpak, and A. Antoniou, "NEXT mitigation using wavelets," *2006 IEEE Int. Conf. Acoustics, Speech, Signal Processing (ICASSP 2006)*, Toulouse, France .

UNIVERSITY OF VICTORIA PARTIAL COPYRIGHT LICENSE

Title of Dissertation:

Near-End Crosstalk Cancellation in xDSL Systems

Author: _____

RAJEEV CONRAD NONGPIUR

December 5, 2005

DISSERTATION WITHHOLDING FORM

At our request, the commencement of the period for which the partial licence shall operate shall be delayed from December 5, 2005 for a period of at least six months.

_____

(Supervisor)

_____

(Department Chairman)

_____

(Dean of Graduate Studies)

_____

(Signature of Author)

_____

(Date)

Date Submitted to the Dean's Office: _____